AFAPL-TR-71-34

A REVIEW OF CURRENT AND PROJECTED ASPECTS OF TURBINE ENGINE PERFORMANCE EVALUATION

ROBERT J. MAY, JR., 1/LT, USAF
BARRY J. BROWNSTEIN, 1/LT, USAF
STEPHEN J. PRZYBYLKO
RICHARD L. McTASNEY, CAPT, USAF
ANTHONY T. MOLISSE

TECHNICAL REPORT AFAPL-TR-71-34

FEBRUARY 1972

AIR FORCE AERO PROPULSION LABORATORY
AIR FORCE SYSTEMS COMMAND
WRIGHT-PATTERSON AIR FORCE BASE, OHIO 45433

NOTICE

When Government drawings, specifications, or other data are used for any purpose other than in connection with a definitely related Government procurement operation, the United States Government thereby incurs no responsibility nor any obligation whatsoever; and the fact that the government may have formulated, furnished, or in any way supplied the said drawings, specifications, or other data, is not to be regarded by implication or otherwise as in any manner licensing the holder or any other person or corporation, or conveying any rights or permission to manufacture, use, or sell any patented invention that may in any way be related thereto.

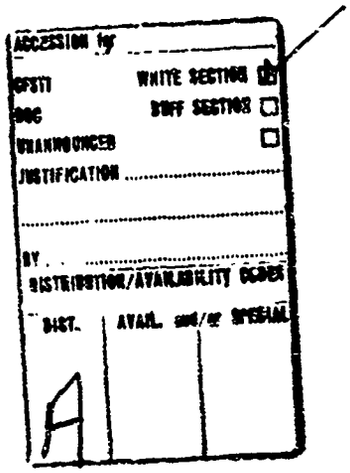

Copies of this report should not be returned unless return is required by security considerations, contractual obligations, or notice on a specific document.

AIR FORCE: 30-3-72/100

UNCLASSIFIED

Security Classification

DOCUMENT CONTROL DATA - R & D

(Security classification of title, body of abstract and indexing annotation must be entered when the overall report is classified)

1 ORIGINATING ACTIVITY (Corporate author) Air Force Aero Propulsion Laboratory Wright-Patterson AFB, Ohio 45433	2a. REPORT SECURITY CLASSIFICATION UNCLASSIFIED 2b. GROUP

3 REPORT TITLE

A Review of Current and Projected Aspects of Turbine Engine Performance Evaluation

4 DESCRIPTIVE NOTES (Type of report and inclusive dates)

5 AUTHOR(S) (First name, middle initial, last name)

Robert J. May, Jr., 1/LT, USAF
Barry J. Brownstein, 1/LT, USAF
Stephen J. Przybylko
Richard L. McTasney, Capt, USAF
Anthony T. Molisse

6 REPORT DATE February 1972	7a. TOTAL NO OF PAGES 120	7b. NO. OF REFS
8a. CONTRACT OR GRANT NO b. PROJECT NO 3066 c. d.	9a. ORIGINATOR'S REPORT NUMBER(S) AFAPL-TR-71-34 9b. OTHER REPORT NO(S) (Any other numbers that may be assigned this report)	

10 DISTRIBUTION STATEMENT

Approved for public release; distribution unlimited

11 SUPPLEMENTARY NOTES	12. SPONSORING MILITARY ACTIVITY Air Force Aero Propulsion Laboratory Wright-Patterson AFB, Ohio 45433

13 ABSTRACT

This report is actually a compilation of four separate papers which, in total, represent a survey of several important aspects of turbine engine performance analysis. The first paper describes a digital computer method which has become a powerful tool for simulation of steady-state engine operation. A discussion of inlet airflow distortion is the topic of the second paper. It elaborates on a theory of rotating stall generation and a unique method which was encountered for determining how this distortion propagates through the compression components and produces surge. The third paper addresses the problems associated with the engine control system and the techniques for computer simulation of transient engine operation. A discussion of the performance predictions of complex multimission aircraft weapon systems comprise the final section of this technical report. Emphasis is placed upon the use of inlet and exhaust nozzle maps to alleviate some serious shortcomings in past performance prediction methods.

ia

DD FORM 1 NOV 68 1473

UNCLASSIFIED

Security Classification

14 KEY WORDS	LINK A		LINK B		LINK C	
	ROLE	WT	ROLE	WT	ROLE	WT
° Steady-State Engine Simulations						
° Inlet Distortion						
° Turbine Engine Control Systems						
° Installed Turbine Engine Performance						
° Inlet and Exhaust System Performance						
° Computer Simulation of Turbine Engine Performance						
° Dynamic Engine Simulations						

*U.S.Government Printing Office: 1972 — 759-084/452

AFAPL-TR-71-34

A REVIEW OF CURRENT AND PROJECTED ASPECTS OF TURBINE ENGINE PERFORMANCE EVALUATION

ROBERT J. MAY, JR., 1/LT, USAF
BARRY J. BROWNSTEIN, 1/LT, USAF
STEPHEN J. PRZYBYLKO
RICHARD L. McTASNEY, CAPT, USAF
ANTHONY T. MOLISSE

ic

FOREWORD

This report was prepared in the Performance Branch (TBA), Turbine Engine Division, Air Force Aero Propulsion Laboratory, Wright-Patterson Air Force Base, Ohio, under Project 3066, "Gas Turbine Technology."

The report, compiled by Anthony T. Molisse, is comprised of four individual papers which were presented 8, 9 December 1970 to Swedish Military and Civilian Aviation representatives. All of the authors of this report are personnel of the Performance Branch. The contents of this technical report cover work conducted in the time period between July 1968 and December 1970.

This Technical Report has been reviewed and is approved.

Ernest C. Simpson

ERNEST C. SIMPSON, Director
Turbine Engine Division
Air Force Aero Propulsion Laboratory

ABSTRACT

This report is actually a compilation of four separate papers (designated sections) which in total represent a survey of several important aspects of turbine engine performance analysis. The first section describes a digital computer method which has become a powerful tool for simulation of steady-state engine operation. A discussion of inlet airflow distortion is the topic of the second section. It elaborates on a theory of rotating stall generation and a unique method which was encountered for determining how this distortion propagates through the compression components and produces surge. The third section addresses the problems associated with the engine control system and the techniques for computer simulation of transient engine operation. A discussion of the performance predictions of complex multimission aircraft weapon systems comprises the final section of this technical report. Emphasis is placed upon the use of inlet and exhaust nozzle maps to alleviate some serious shortcomings in past performance prediction methods.

TABLE OF CONTENTS

SECTION		PAGE
I	"APPLICATION OF STEADY-STATE ENGINE SIMULATIONS" by R.J. May, Jr., 1/Lt, USAF	1
II	"ENGINE RESPONSE TO INLET AIRFLOW DISTORTION" by B.J. Brownstein, 1/Lt, USAF	31
III	"CONTROL SYSTEMS AND TRANSIENT SIMULATIONS" by S.J. Przybylko	67
IV	"A TECHNIQUE FOR PREDICTING INSTALLED INLET AND EXHAUST SYSTEM PERFORMANCE" by R.L. McTasney, Captain, USAF	85

ILLUSTRATIONS

FIGURE		PAGE
1.	Flow Diagram of the SMOTE (Simulation of a Turbofan Engine) Computer Program	4
2.	Typical Fan or Compressor Map	6
3.	Typical Combustor Map	8
4.	Typical Turbine Map	9
5	Design Point Input	10
6.	Curve of Predicted Thrust Performance at Sea Level Static Conditions	12
7.	Curve of Predicted Fuel Flow Performance at Sea Level Static Conditions	13
8.	Nonaugmented T-Fan Mixed-Flow Test Model to Show Engine Output	15
9.	Bypass Ratio and Turbine Inlet Temperature Relationship	17
10.	Comparison Curves of Thrust Performance at Sea Level Static Conditions	18
11.	Comparison Curves of Fuel Flow Performance at Sea Level Static Conditions	20
12.	Comparison Curves of Thrust Performance Using the Modified Tailpipe at Sea Level Static Conditions	21
13.	Comparison Curves of Fuel Flow Performance Using the Modified Tailpipe at Sea Level Static Conditions	23
14.	Comparison Curves of Thrust Performance Using the Modified Tailpipe at 40,000 Feet and Mach 0.8	24
15.	Comparison Curves of Fuel Flow Performance Using the Modified Tailpipe at 40,000 Feet and Mach 0.8	26
16.	Comparison Curves of Bypass Ratio (BPR) at Sea Level Static Conditions	28
17.	Rotating Stall Theory	32
18.	Rotating Stall in Measurable Quantities	34
19.	Effect of Unsteady Flow on Lift Coefficient	35

ILLUSTPATIONS (CONTD)

FIGURE		PAGE
20.	Surge Phenomenon	36
21.	Surge at Compressor Discharge	38
22.	Stable Operation Compressor Map	39
23.	Compressor Surge Margin Allocation	41
24.	Total Pressure Pattern	43
25.	The Engine's View of Distortion	44
26.	Typical Supersonic Inlet Flow Conditions	46
27.	Typical Distortion Screen	48
28.	Correlation of Stall with Distortion Pattern (Instantaneous)	49
29.	Correlation of Stall with Distortion Pattern (1 MSec)	51
30.	Correlation of Stall with Distortion Pattern (2 MSec)	52
31.	Correlation of Stall with Distortion Pattern (3 MSec)	54
32.	Correlation of Stall with Distortion Pattern (6 MSec)	55
33.	Distortion Transport Time	56
34.	Probe Data Station 3	58
35.	Growth Cell Rotation Rate	60
36.	Correlation of Stall with Distortion Pattern	61
37.	Fan Map	63
38.	Distortion Pattern Fan Inlet	64
39.	Distortion Pattern Fan Exit	65
40.	Engine Control Problem	68
41.	Core Control	70
42.	Fan-Augmentor Control	71
43.	Supervisory Control	73

ILLUSTRATIONS (CONTD)

FIGURE		PAGE
44.	Engine Simulation Schematic	74
45.	Typical Output of a Simulation	76
46.	Effect of Aircraft and Engine Transients on Inlet Stability	77
47.	Overall System Simulation	78
48.	Fan Distortion Phenomenon	79
49.	Compressor Stage Model	80
50.	Parallel Compressor	82
51.	Compressor Row Model	83
52.	Installation Performance Losses During the Cruise-Loiter Operation	86
53.	External Exhaust System Thrust Losses (A Function of "Unfilled" Exhaust Area)	88
54.	Part-Power Engine Exhaust Performance Match at Sea Level Static and Mach 0.85	90
55.	Part-Power Engine-Exhaust Performance Match at Sea Level Static and Mach 0.85	91
56.	Exhaust System Performance (Typical)	93
57.	Reference Drag Effect on CFG	94
58.	Thrust Losses Due to Excessive Inlet Airflow	98
59.	Exhaust System Installed Performance	99
60.	Nozzle Operating Line at Sea Level Static and Mach 0.9	101

TABLES

TABLE		PAGE
I	Performance Comparison of Pretest and Test Results at Sea Level Static Conditions and Maximum Power	21
II	Performance Comparison of Results (Pretest, Test, and With Modified Tailpipe) at Sea Level Static Conditions and Maximum Power	24
III	Performance Comparison of Results (Pretest and with Modified Tailpipe) at 40,000 Feet, Mach 0.8, and Maximum Power	28

SYMBOLS AND UNITS

SYMBOL	DEFINITION	CONVENTIONAL UNITS
A	area	ft^2
A_8, A_j	nozzle throat area	ft^2
A_{8_M}	maximum nozzle throat area	ft^2
A_{91}	ideal plume area	ft^2
A_{10}	aircraft cross-sectional area	ft^2
BPR	bypass ratio (duct flow/core flow)	
C_{TEX}	external thrust coefficient	
C_{TIN}	internal thrust coefficient	
C_{TT}	gross thrust coefficient	
ΔD	external drag	lb_f
F_{GID}	ideal gross thrust	lb_f
FN	net thrust	lb_f
ΔH	change in enthalpy	
H	enthalpy	Btu/lb_m
HP	high pressure compressor	
i	incidence angle	degrees
LP	low pressure compressor	
N	rotational speed	RPM
N_1	fan speed	RPM
N_2	high compressor speed	RPM
N_d	speed demand	RPM
N_s	speed sensed	RPM
NPR	nozzle pressure ratio (P_{T8}/P_o)	

SYMBOLS AND UNITS (CONTD)

SYMBOL	DEFINITION	CONVENTIONAL UNITS
NPR_M	maximum nozzle pressure ratio	
P	pressure	lb_f/in^2
P_o	ambient pressure	lb_f/in^2
P_2	engine face total pressure	lb_f/in^2
P_8	nozzle throat pressure	lb_f/in^2
P_{8M}	maximum nozzle throat pressure	lb_f/in^2
P_T	total pressure	lb_f/in^2
PLA	power level angle	degrees
PR	pressure ratio (P_{out}/P_{in})	
Q	dynamic pressure	lb_f/in^2
SFC	specific fuel consumption	$lb_M/hr/lb_f$
ΔT	temperature difference ($T_{out}-T_{in}$)	
T	temperature	°R
T_2	engine face total temperature	°R
T_{25}	fan exit total temperature	°R
T_5	inter-turbine temperature	°R
T_8	nozzle throat temperature	°R
T_{8M}	maximum nozzle throat temperature	°R
WA	airflow	lb_M/sec
WAC	corrected airflow	lb_M/sec
WF	fuel flow	lb_M/sec
W_8	nozzle throat airflow	lb_M/sec
W_{8M}	maximum nozzle throat airflow	lb_M/sec

SYMBOLS AND UNITS (CONTD)

SYMBOL	DEFINITION	CONVENTIONAL UNITS
$WF_{A/B}$	afterburner fuel flow	lb_M/sec
W_g	gas flow	lb_M/sec
δ	pressure ratio (P/14.696)	
η	efficiency	
ω	pressure loss coefficient	
θ	temperature ratio (T/518.67)	

SECTION I

APPLICATIONS OF STEADY-STATE ENGINE SIMULATIONS

This three-part section describes digital simulations of turbine engines. It includes the applications and importance of steady-state computer engine models; a computer program used to predict design and off-design performance of turbofan engines; and an example of how a steady-state engine simulation is put together and used. This example is intended to explain why a computer model is necessary for isolating causes of poor engine performance and investigating the possible solutions to these problems.

BACKGROUND

First of all, just what is a steady-state engine simulation? A turbine engine may be described by a set of mathematical equations which define the steady-state aerodynamic and thermodynamic interactions which occur. These processes are very complex and iterative, and thus lend themselves very nicely to solution by a digital computer. The computer solution of these equations using major engine component (i.e., fan, compressor, turbines) test data and various mathematical techniques is known as a turbine engine simulation.

Why do we need steady-state engine simulations? There are four principal uses for these turbine engine models: 1) monitor present or "in use" engines, 2) explore the advantages and disadvantages of proposed advanced engines for future aircraft, 3) determine sensitive or critical areas in near future engines now under development, and 4) provide an economical means of obtaining engine data for aircraft

mission analysis. As a government organization, the Air Force Aero Propulsion Laboratory uses engine simulations to evaluate proposals, support government test facilities, assess the performance of development engines, and aid in advanced planning.

What are the advantages of computer engine models? First of all they are very fast. A typical simulation can run a complete point in one second or less. They are also economical. Running a series of points with the model is much less expensive than running the engine itself. Computer models are flexible. Component changes or even changes in geometry can be made very easily and quickly. Simulations are very reliable, and also very accurate. In the past, computer simulation performance has closely matched actual engine test cell data.

SMOTE

Now that some of the background on steady-state simulations has been covered, a discussion of what is used to build a turbine engine model is in order. A basic tool for simulating an engine cycle is a computer program called SMOTE - or Simulation of a Turbofan Engine. It is a balancing program used to predict performance at design and off-design conditions. The original SMOTE program was developed in the Air Force Aero Propulsion Laboratory and provided much of the impetus to the airframe and engine industries to use and further improve this type of engine simulation.

In order to run SMOTE, a set of flight conditions and a power setting, representative of the real engine being simulated, must be chosen. The power setting can be either turbine inlet temperature, fuel flow,

percent compressor speed, or percent fan speed. Component performance is made available to the program through performance maps. Several variables must be known before it is possible to enter the performance maps. These variables are called the independent variables. Their values are initially guessed using empirical data, and continually updated before each iterative pass through the engine. Once the independent variables have been determined the cycle calculations can be accomplished using component characteristics obtained from the component maps. Figure 1 is a flow diagram of the SMOTE computer simulation program.

The work from the turbines can be calculated but will not necessarily equal the work required by the compressors. Similarly, a nozzle throat area is known and the pressure required to drive the gas flow through this area can be calculated. This pressure may not necessarily equal the actual pressure of the gas stream. The duct discharge static pressure and low turbine discharge static pressure are known but are not necessarily equal. The difference between the available turbine work and the required compressor work, the difference between the actual nozzle pressure and the required nozzle pressure, and the difference between the duct and low turbine discharge static pressures become the dependent variables. By varying the independent variables it is possible to zero the dependent variables. The final result then, when the dependent variables have been zeroed, is a balanced off-design point where each of the components has been matched and their characteristics are compatible.

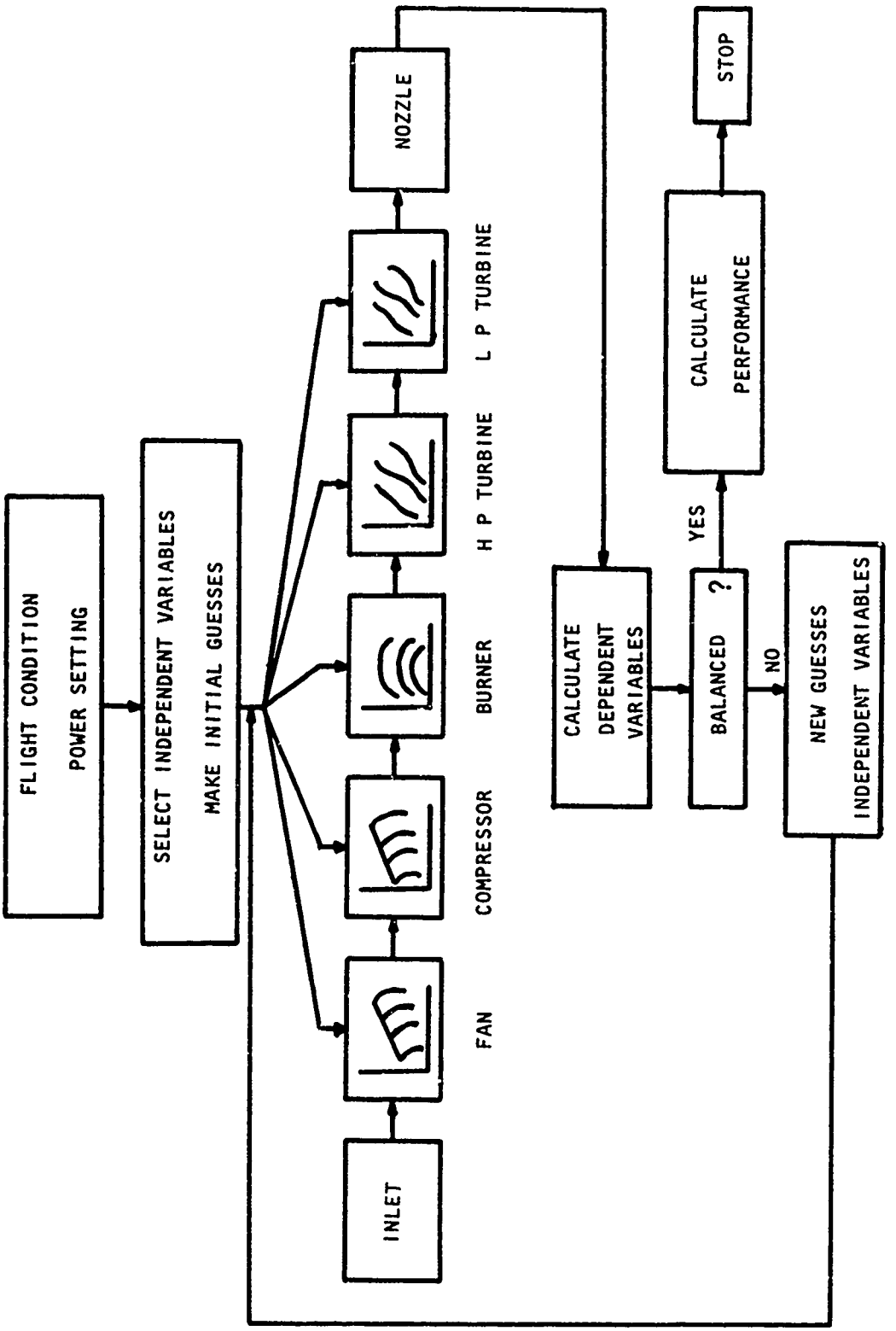

Figure 1. Flow Diagram of the SMOTE (Simulation of a Turbofan Engine) Computer Program

Setting up SMOTE correctly requires component performance maps and a detailed design point for the engine being modeled. (Throughout this paper, the term "design point" is defined as those parameters needed to specify the engine operating point at the sea level static, maximum thrust condition.) It is most important to input correct maps and a precise design point since the accuracy of the off-design performance is directly related to the accuracy of these two inputs.

The basic SMOTE program requires component performance maps for the fan, compressor, main burner, and both turbines. These maps are obtained from analytical methods or rig testing and converted into tabular form for use by the program. In addition, SMOTE may be modified to include other component performance maps, such as an afterburner or nozzle map. At the present time, these components are represented in the program in a general form. Other characteristics of the specific engine being modeled, such as pressure drops and bleed schedules may also be input, but again are not required. If a particular component map is not available, it is possible to use a representative component map and SMOTE will automatically scale it to fit the given design point. While this method is acceptable, it is not as accurate as using the actual component map.

Figure 2 represents a typical fan or compressor map in a form compatible with SMOTE. It is basically a plot of corrected airflow $WA\sqrt{\theta}/\delta$ versus pressure ratio. The upper line is the surge line. The near-vertical lines are lines of constant corrected speed, $N/(\sqrt{\theta})$,

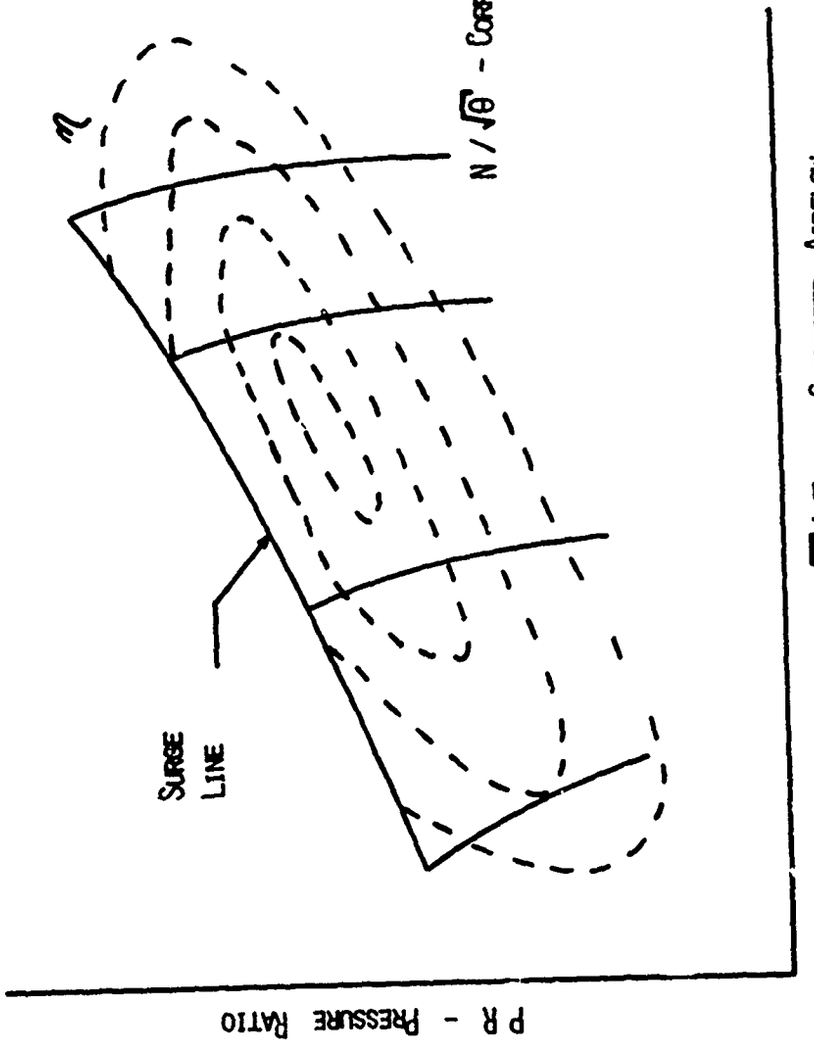

Figure 2. Typical Fan or Compressor Map

and the dotted lines are constant efficiency islands. Corrected flow and efficiency are input along a given corrected speed line for pressure ratios ranging from surge down to 1.

A typical combustor map, as used in SMOTE, is shown in Figure 3. It is a plot of burner efficiency versus burner temperature rise for lines of constant burner inlet pressure.

Figure 4 represents a turbine map suitable for use in SMOTE. It is a plot of work function, $\Delta H/T$, versus speed function $N/\sqrt{T}$, for lines of constant flow function or $W_g \sqrt{T}/P$. The dotted lines are lines of constant turbine efficiency. SMOTE requires $\Delta H/T$, $N/\sqrt{T}$, and efficiency be input along lines of constant flow function.

As stated earlier, in addition to component maps SMOTE requires a detailed design point in order to properly model the engine. The design point is required to set the mixing and nozzle throat areas as well as to scale the component maps. It is made up of those parameters needed to simulate the real engine at its design point or where it is sized, usually sea level static. If test data is being matched the design point is set up around the sea level static maximum speed point. Figure 5 is a list of the parameters required for a SMOTE design point.

EXAMPLE

As previously stated, one of the most important uses of steady-state engine simulations is to determine sensitive or critical areas in near future engines now under development. The following is an example of how this is accomplished. It necessitates the use of an engine simulation or model coupled with test cell data. Basically, one engine

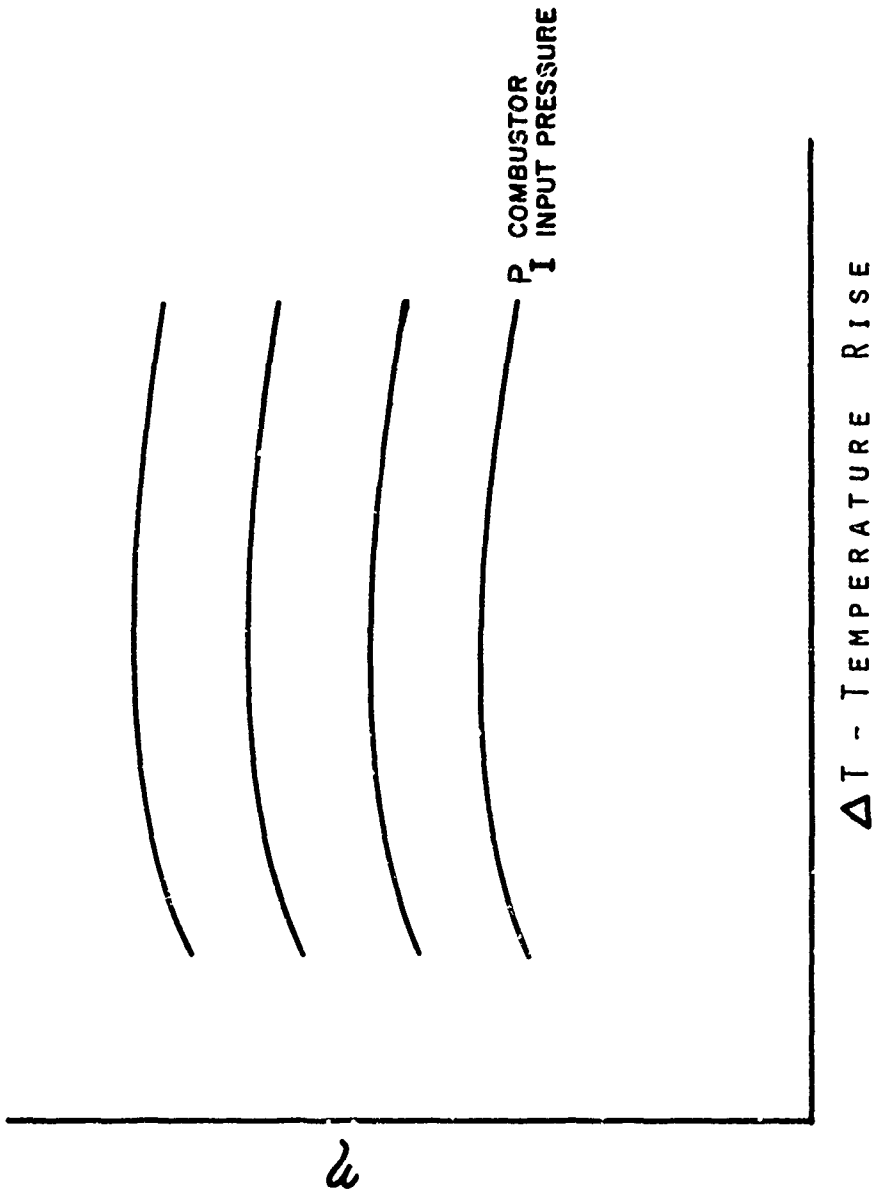

Figure 3. Typical Combustor Map

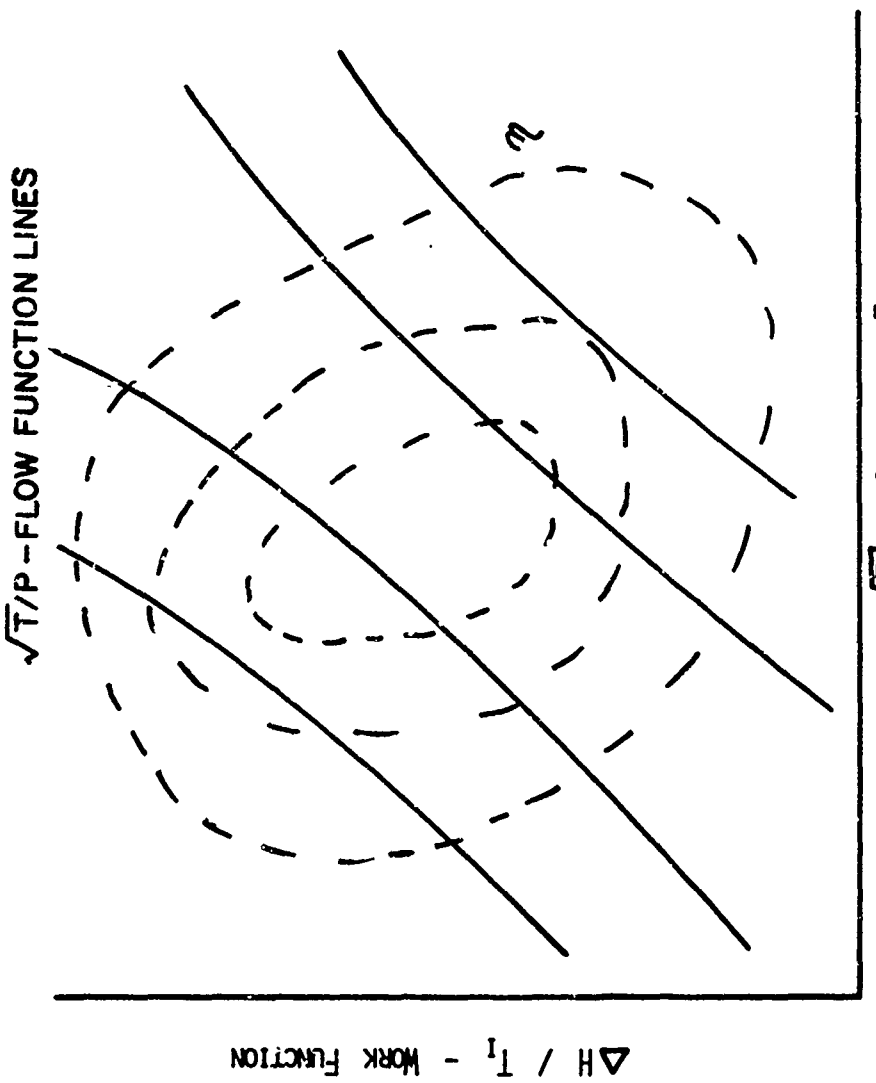

Figure 4. Typical Turbine Map

FAN COMPRESSOR	COMBUSTOR	HP & LP TURBINE	PRESSURE DROPS
Pressure Ratio	Efficiency	Efficiency	Main Burner
Airflow			Afterburner
Efficiency			Duct
% Speed			

BLEED FLOWS	MISCELLANEOUS	POWER SETTINGS
Overboard Bleed	Horsepower Extracted	Fuel Flow
HP & LP Turbine Cooling Air	Turbine Discharge Mach No.	Turbine Inlet Temperature
Leakage To Duct	Nozzle Velocity Coefficient	% Compressor Speed

Figure 5. Design Point Input

model is used to make pretest performance predictions. This simulation is essentially just the "spec" engine run on the SMOTE computer program. Another model is used to accurately match actual test cell performance. If these two simulations are not in agreement, they can then be used together to isolate the reason for the poor performance and to investigate any proposed solutions. This type of exercise could possibly require three separate engine simulations; one representing the pretest predicted or spec engine performance, a second matching actual test cell data, and a third incorporating proposed changes in the test engine. For the following example, data from a typical nonaugmented, mixed flow engine with a fixed nozzle throat area will be used.

PRETEST PREDICTIONS

The first step in determining whether or not a problem exists is to set up some sort of baseline performance so that there is something with which to compare the test engine. This is the "pretest" engine model. Generally, when comparing engine cycle performance, net thrust and fuel flow are examined as a function of power setting. However, in this example, t rbine inlet temperature is used as the indication of power setting. In the pretest engine model, component performance is based on the most recent rig test results. The design point is the projected operating point of each component at the maximum power setting. This is also based on the most recent rig test data. The combination of rig test component performance and design point becomes the basis for the pretest model performance predictions.

Figures 6 and 7 were generated by running the pretest engine model at a series of different power settings at sea level static conditions.

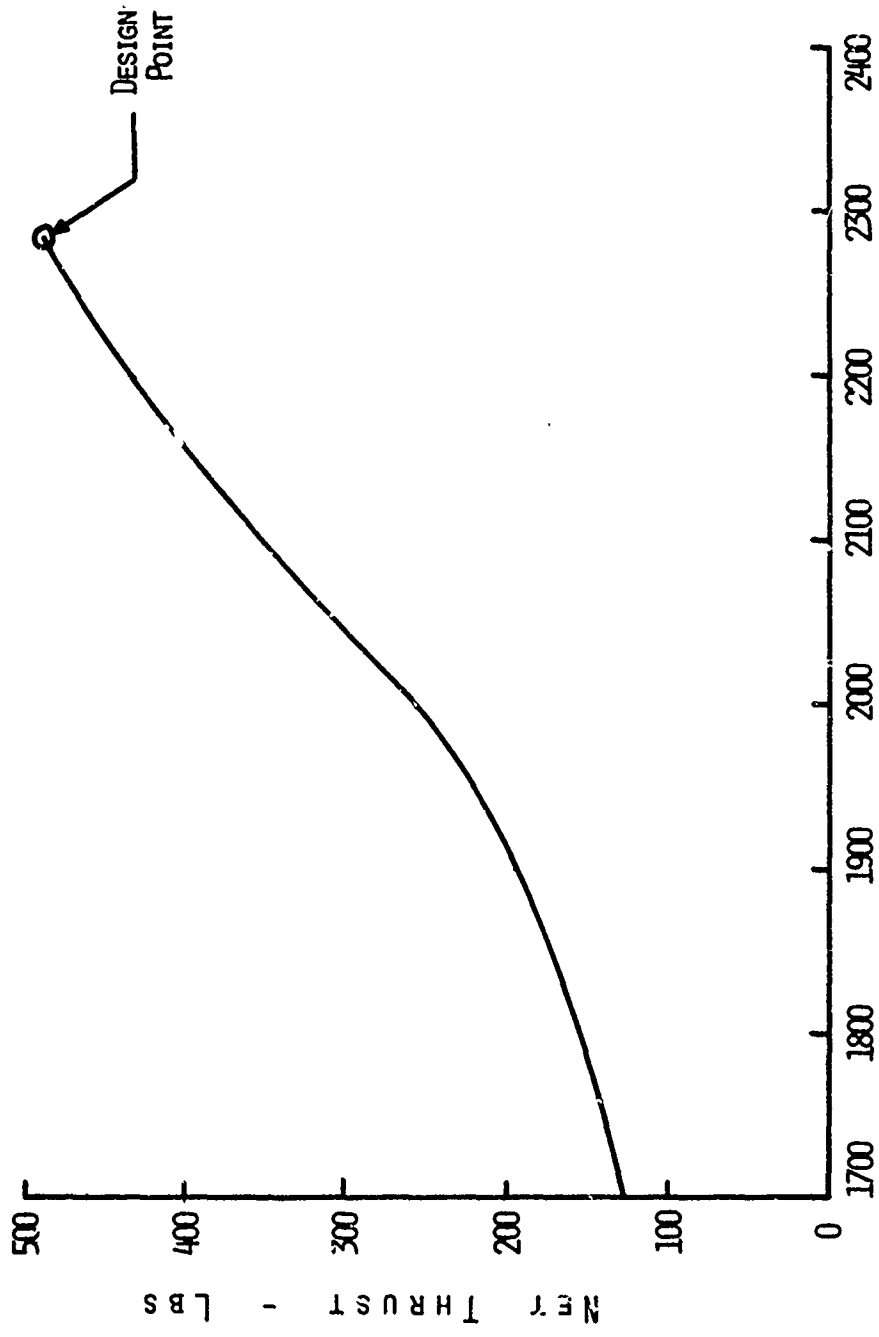

Figure 6. Curve of Predicted Thrust Performance at Sea Level Static Conditions

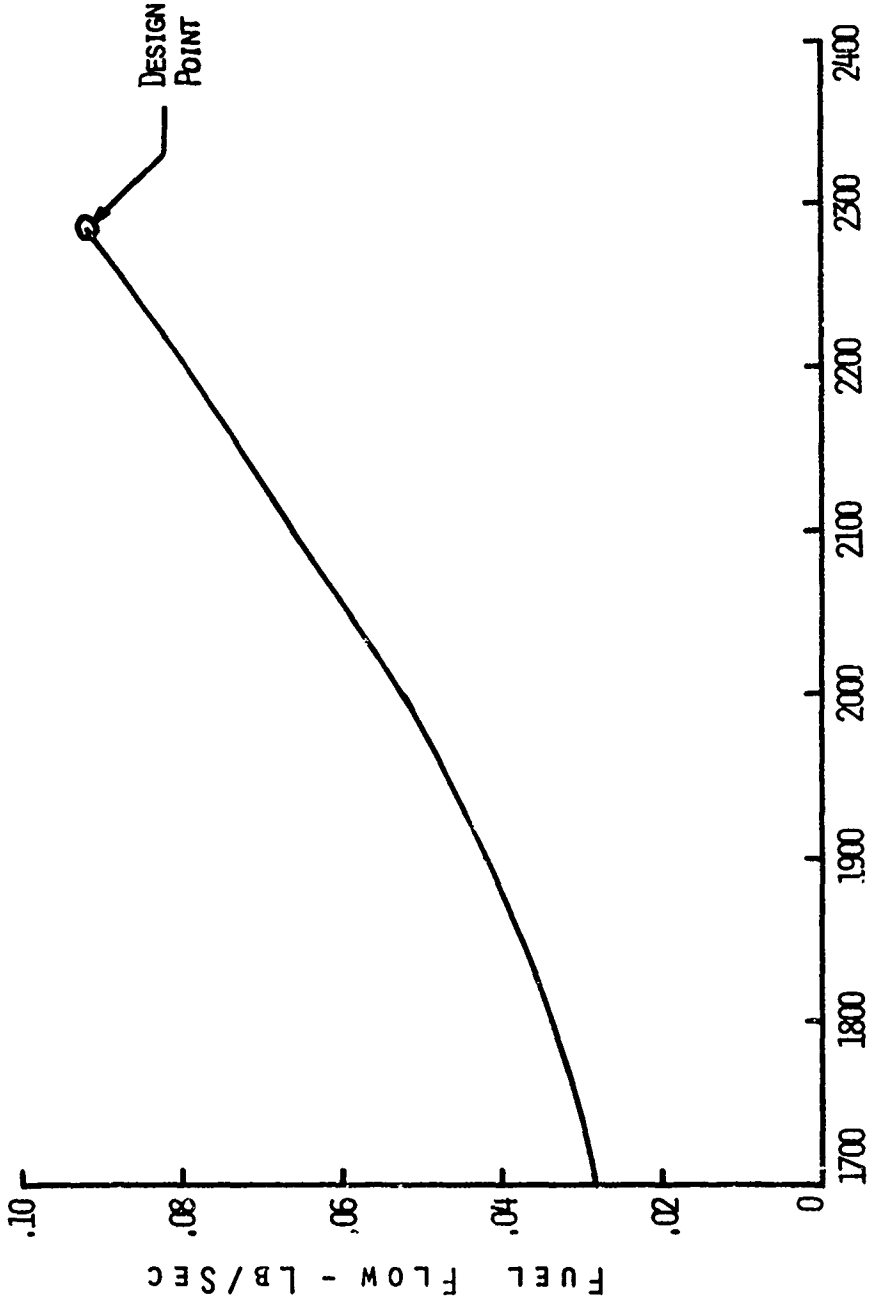

Figure 7. Curve of Predicted Fuel Flow Performance at Sea Level Static Conditions

Figure 6 represents the expected variation of net thrust with turbine inlet temperature if each component were operating as expected. The circled point is what is referred to as the design point of the engine. Similarly, Figure 7 shows the predicted change in fuel flow in lbs/sec with a change in power setting. The circled point is the design point, or expected fuel flow at the maximum power setting. Once again, this curve has been projected from the latest rig test data and the predicted sea level static, maximum power match point of the engine. (These last 2 performance curves now become the baseline about which the actual test cell engine performance is evaluated.)

TEST ENGINE SIMULATION

Now that the "baseline" engine model has been assembled, the test cell engine performance must be accurately simulated. This requires translating test data into a new design point. Typical test cell output as indicated on Figure 8 includes the following parameters: fan, intermediate and high pressure compressor speeds; and fuel flow, total inlet airflow and thrust. Also available are pressure and temperature at the fan inlet, intermediate pressure compressor inlet, high pressure compressor inlet and exit, low turbine exit and the duct discharge. Most of the SMOTE design point variables can easily be calculated from this data at the sea level static maximum power point. However, two very important variables are not measured, bypass ratio and turbine inlet temperature. Both are critical and must be known precisely at the match point if an accurate simulation of the test engine is to be made.

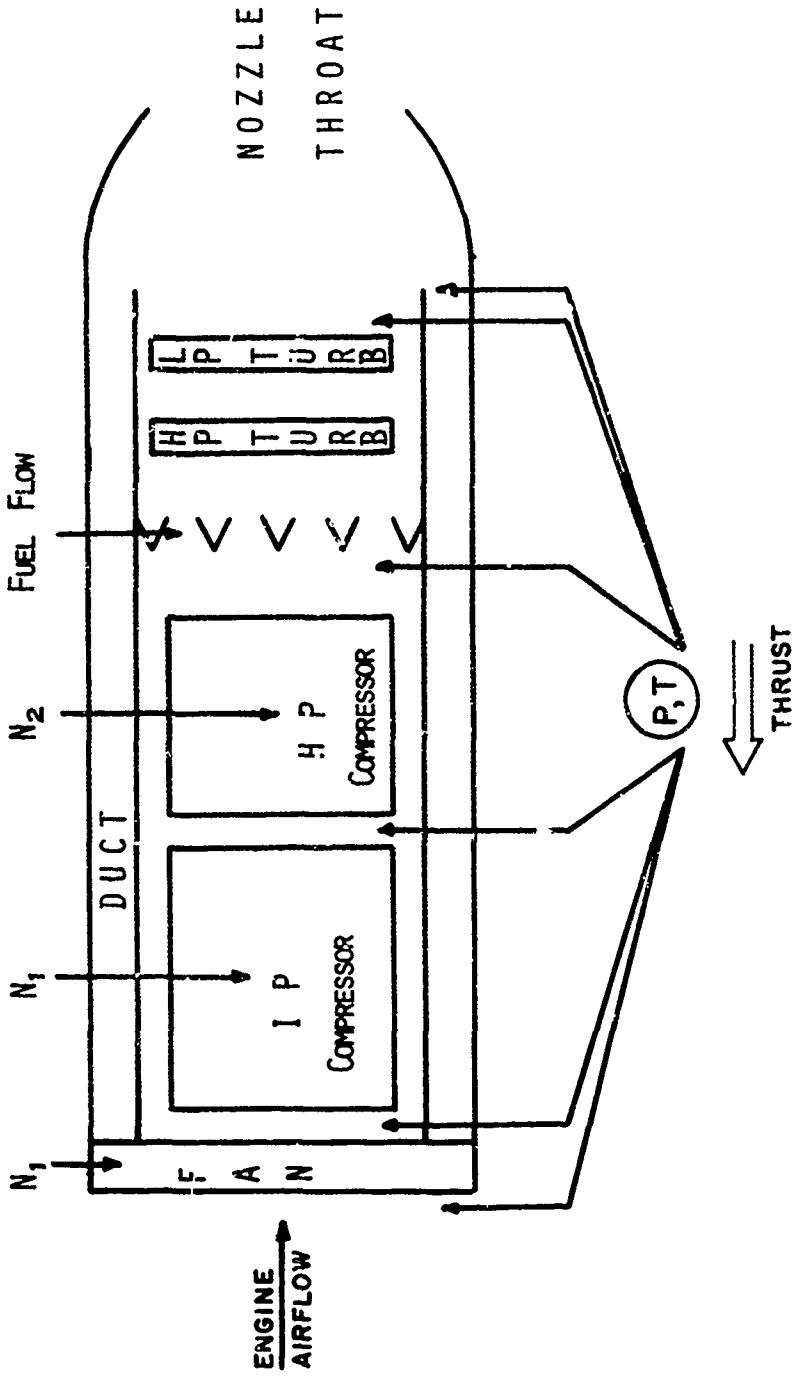

Figure 8. Nonaugmented T-Fan Mixed-Flow Test Model to Show Engine Output

To find the correct bypass ratio and turbine inlet temperature, a matrix of computer runs (using the test engine simulation) is made varying bypass ratio for a constant turbine inlet temperature and then varying turbine inlet temperature for a constant bypass ratio. From the output of these runs, a plot of fuel flow versus exhaust gas temperature is made for lines of constant turbine inlet temperature and constant bypass ratio (see Figure 9). Exhaust gas temperature and fuel flow are both measured during the test. This combination of variables at the maximum speed point uniquely defines the turbine inlet temperature and bypass ratio at this match point. The test engine design point is now completely defined. A series of points at different power settings (power hook) is run and compared with the reduced test data. Adjustments (e.g., component map multipliers) are then made to the design point parameters in order to more perfectly match the test results. Once the computer power hook correlates with the test power hook, an accurate representation of the test engine has been made. It is then possible to compare the test engine performance with the baseline engine performance at any other point in the operating envelope.

The test engine simulation performance is compared with the previously defined baseline performance at a given flight condition. Figure 10 is a plot of net thrust versus turbine inlet temperature at sea level static. The upper line represents the pretest model performance predictions. The lower line is the performance prediction of the test engine simulation, and the solid circles are the actual test points. Notice the excellent correlation between the actual test points and test engine model.

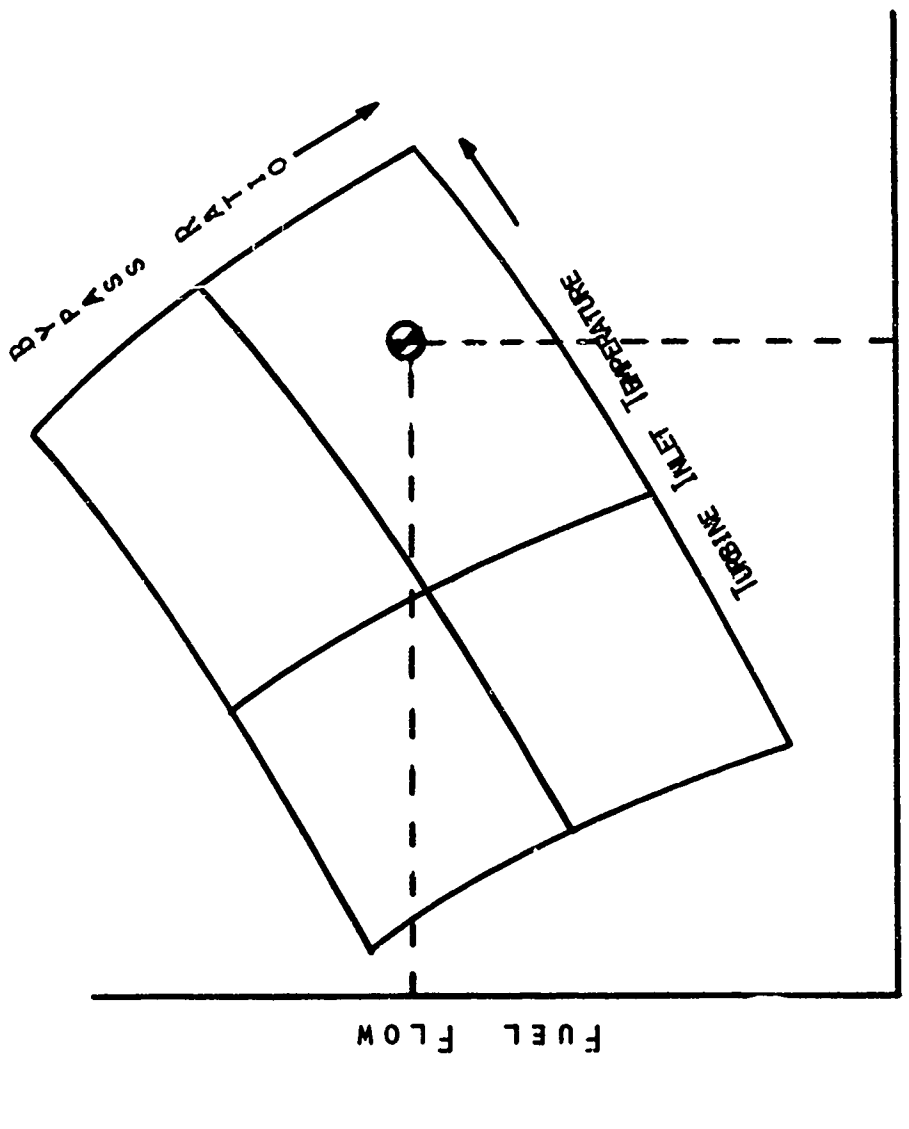

Figure 9. Bypass Ratio and Turbine Inlet Temperature Relationship

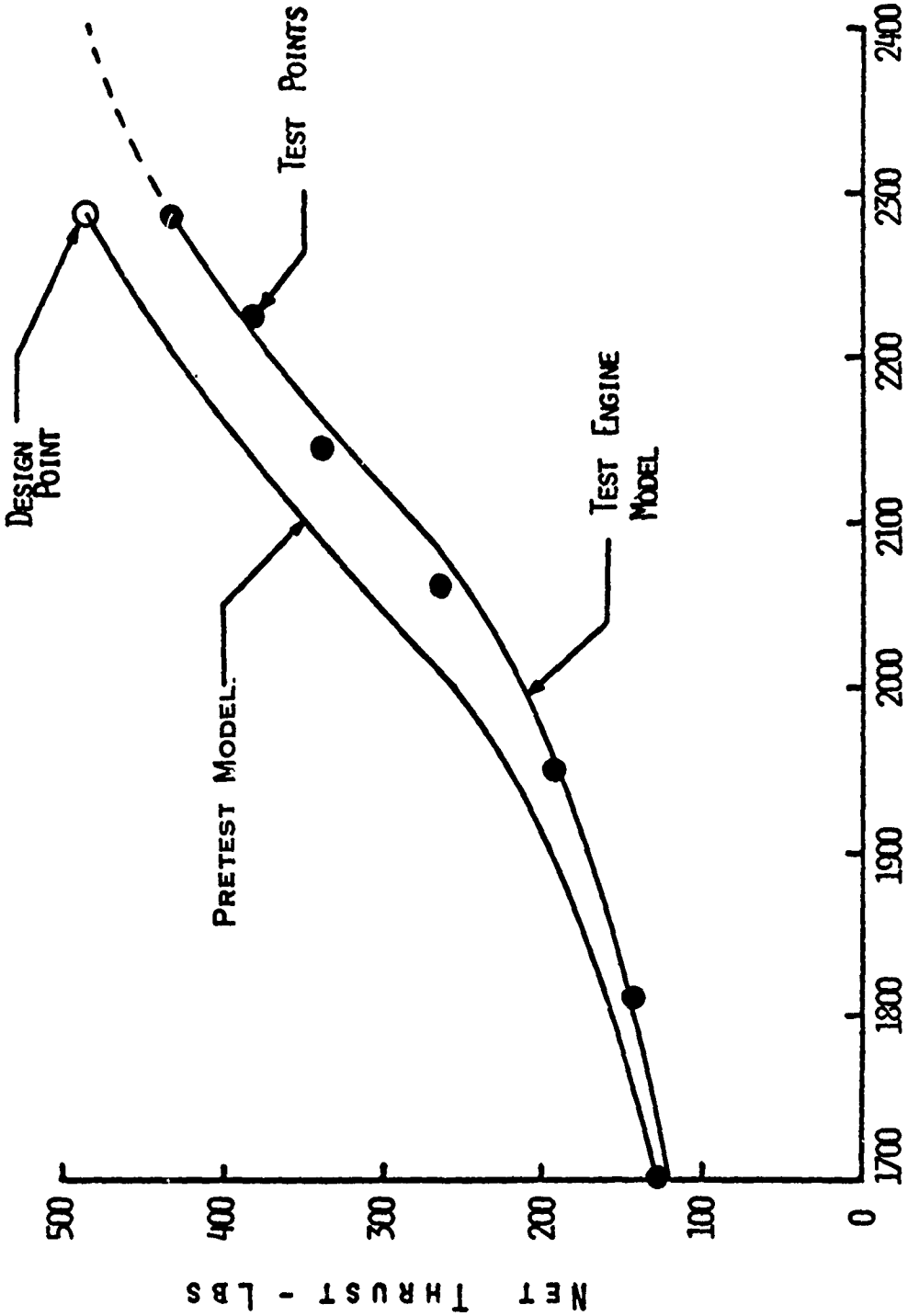

Figure 10. Comparison Curves of Thrust Performance at Sea Level Static Conditions

From this plot it is evident that at high power settings, the test engine is operating significantly below expected baseline performance. In fact, in order to reach the projected maximum thrust level, the test engine must be "over-temperatured" by about 125° to a temperature of 2400°R as represented by the dashed line. However, well in advance of this temperature, an exhaust gas temperature limit is hit making it impossible to reach the expected maximum thrust level.

The fuel flow curve of Figure 11 shows a similar story; that is, the test engine is not performing as expected. Again, the upper line represents the baseline performance and the lower line is the test engine model performance. The solid circles are the actual test points. At high power settings the fuel flow is down slightly; however, the dotted portion of the lower curve shows that in order to reach the desired maximum thrust level it would take a significantly higher fuel flow than predicted.

Table I is a closer look at the sea level static maximum power performance. The pretest model predicted a net thrust of 487 lbs at a fuel flow rate of 0.0915 lbs/sec, which is a specific fuel consumption of 0.676. The test results show the engine only made a net thrust of 435 lbs at a fuel flow of 0.0837 lb/sec for a specific fuel consumption of 0.692. In other words, the net thrust is down by almost 11% and the specific fuel consumption is up 3%. This degraded sea level static performance is unacceptable and must be corrected.

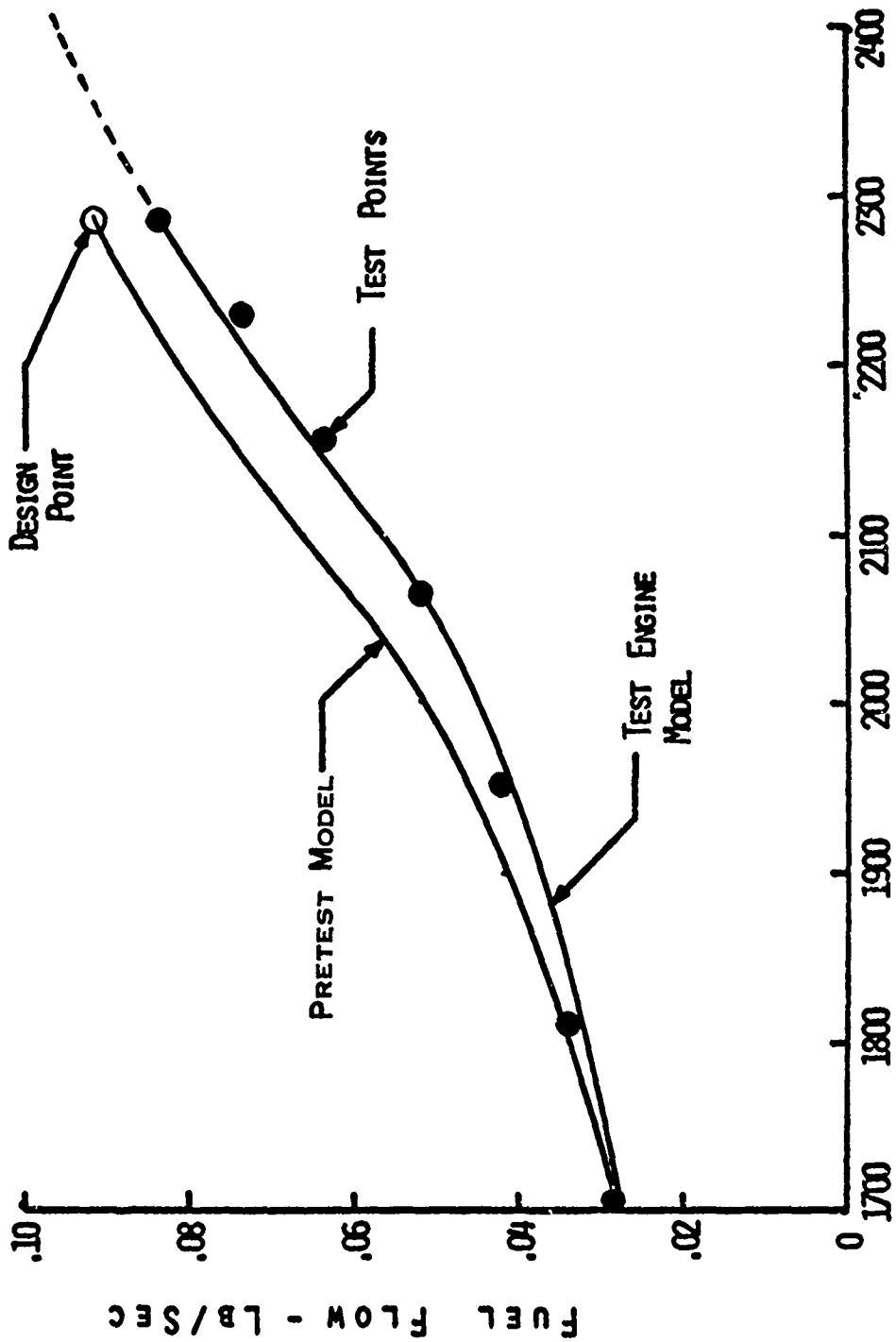

Figure 11. Comparison Curves of Fuel Flow Performance at Sea Level Static Conditions

TABLE I

PERFORMANCE COMPARISON

OF PRETEST AND TEST RESULTS

AT SEA LEVEL STATIC CONDITIONS

AND MAXIMUM POWER

	FN	WF	SFC
PRETEST	487	.0915	.676
TEST	435	.0837	.692

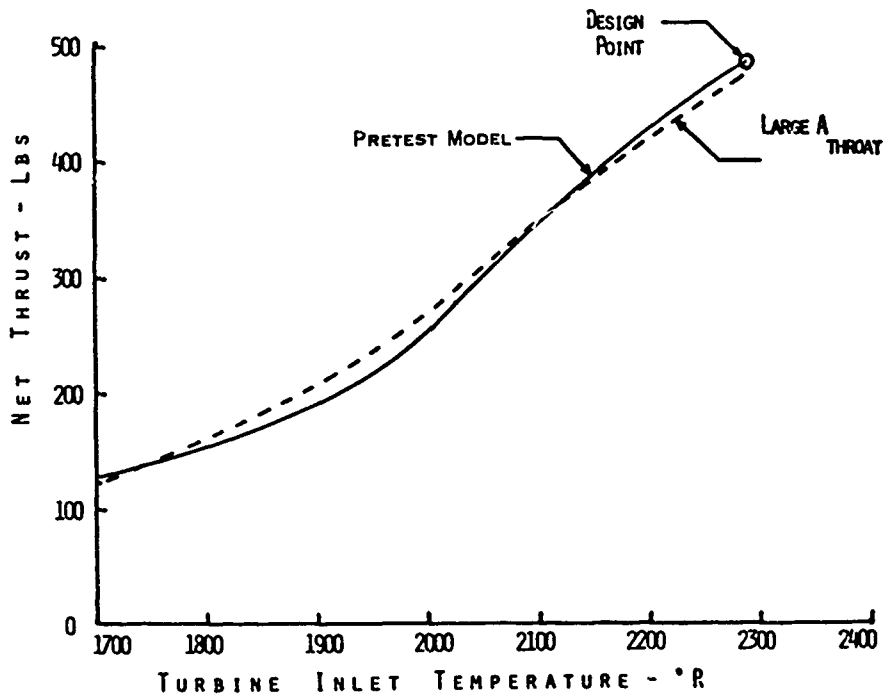

Figure 12. Comparison Curves of Thrust Performance Using the Modified Tailpipe at Sea Level Static Conditions

Generally, when an engine is not performing up to specifications there are several easily implemented solutions. One of these is to over-temperature the engine. This will result in the desired thrust level but at a higher specific fuel consumption and a reduced engine life. With this particular engine, however, an exhaust gas temperature limit is encountered before a significant increase in thrust is felt. A second possible solution is to open up the nozzle throat area, which slightly overspeeds the fan. After a few quick checks with the test engine model, this appears to be a feasible solution to the low thrust, high specific fuel consumption problem of the test engine. The model can also be used to determine a suitable change in area for regaining the lost performance.

Again a power hook is run with the test engine model, only this time with an expanded tailpipe area. This new performance is compared to the originally predicted sea level static performance. The dashed line on Figure 12 represents the net thrust of the test engine with a larger nozzle throat area. There is a significant improvement in performance over the original test engine. In fact, by slightly over-temperaturing the engine the required maximum net thrust level can be met.

Figure 13 is a performance curve comparing the baseline fuel flow with the fuel flow of the engine with the modified tailpipe at sea level static. It indicates that the fuel flow will not be excessive even if the engine is over-temperatured to reach maximum desired net thrust.

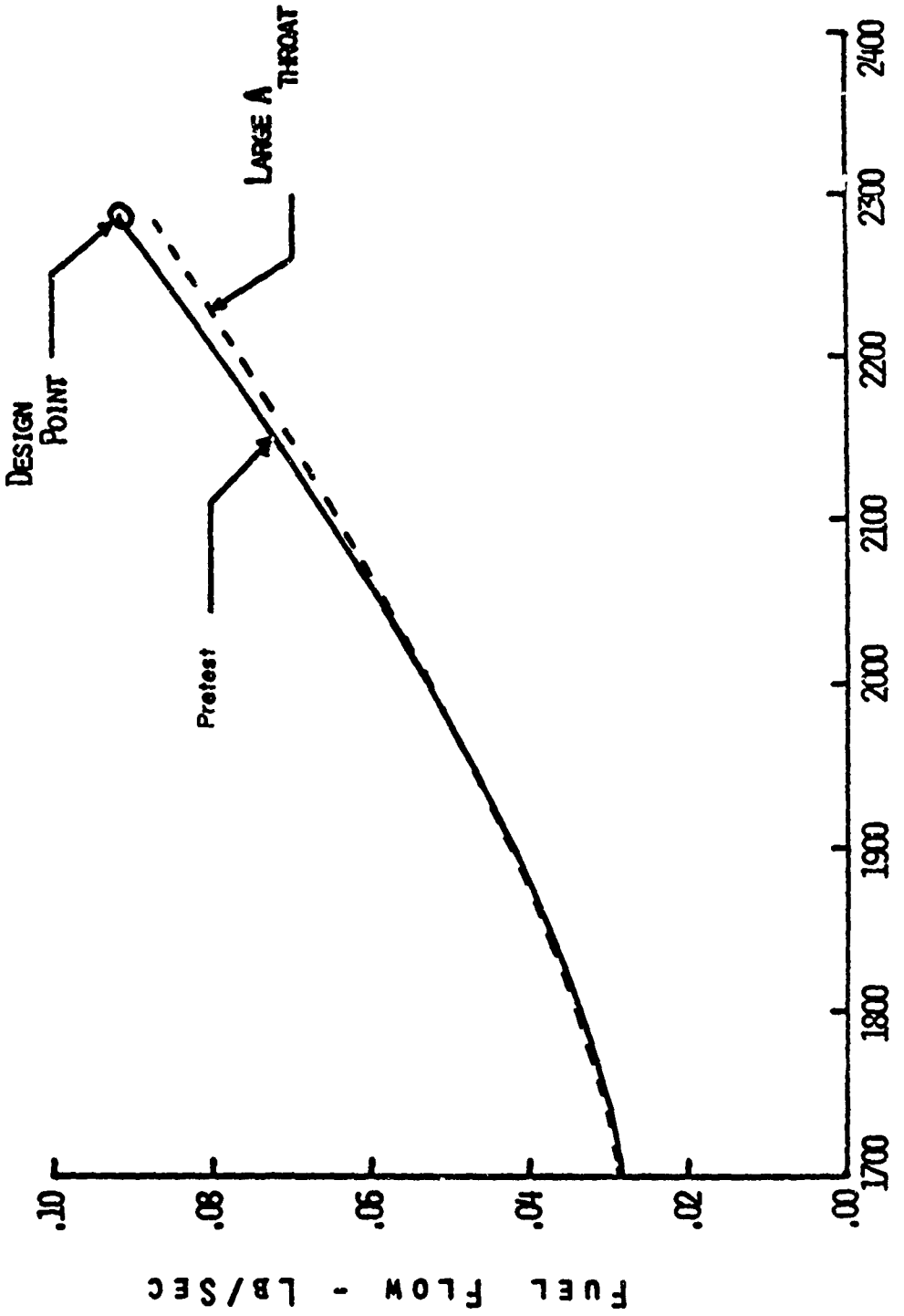

Figure 13. Comparison Curves of Fuel Flow Performance Using the Modified Tailpipe at Sea Level Static Conditions

TABLE II

PERFORMANCE COMPARISON OF RESULTS (PRETEST, TEST, AND WITH MODIFIED TAILPIPE) AT SEA LEVEL STATIC CONDITIONS AND MAXIMUM POWER

	FN	WF	SFC
PRETEST	487	.0915	.676
TEST	435	.0837	.692
LARGE A_{THROAT}	475	.0885	.672

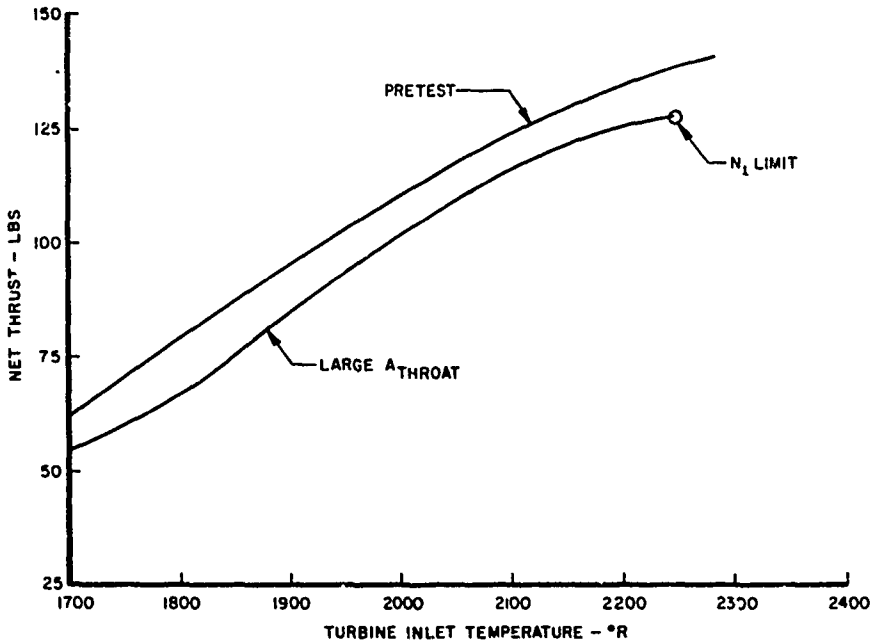

Figure 14. Comparison Curves of Thrust Performance Using the Modified Tailpipe at 40,000 Feet and Mach 0.8

Table II shows a detailed comparison of the sea level static maximum power performance of the three engine models. The pretest model predicted a net thrust of 487 lbs, but the test engine only produced 435 lbs of thrust. However, by opening up the nozzle throat area all but about 2% of the lost thrust was regained and this fraction could be recovered by slightly over-temperaturing the engine. In addition, this thrust increase did not result at the expense of specific fuel consumption. In fact, the specific fuel consumption of the engine with the modified tailpipe has decreased to slightly below the baseline level. From the data on this chart, it appears that the desired thrust and SFC levels were attained by a simple change in the nozzle. However, the investigation cannot stop here, as might be the tendency if a computer model were not available. The sea level static performance problem has been solved but how does the solution affect performance at another flight condition? The computer models can quickly supply the answer to this question.

FURTHER CHECKOUT

With this particular engine, another important operating point is at an altitude of 40,000 feet and a Mach number of 0.8. Once again a power hook is run at these flight conditions with the pretest engine model in order to establish a baseline of performance for comparison. The upper line on this curve (Figure 14) of net thrust versus turbine inlet temperature represents this predicted performance. The lower line is obtained by running a power hook at the given altitude and Mach number with the test engine model and the modified tailpipe. Despite the fact that, at sea level static, these two models predicted nearly

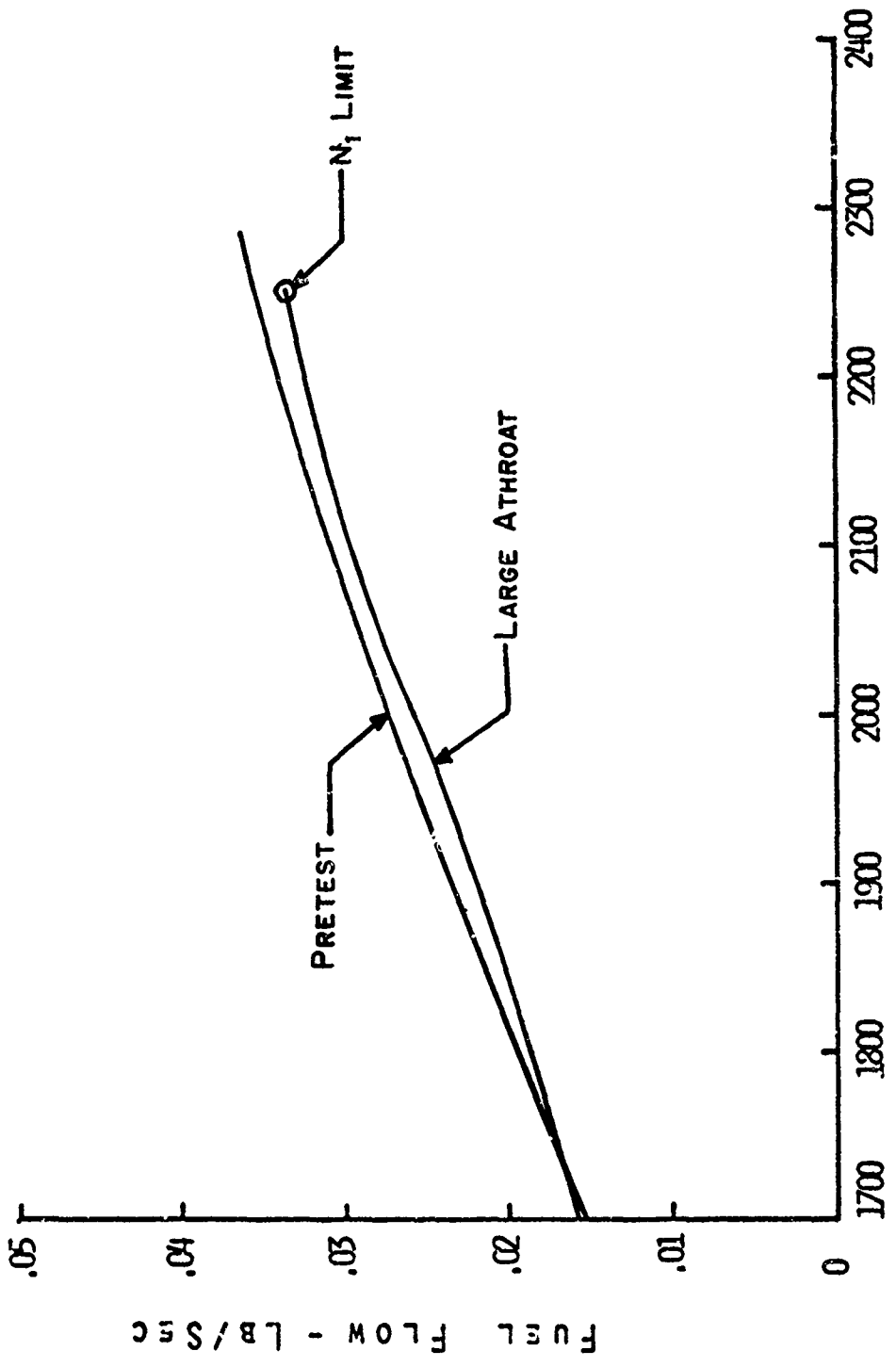

Figure 15. Comparison Curves of Fuel Flow Performance Using the Modified Tailpipe at 40,000 Feet and Mach 0.8

the same performance, Figure 14 shows that the modified test engine is not performing up to predictions. At any given power setting the thrust of this engine is down considerably. In fact, a fan overspeed limit is hit before the desired maximum turbine inlet temperature can be reached.

The fuel flow comparison curve (Figure 15) was generated in the same way as the preceding chart. The upper line is the baseline fuel flow at an altitude of 40,000 feet at Mach 0.8. The lower line is the fuel flow for the test engine model with the modified tailpipe at the same flight conditions. The fuel flow of this engine is down only slightly from pretest prediction even though net thrust is down considerably.

Table III compares the maximum power performance of the two engines at 40,000 feet Mach 0.8. The pretest model predicted a net thrust of 142 lbs at a fuel flow of 0.0366 lbs/sec for a specific fuel consumption of 0.932. The engine model with the modified tailpipe showed a thrust of only 127 lbs or down 11% from the defined baseline performance. If this engine had an energy maneuverability requirement at this flight condition, the degraded thrust performance would not be acceptable. Also, this lost thrust cannot be regained by over-temperaturing the engine due to the 105% fan speed limit. In other words, changing the tailpipe size was not the correct "fix" for the test engine. It worked nicely at sea level static but not at other flight conditions. The test engine has a more serious problem than just an improperly sized tailpipe. To isolate the problem the internal performance of the pretest model and the test model must be compared.

TABLE III

PERFORMANCE COMPARISON OF RESULTS (PRETEST AND WITH MODIFIED TAILPIPE) AT 40,000 FEET, MACH 0.8, AND MAXIMUM POWER

	FN	WF	SFC
PRETEST	142	.0366	.932
LARGE A_{THROAT}	127	.0335	.932

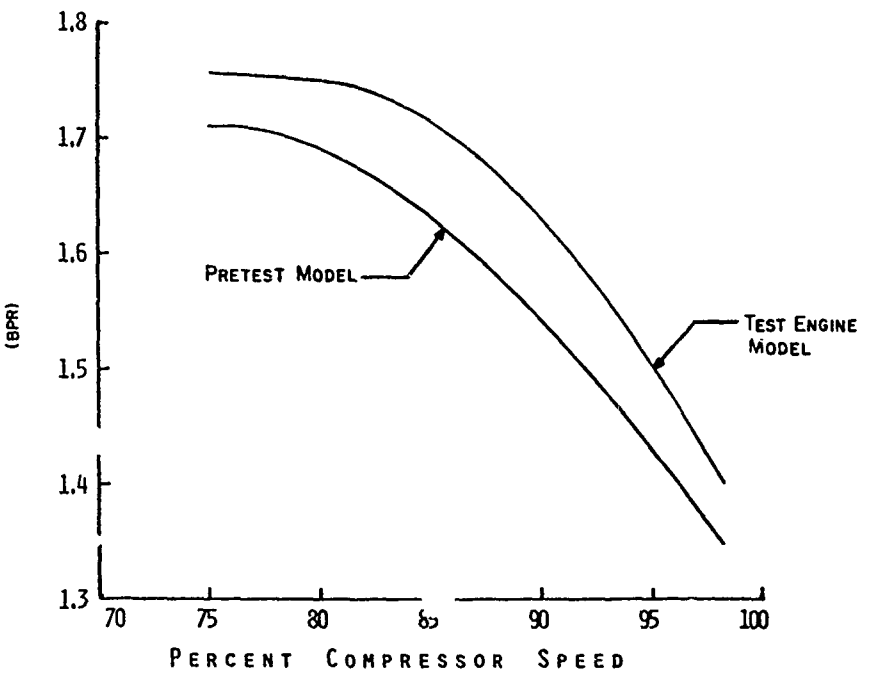

Figure 16. Comparison Curve Bypass Ratio (BPR) at Sea Level Static Conditions

In this particular example the poor test performance can be traced back to a low core flow. Figure 16 is a plot of bypass ratio versus percent compressor speed. The lower line is the pretest prediction while the upper line is the test engine model. The test engine bypass ratio is much higher than it should be. This must be corrected by a design change in either the fan hub or the high pressure compressor. Once this is taken care of the test engine model shows performance will return close to the established spec level.

SUMMARY

In summary, troubleshooting this engine required three separate cycle models: the pretest or baseline model, the actual test engine model, and the test engine model with the modified tailpipe. The baseline and test performance were compared at sea level static. Possible modifications to the cycle were investigated at different flight conditions and rejected. Finally, by using the model to check internal performance of the test engine, the problem area was isolated. The computer simulation enabled a detailed investigation of the engine without wasting valuable test time as well as giving greater visibility to the actual problem areas, and their proposed solutions. Although, at the present, steady-state engine simulations are very useful tools, there is still plenty of room for improvement. Engine models could be used for a broader range of applications. Also, continued development of better techniques to make these computer programs faster and more manageable are required. Even more important is the need for a computer model of the total propulsion system. As discussed in Section IV of this report, in the future, inlet and nozzle performance will be defined in map form, just

like any other engine component. These maps should be incorporated into the present steady-state engine models to predict and optimize installed performance for the inlet, engine, and nozzle combination.

SECTION II

ENGINE RESPONSE TO INLET AIRFLOW DISTORTION

With the advent of high performance aircraft, the subject of inlet-engine compatibility has become increasingly important. Not only does supersonic flight at severe angles-of-attack and yaw produce highly distorted inlet flow, but the introduction of the afterburning turbofan engine has complicated the problem of engine tolerance to distortion.

The points to be covered here include a description of the surge phenomenon, which is, after all, the ultimate result of poor inlet-engine compatibility. On the inlet side of the problem, we will look at flow distortion, what it is, where it comes from, and more importantly, what it does in the engine. The propulsion system's reaction to the distorted flow is complicated, and we will briefly discuss the effect of component interactions on the distortion pattern as it proceeds through the engine.

THE SURGE PHENOMENON

There are occasional misunderstandings concerning the usage of the words "stall" and "surge." For the purposes of this report we will define stall to be the breakdown in flow in some portion of a stage of a compression unit, for example: a "fifth stage high pressure compressor stall." Surge will be used to mean complete flow breakdown throughout the engine compression system as characterized by a drop-off in the total pressure measured at the exit of the last compressor stage. This condition will be described in greater detail later.

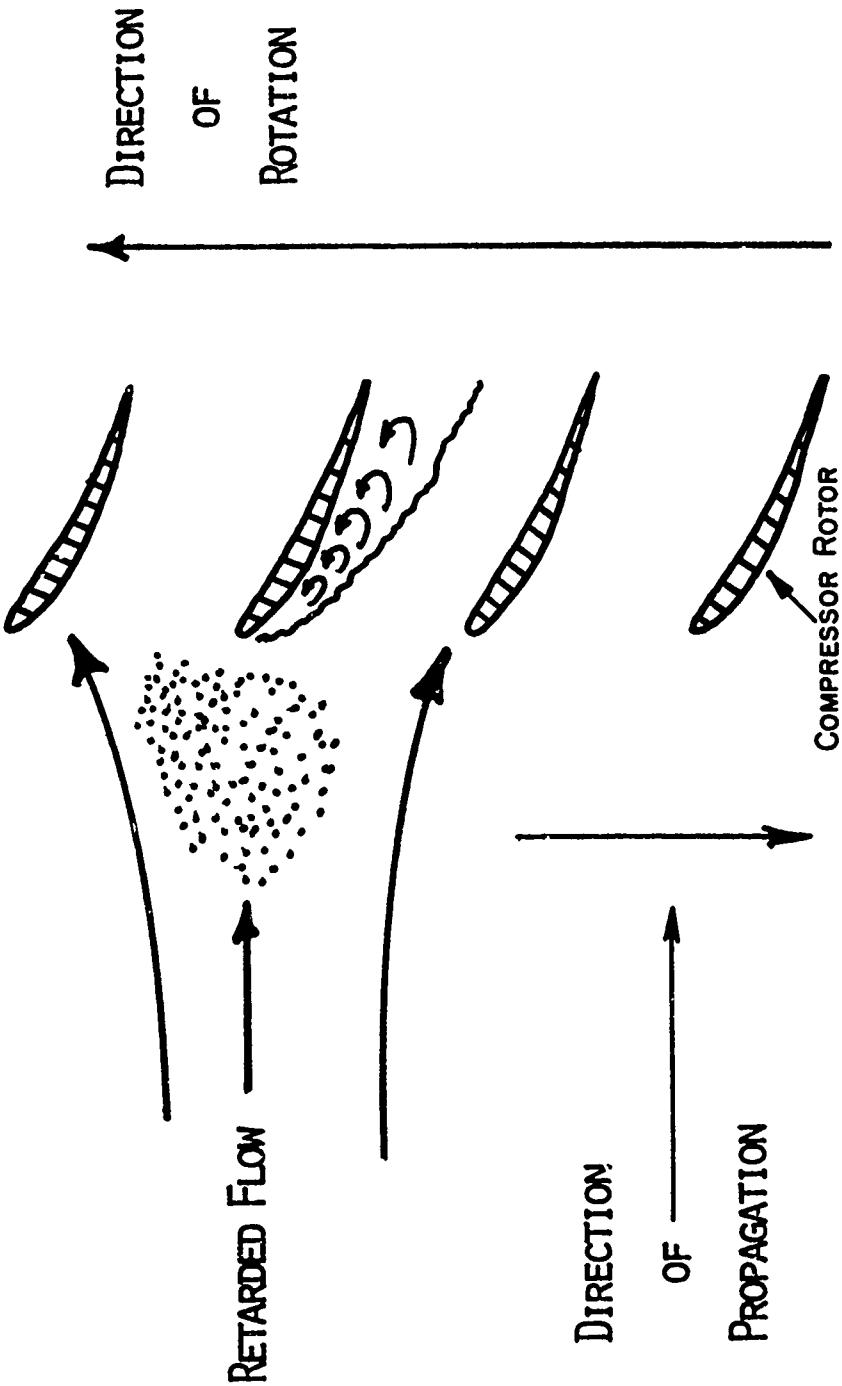

Figure 17. Rotating Stall Theory

Figure 17 is a visualization of the flow through one stage of a compressor. The blades are a cascade representation of the blade row with the direction of rotation upward on the figure. The flow is entering from the left. Due to some perturbation in the flow, the second blade from the top becomes aerodynamically stalled. The result of this is that the pressure rise across the cascade drops locally, causing a decrease in flow in the vicinity of the stalled blade. To bypass this region of retarded flow, incoming air is diverted in such a manner as to decrease the effective angle-of-attack on the blade above the stalled blade, and increase the angle on the blade below. If the upper blade had been stalled previously, it would now tend to recover, while the lower blade now would tend toward stall. The net effect is to produce a pocket of retarded flow and locally low pressure that moves in the opposite direction of rotation of the blade row at about one-half the rotational speed. This condition is known as rotating stall.

A view of rotating stall in terms of measurable quantities is presented in Figure 18. Here the rotating region of retarded flow is seen as a rotating zone of low total pressure. If we locate two total pressure probes 180° from each other on the compressor face, the stall cell can be observed. A low pressure zone with a depth of about ten percent of the face average total pressure is seen rotating with a period on the order of 0.01 sec.

The cause of rotating stall at its initial onset was glossed over in the discussion above due to the uncertain nature of unsteady flow. The solid line in Figure 19 represents the familiar lift coefficient versus angle-of-attack curve for steady flow. Within rotating machinery,

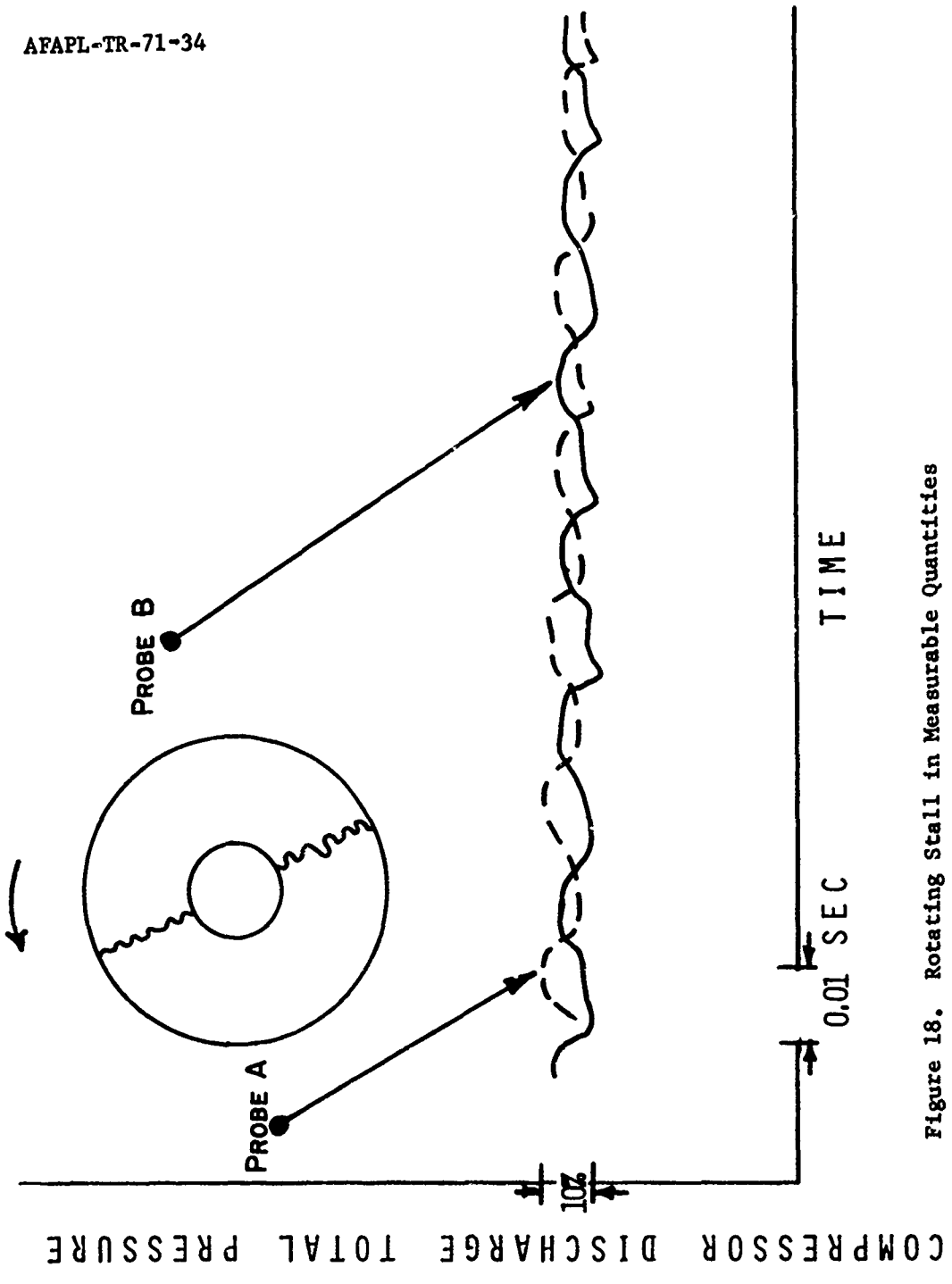

Figure 18. Rotating Stall in Measurable Quantities

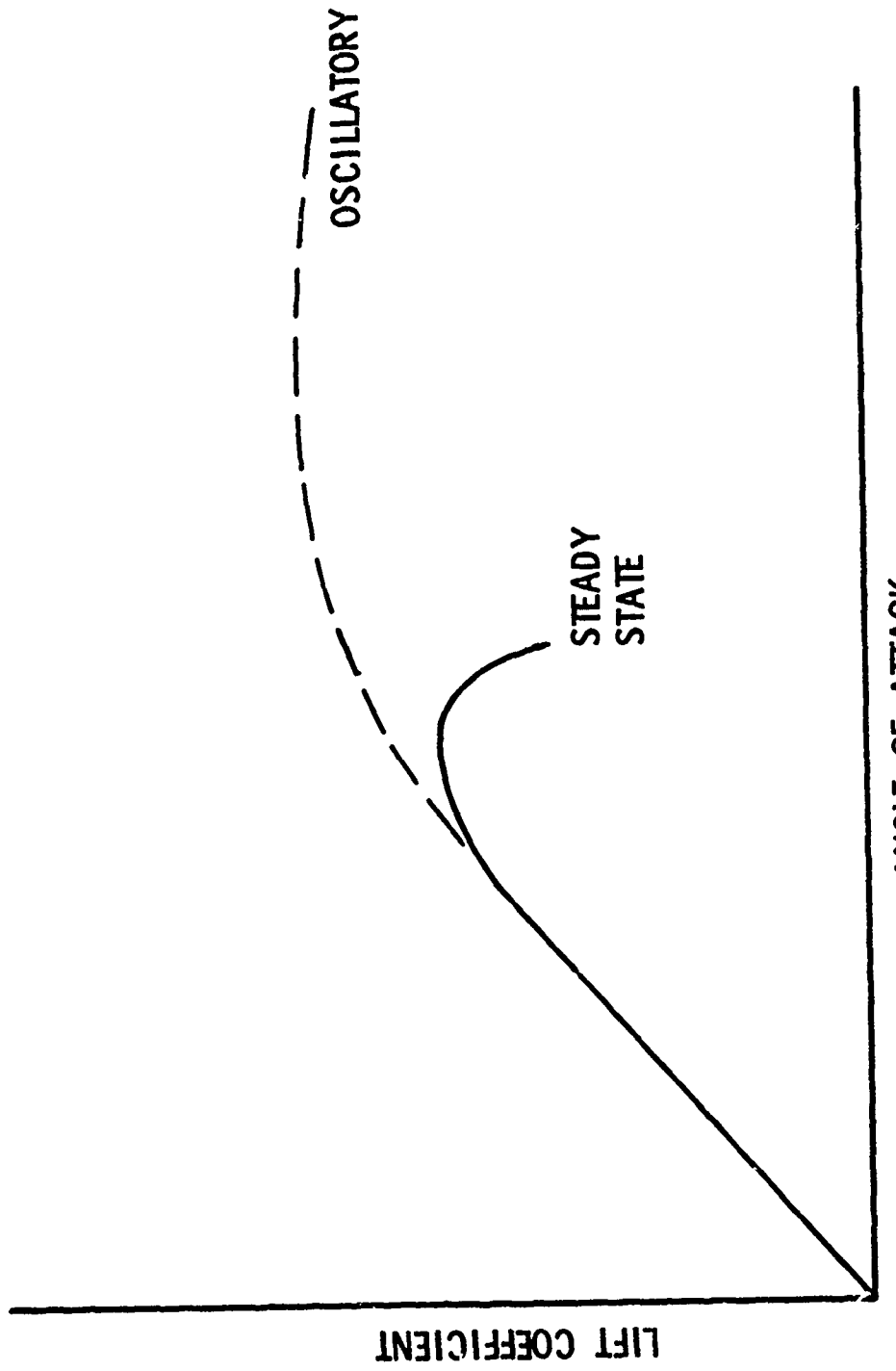

Figure 19. Effect of Unsteady Flow on Lift Coefficient

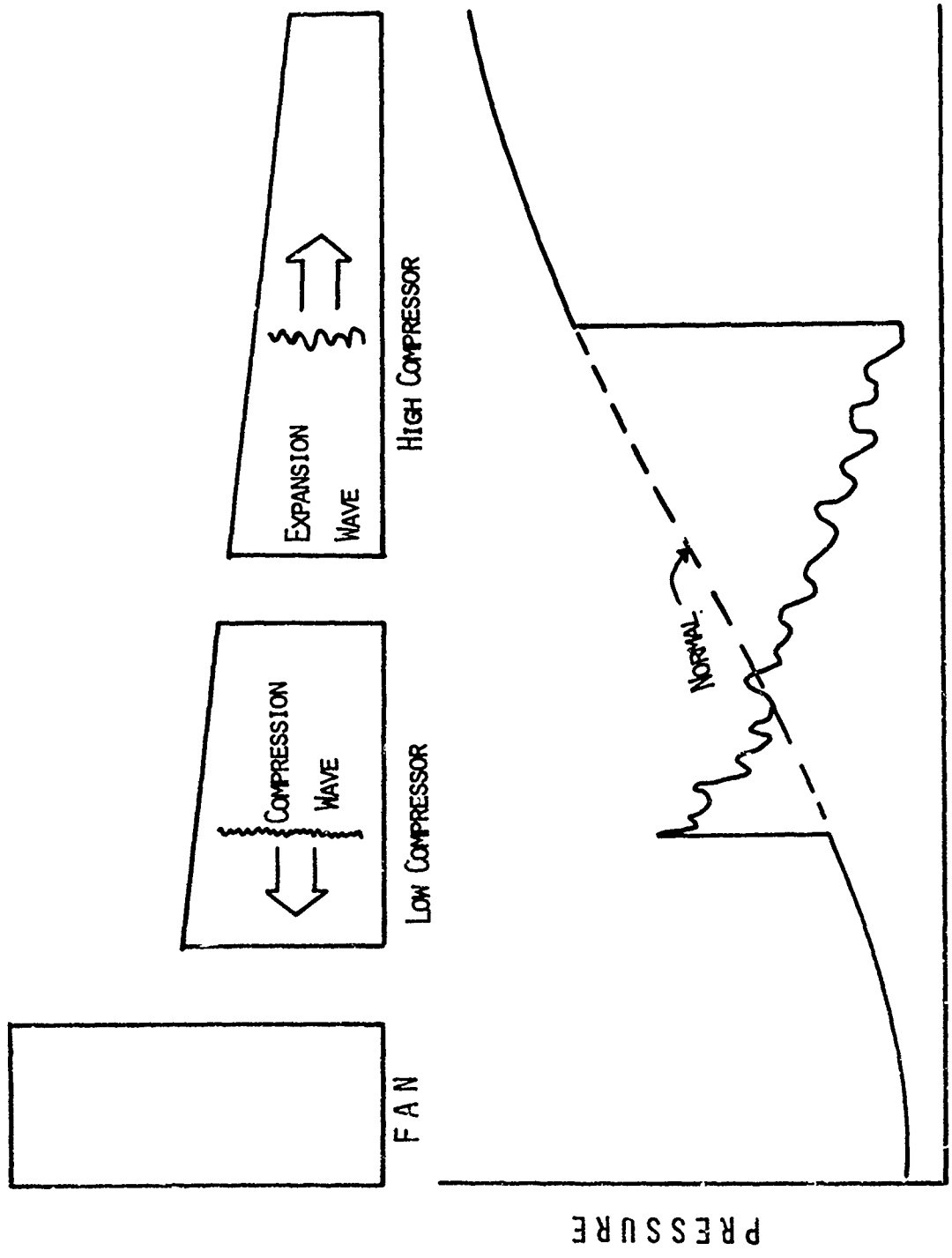

Figure 20. Surge Phenomenon

any entering perturbation is felt as an oscillating disturbance. For such a condition the lift curve is similar to the dashed line in Figure 19. The important difference between the steady and unsteady curves is the absence of a well-defined stall point on the unsteady curve. It is this feature that makes it difficult to predict the onset of rotating stall.

Regardless of the initiating mechanism, the rotating stall cell continues to rotate and, if the triggering disturbance is severe enough, to grow in both magnitude and circumferential extent. Eventually, the flow will break down completely in the stage, triggering what is referred to as surge. The flow regime just after the onset of surge in a compression system is shown in Figure 20. The stage that was in rotating stall and triggered the surge was in the vicinity of the low compressor discharge. When the surge occurred, it triggered a compression wave and an expansion wave, which are seen traveling through the system. We note the peculiar pressure pattern of a compression-expansion system at the bottom of the figure. This gradient occurs in conjunction with large flow changes throughout the entire engine, which can lead to complete flow reversal. This change in flow can cause flameout and structural damage to the blades.

Surge in terms of measurable quantities is shown in Figure 21. A total pressure probe at the high compressor discharge plane shows a large oscillation in pressure (about 75% of the face average) occurring over a period of approximately 0.1 sec. The oscillatory nature is caused by the reflection of the waves.

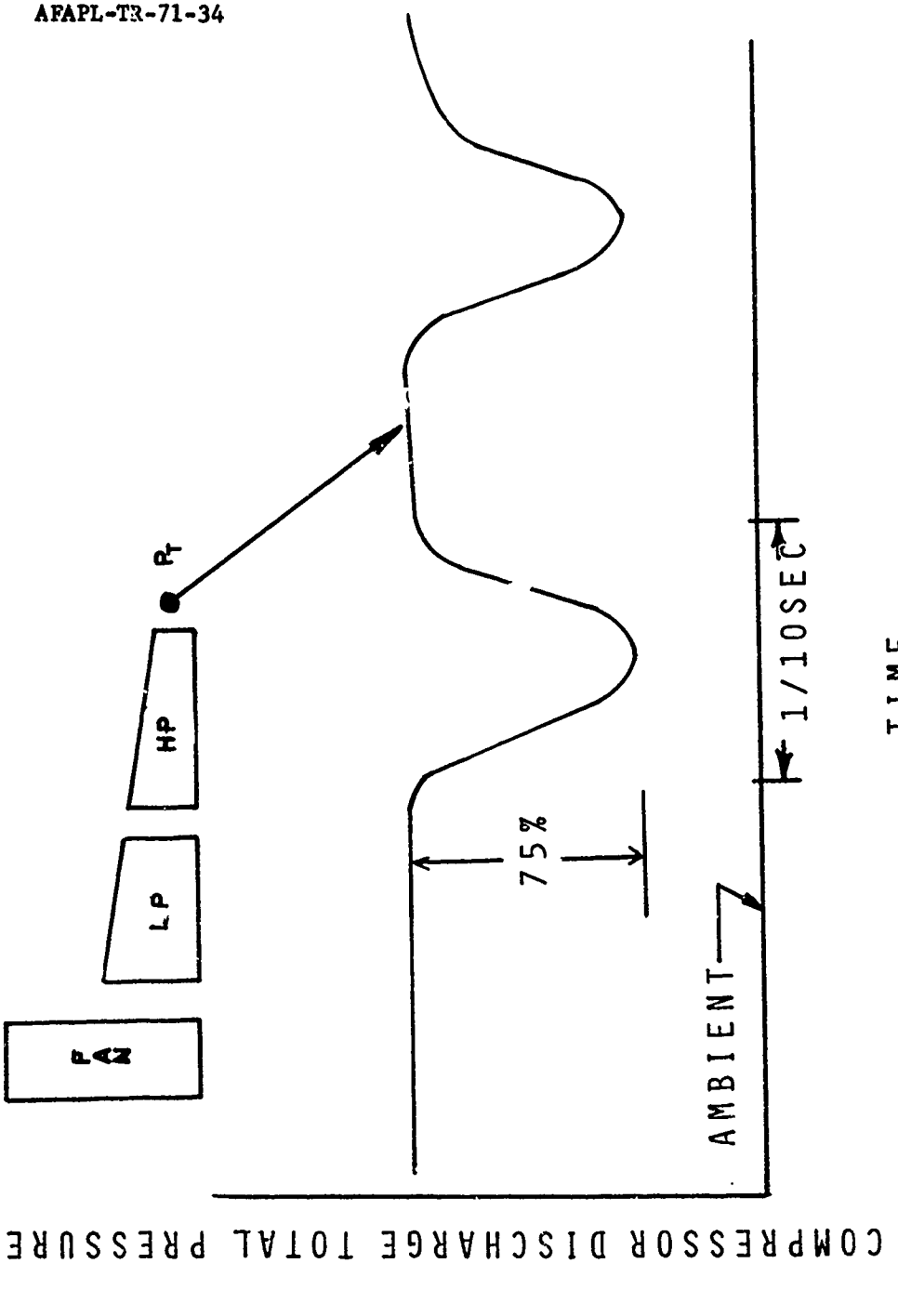

Figure 21. Surge at Compressor Discharge

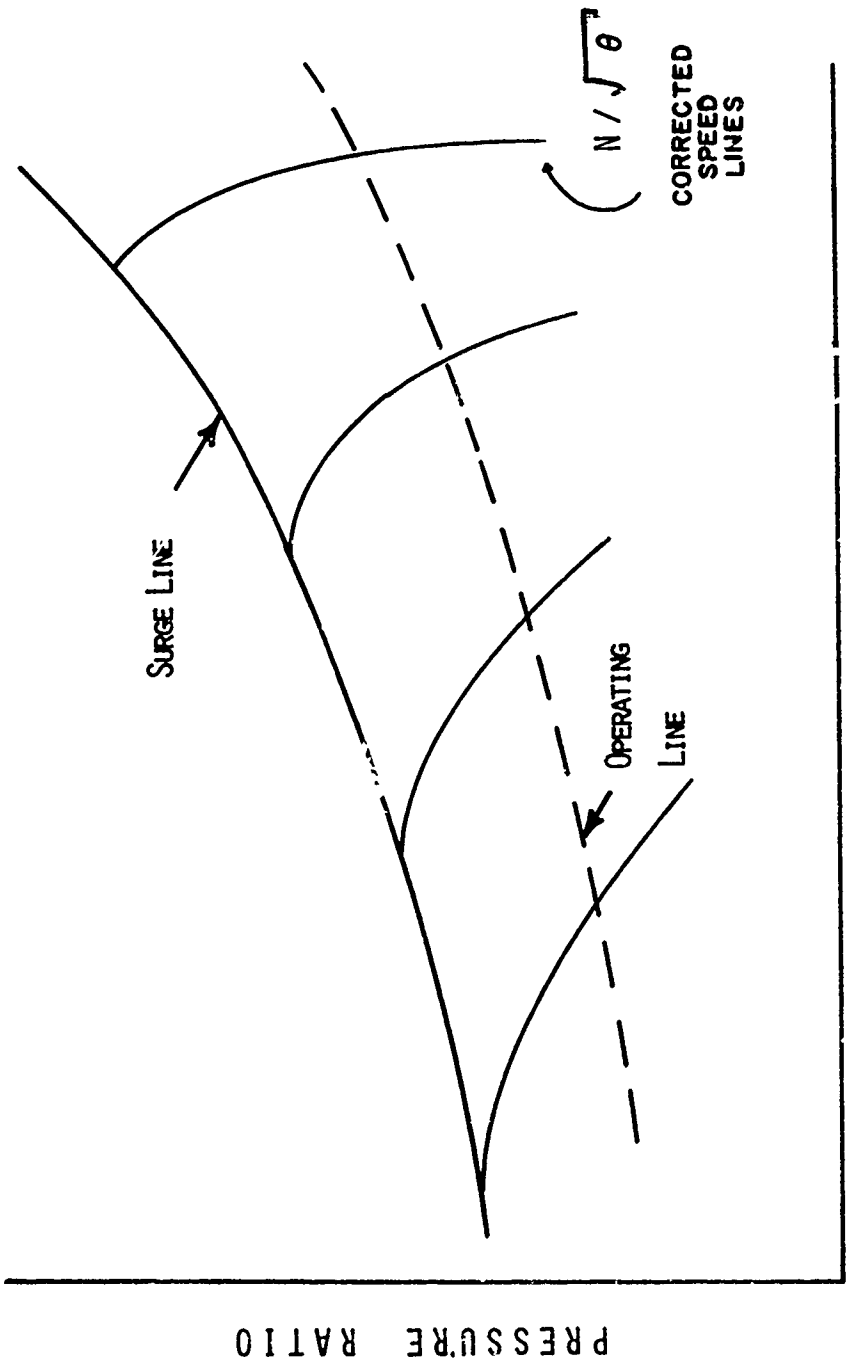

Figure 22. Stable Operation Compressor Map

STABILITY MARGIN

The surge condition defines an envelope for compressor operation. A typical compressor map is shown in Figure 22. Under normal conditions, the compressor is matched to the rest of the engine in such a manner as to be operating along the dashed line. Although certain engine transients can cause the compressor to operate at a point below the normal operating line, such movement is not critical to stability as long as air is delivered to the burner at high enough pressure to support combustion. Motion on the map above normal operating line is another matter. As the operating point moves toward the surge line, rotating stall cells begin to appear which do not interfere with engine operation. In many engines, rotating stall in one stage or another is a continual occurrence. Eventually, if the operating point reaches the surge line, the destabilizing events previously described will occur.

Unfortunately this compressor map does not tell the complete story with respect to inlet-engine compatibility. By looking at Figure 23, the other effects can be observed. Due to the causes shown, the normal surge line and the normal operating line are moved toward each other. Hence it is possible to be operating below the nominal surge line, and suddenly experience surge due to a decay in the surge line caused by an increase in distortion. In other words, the surge event occurred because the stability margin indicated on the figure becomes "negative." Hence the entire problem of engine-inlet compatibility can be expressed with Figure 23 and the statement: "compatibility means maintaining a positive stability margin throughout the aircraft's flight regime."

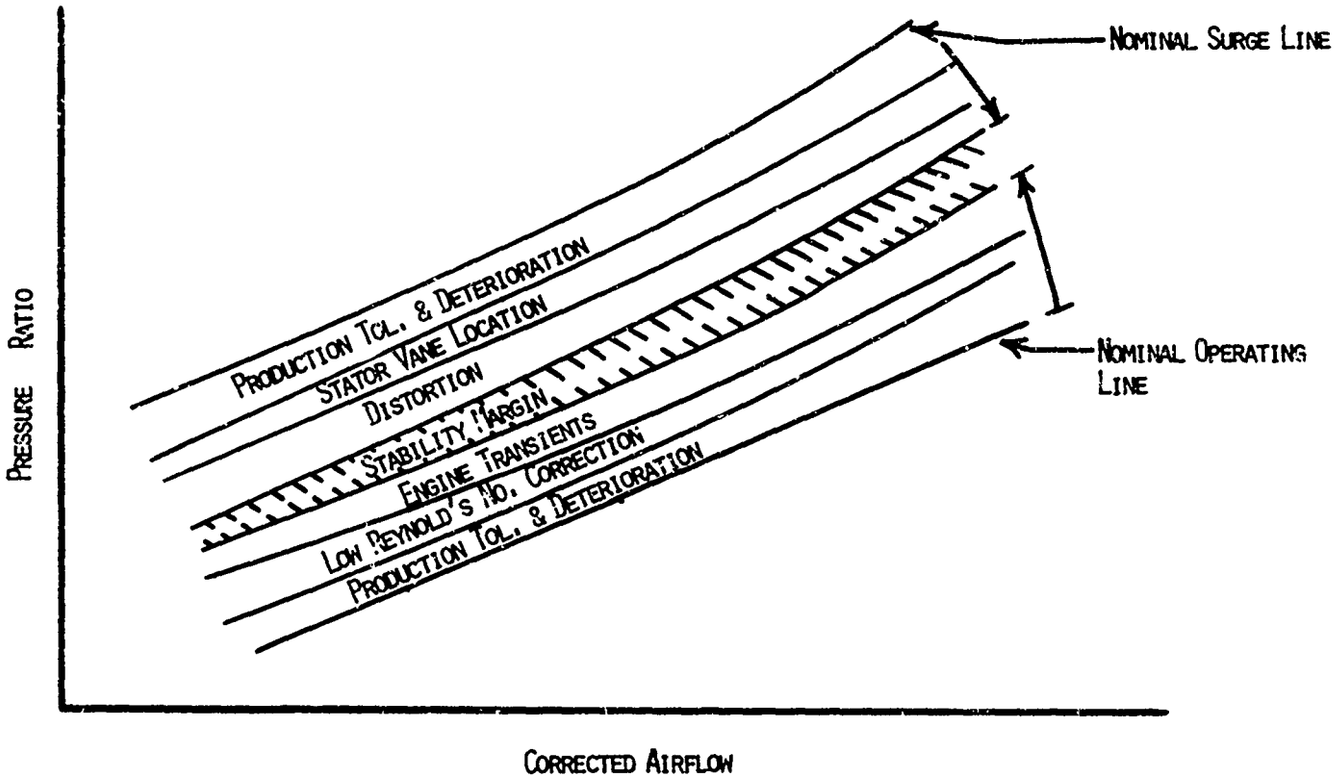

Figure 23. Compressor Surge Margin Allocation

INLET FLOW DISTORTION

Inlet distortion is only one of many destabilizing effects on an engine. For a considerable period of time there has been discussion concerning the best physical properties to use to describe the phenomenon. Various flow fields in an inlet can be attributed to vorticity, and, while some attempts have been made to correlate engine tolerance to such flow properties, they generally fall short of the solution. Additionally, they are difficult parameters to measure in the hostile environment of an engine-inlet interface under flight conditions. The present solution is to use the variation in total pressure to describe the flow field. This approach has two immediate results. The first is that by Crocco's Theorem, vorticity is reflected in the total pressure change. The second is that total pressure is relatively easy to measure. Using total pressure, a distorted flow field can be represented by areas having pressures above and below the face average. This is illustrated in Figure 24.

The effect of distortion on the engine can be described one way by observing that a portion of the compressor inside a low pressure zone is actually experiencing a higher operating pressure ratio than the compressor as a whole. Since both the entire compressor and the section operating at the high pressure ratio are rotating at the same speed, it can be seen on Figure 25 that the operating point of a portion of the compressor is moving up the speed line toward the surge line. This type of reasoning is sometimes referred to as the parallel compressor theory.

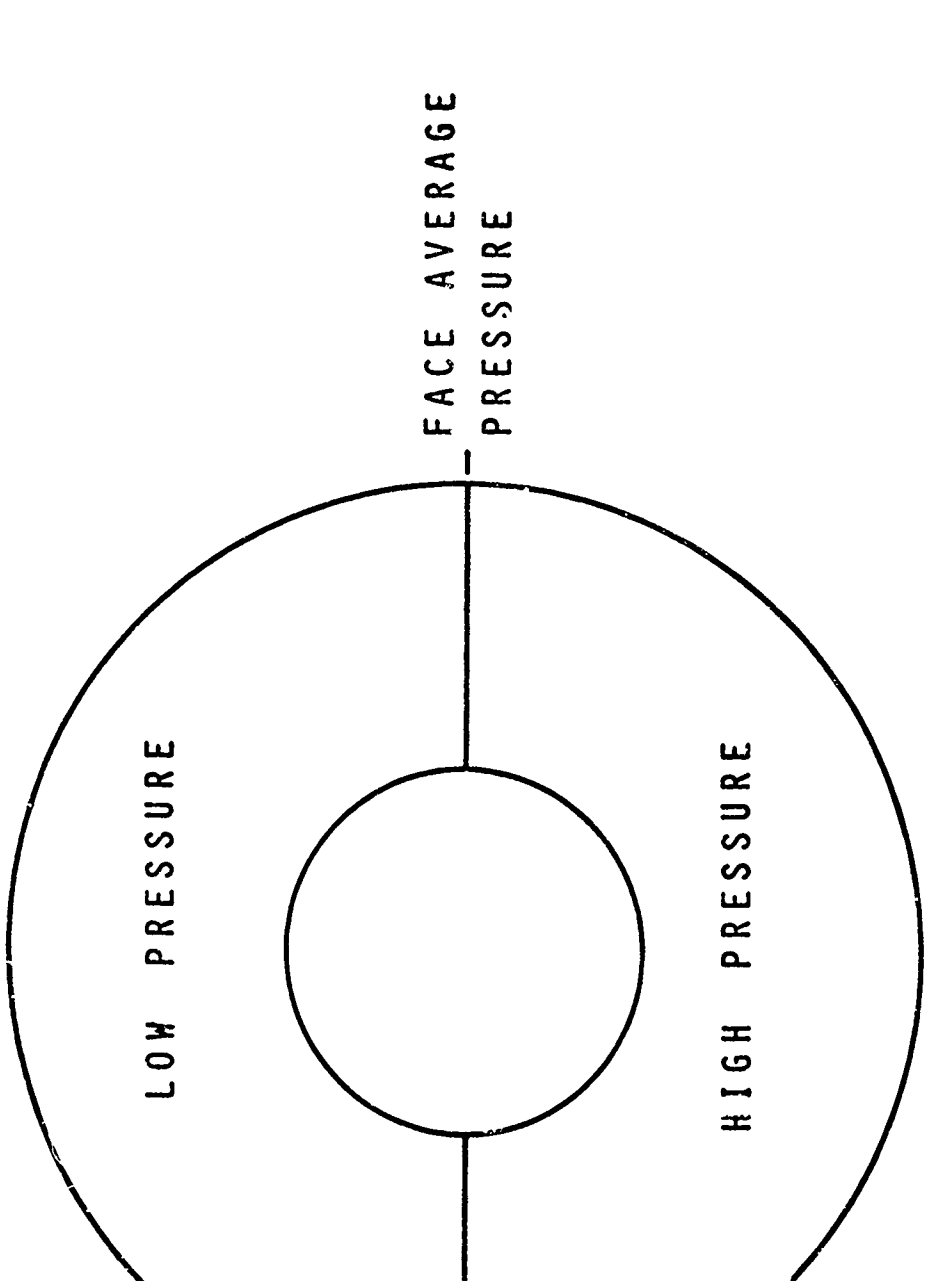

Figure 24. Total Pressure Pattern

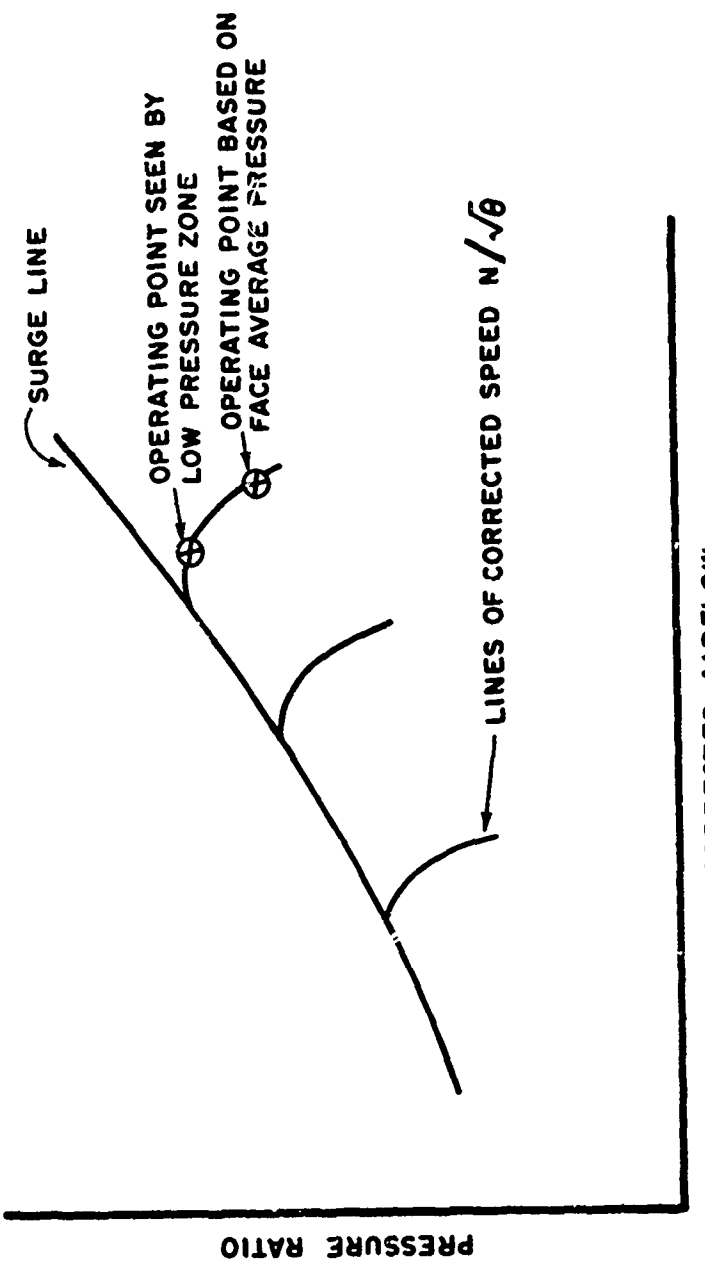

Figure 25. The Engine's View of Distortion

In flight, inlet distortion turns out to be a dynamic condition. This is partly due to the fact that the air entering the inlet is not uniform, but is due more importantly to events occurring inside the inlet. Figure 26 shows a typical supersonic inlet with its characteristic oblique shock structure followed by a normal "Lambda" shock near the inlet throat. The distortion is measured by a total pressure transducer at the end of the inlet duct. We note that the transducer is measuring a random and rapid variation in pressure. This is due to vorticity generated at the inlet's external lip, as well as shock-boundary layer interactions. Changes in flight condition can cause changes in the shock structure. The pressure fluctuations get stronger if the lambda shock moves inward toward the engine, and inlet unstart or "buzz" causes disturbances when the shock moves upstream.

Simulating distortion in isolated engine testing has evolved considerably in recent years. Perhaps the largest stride made was the discovery that a compression element has a critical period: disturbances lasting longer than a certain time span are felt as steady-state perturbations, while those which exist for shorter periods of time are essentially not felt. This is the crucial point in the understanding of time-variant distortion and its effect on the engine. In reality the cutoff is not quite that severe, which will be explained in a later section.

The immediate result, for engine testing purposes, is that the time-variant situation in the inlet can be simulated by steady-state distortion patterns. This is true if the steady-state pattern represents the highest distortion level measured which lasted at least as long as the

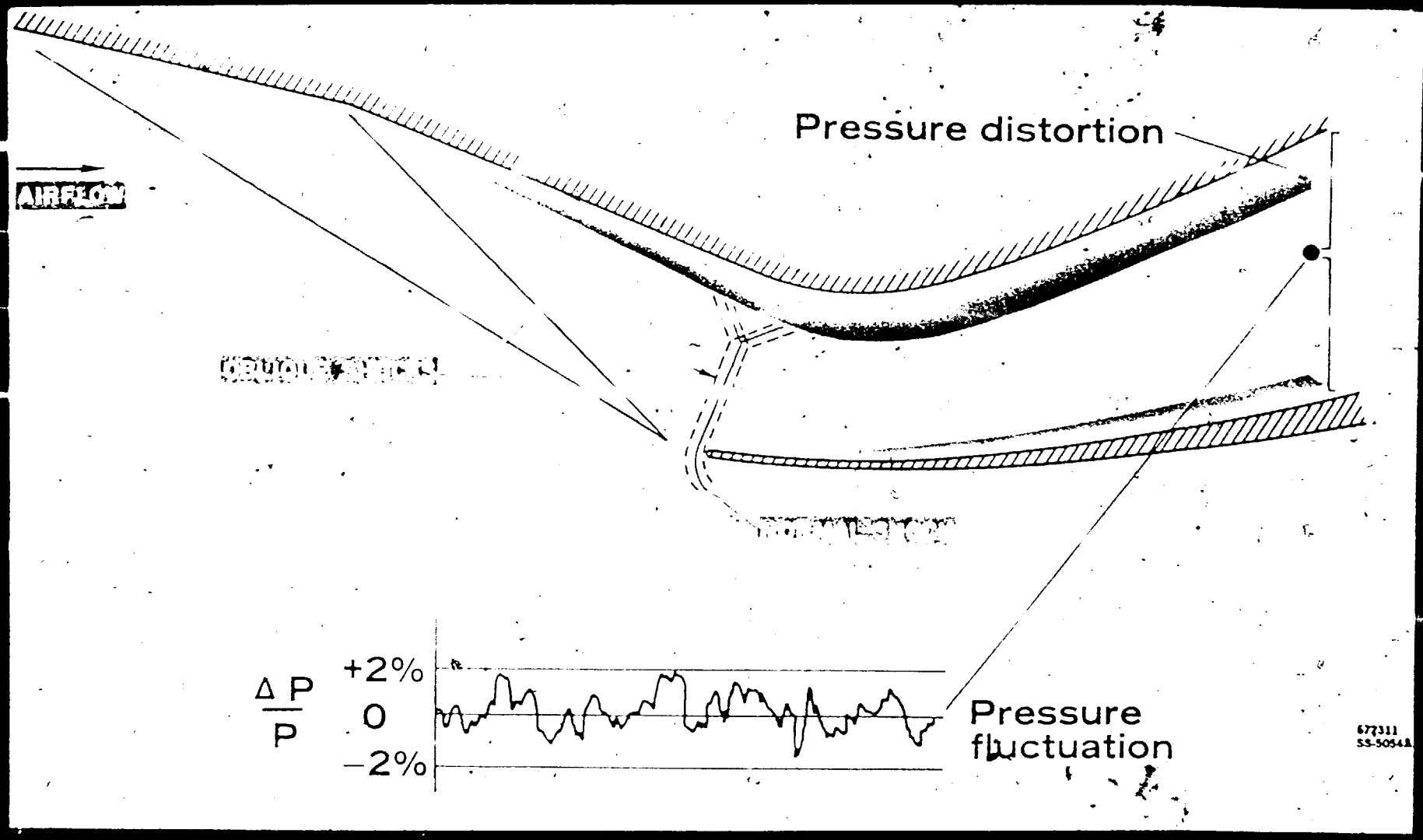

Figure 26. Typical Supersonic Inlet Flow Conditions

critical timespan for the compressor. The most common method of doing this is by using a screen; a typical one is shown in Figure 27. By varying the mesh size and position, it is possible to obtain different total pressure losses over portions of the flow field.

ANATOMY OF A SURGE

Now that we have discussed the theory, let us try to apply it in the analysis of actual data from a complete dual spool compression system test. Distortion has been described as variation in pressure, with space and time --- and with the standard compatibility instrumentation of about forty high-response pressure transducers, the amount of data obtained becomes almost instantly insurmountable. To alleviate this condition, a "distortion factor" is employed.

A distortion factor is the result of some mathematical operations on a set of pressure readings, which accounts for at least some of the following qualities: depth of the pressure variation across the compressor or fan, pressure gradient, shape of the low pressure zone, radial location of the low zone, and circumferential extent of the distortion. The final format of the factor is empirical, since it is correlated with basic screen tests. For our purposes here, the exact form of the distortion factor is immaterial (we will assume those whose job it is to correlate have correlated properly).

In Figure 28 we see the result of pressure readings taken at forty probes (once each four-thousandths of a second) and converted to a distortion factor. Therefore each point on the trace represents a particular distortion pattern that was present during one of the readings.

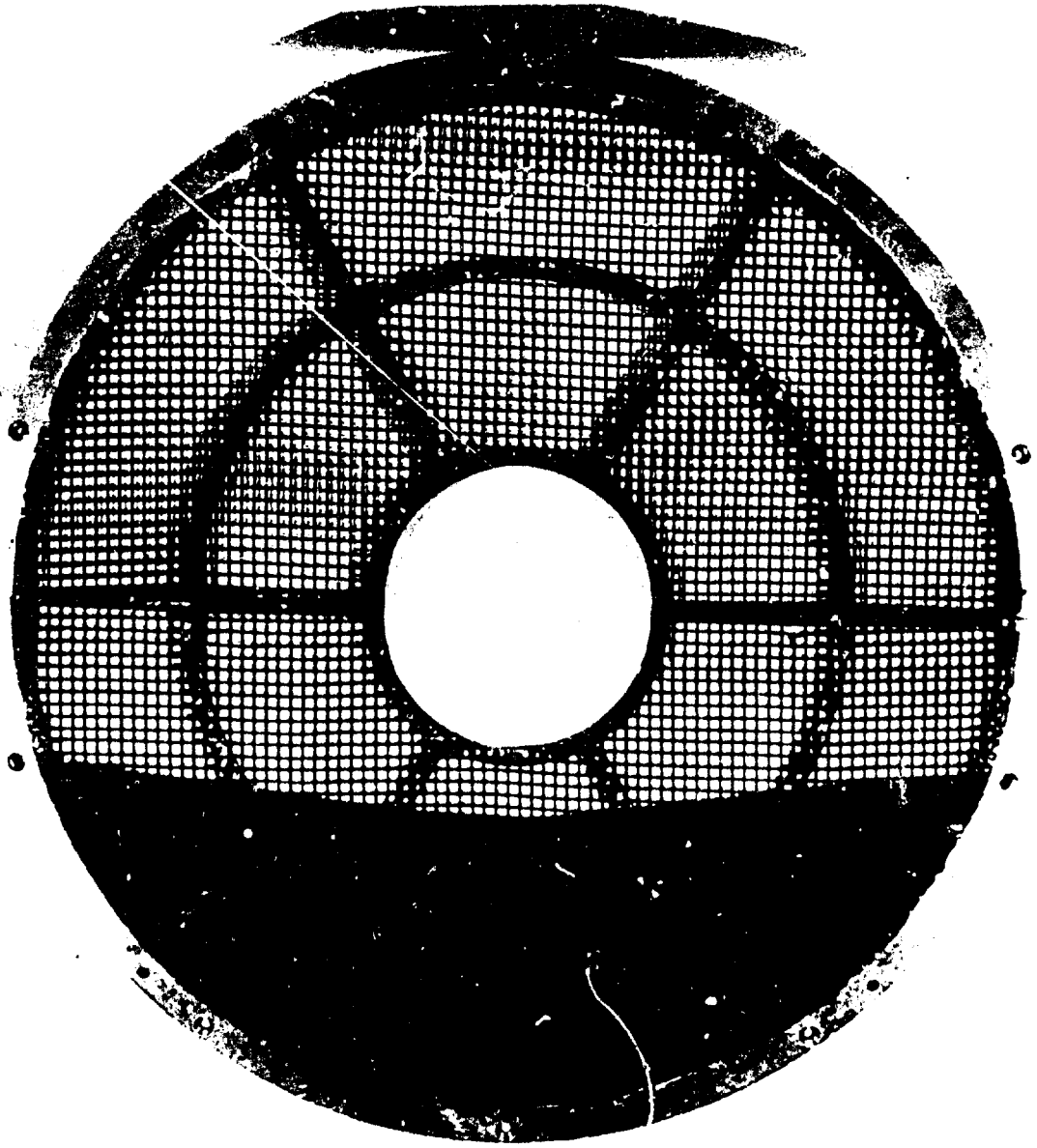

Figure 27. Typical Distortion Screen

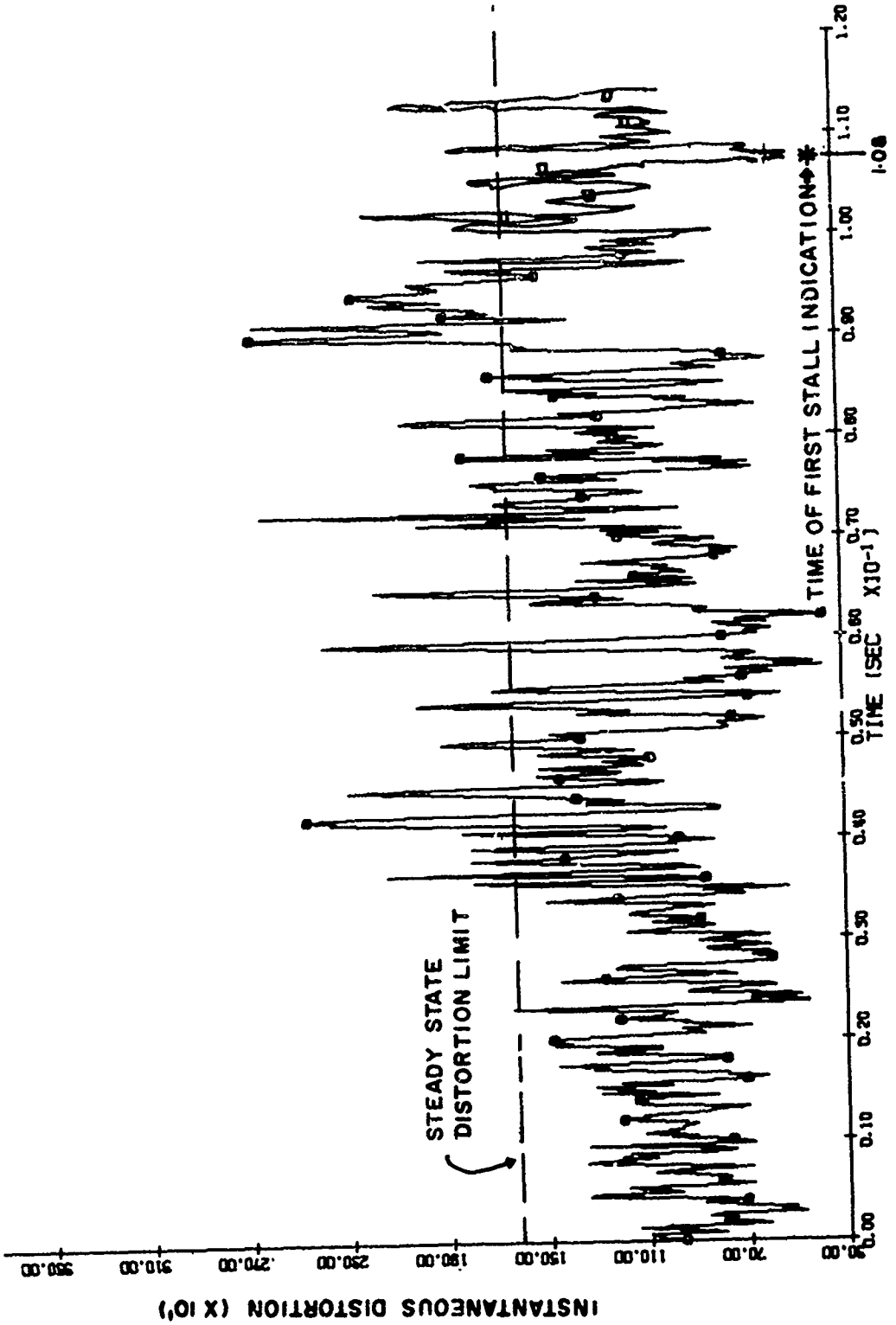

Figure 28. Correlation of Stall with Distortion Pattern (Instantaneous)

The higher the factor the more severe the distortion. The dashed line indicates the limit of stall-free operation under distorted conditions, as obtained from previously conducted screen tests. The limit is commonly referred to as the steady-state distortion limit, since distortion generated by a screen is basically constant with time. This particular test was run in a dual-spool rig, which fully simulates, dynamically, the compression system in flight.

The most striking feature of this trace is that there are several distortion patterns for which the factor is larger than the steady-state distortion limit occurring before the indicated surge, some 0.108 seconds into the run. It was this sort of situation that caused a great deal of "soul-searching" in the compatibility field. There had to be something missing in the correlation of steady-state distortion limits with the normal dynamic disturbances experienced in flight. As it turns out, the missing link is exposure time, or the "critical time" discussed earlier.

If it is hypothesized that the length of time a pattern exists is important --- that is, there is some time that the pattern must exist to affect the engine --- then we should be able to adjust the data to determine an approximation of the critical time. A method of doing this is to time-average the data so as to see the average levels felt during a series of small overlapping periods. The first attempt is to do a running time average for periods of 1 msec, and the resultant plot is shown in Figure 29. We note that the curve is more regular, and there are about ten peaks above the steady-state distortion limit prior to stall.

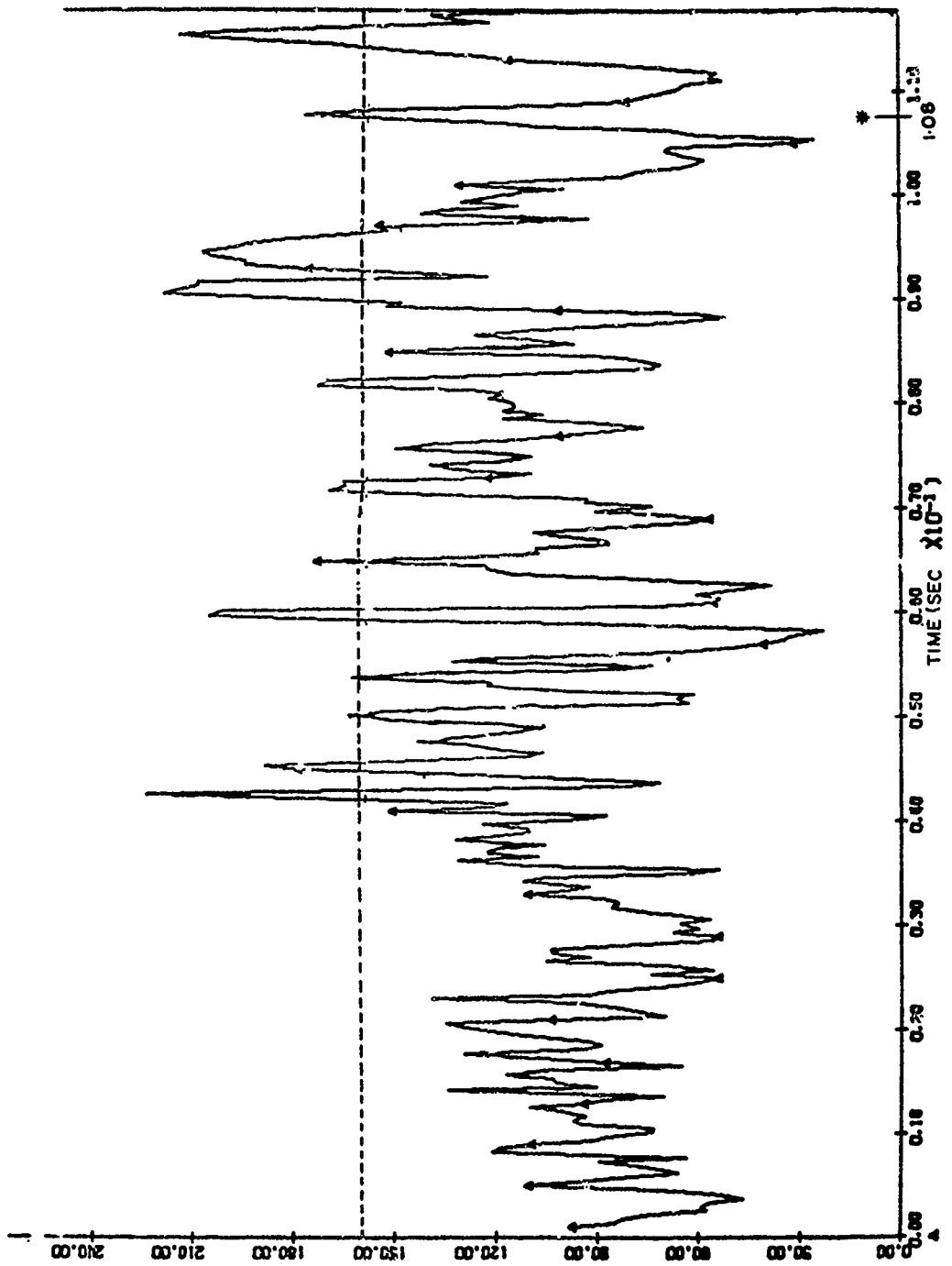

Figure 29. Correlation of Stall with Distortion Pattern (1 MSec)

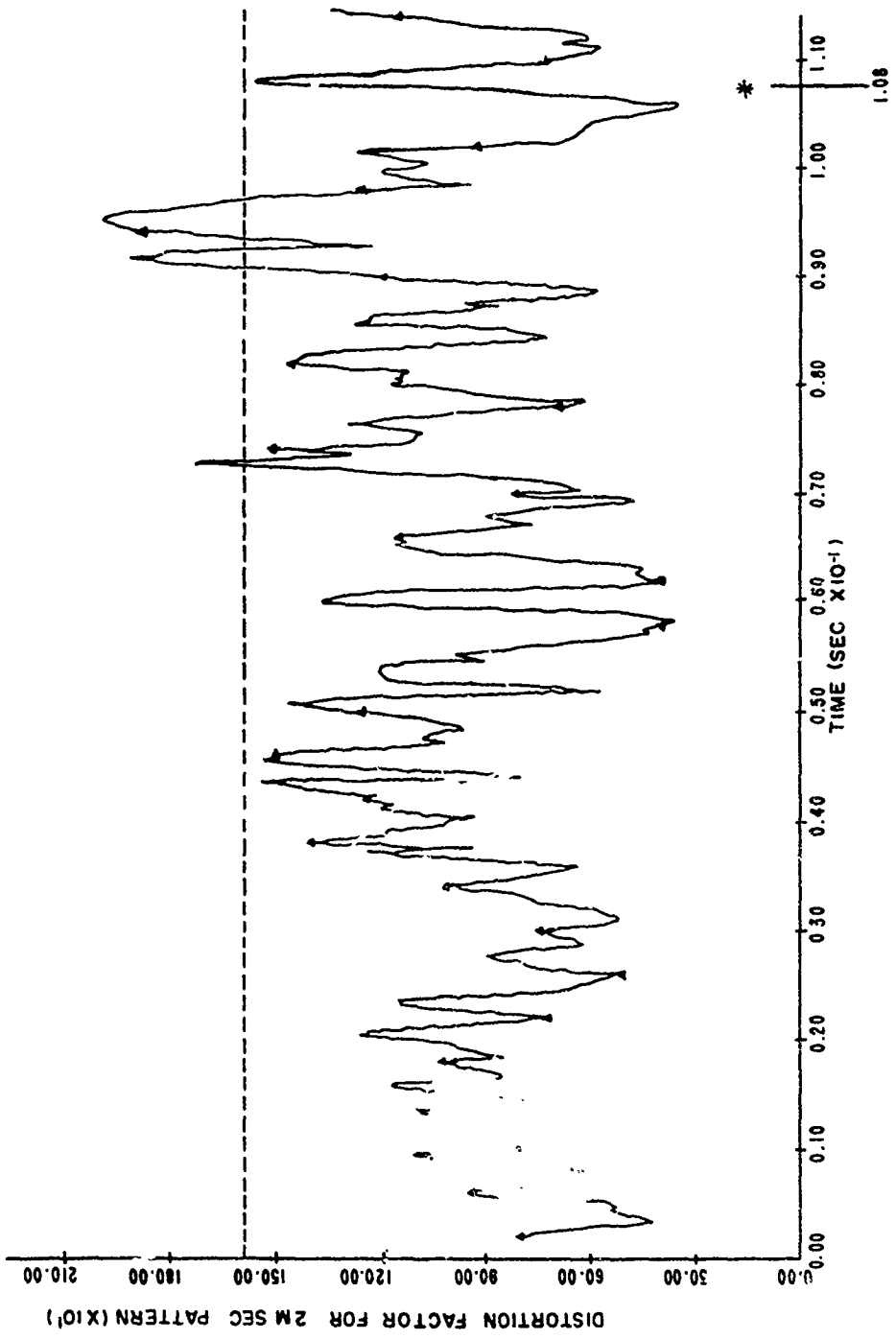

Figure 30. Correlation of Stall with Distortion Pattern (2 MSec)

If we increase the period for the running average to 2 msec, we obtain the curve in Figure 30. Note that the smoothing effect is continuing and that there are fewer peaks. We seem to be on the right track. Figure 31 indicates the result of a 3 msec average, and now there is only one large peak prior to the onset of surge. Figure 32 represents the 6 msec average, which shows the same kind of picture. We note the peak is occurring about 12 msec prior to surge, and the distortion pattern has about the same severity as the steady-state limit.

The conclusions to be drawn are that the distortion pattern causing the surge occurred about 12 msec before the surge, and that the critical time of existence of the pattern is greater than 3 msec. For this particular engine in this specific test, 6 msec is the time it takes to accomplish one revolution of the compressor. Therefore, it can be said: "Steady-state to this particular compressor is anything lasting as long as one revolution." Smaller periods are generally used, to be on the safe side. It is assumed in this analysis that the transport velocity within the engine is essentially equal to the inlet axial velocity.

The next question to answer is why there is a 12 msec delay between the detection of the distortion pattern causing surge, which is measured in front of the fan stage, and the indication of surge behind the last compressor stage. Intuition tells us that at least some of that time can be attributed to the convective transport of the disturbance downstream. The time line at the bottom of Figure 33 indicates the time it takes for a disturbance to travel from the instrumentation plane at station 2 to any point in the compression system. Based on experimental data, it has been determined that at the flight condition simulated in

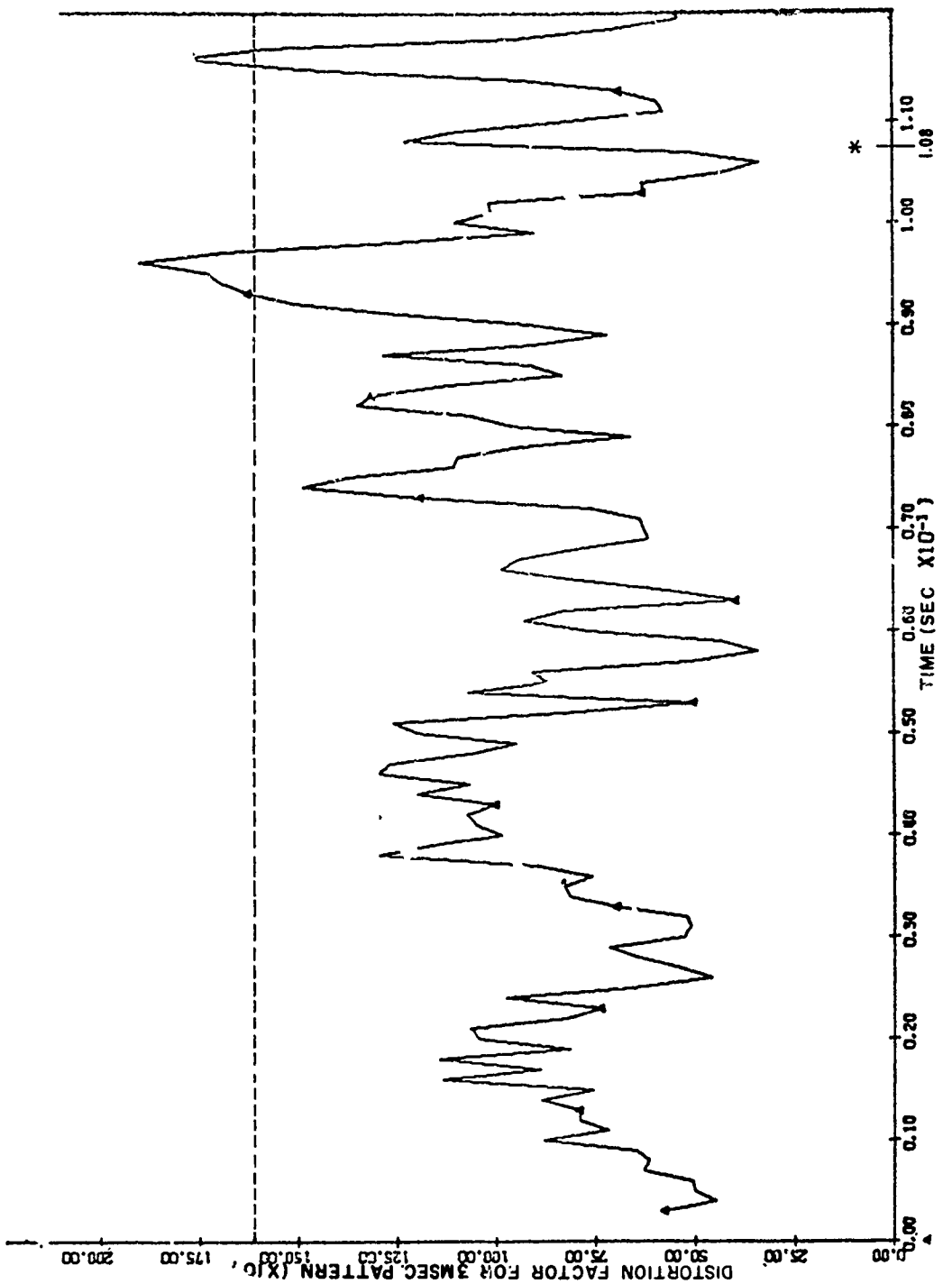

Figure 31. Correlation of Stall with Distortion Pattern (3 MSec)

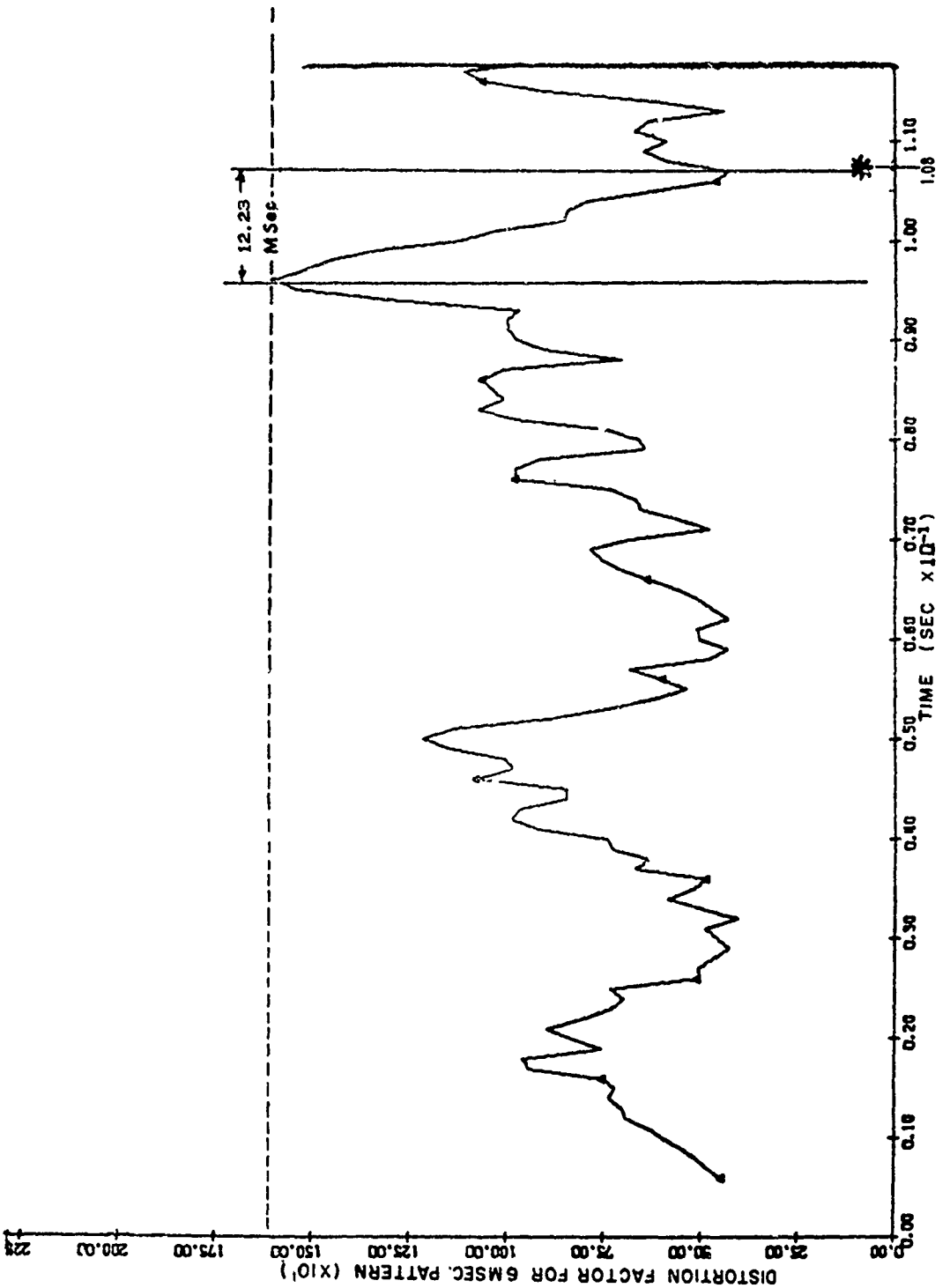

Figure 32. Correlation of Stall with Distortion Pattern (6 MSec)

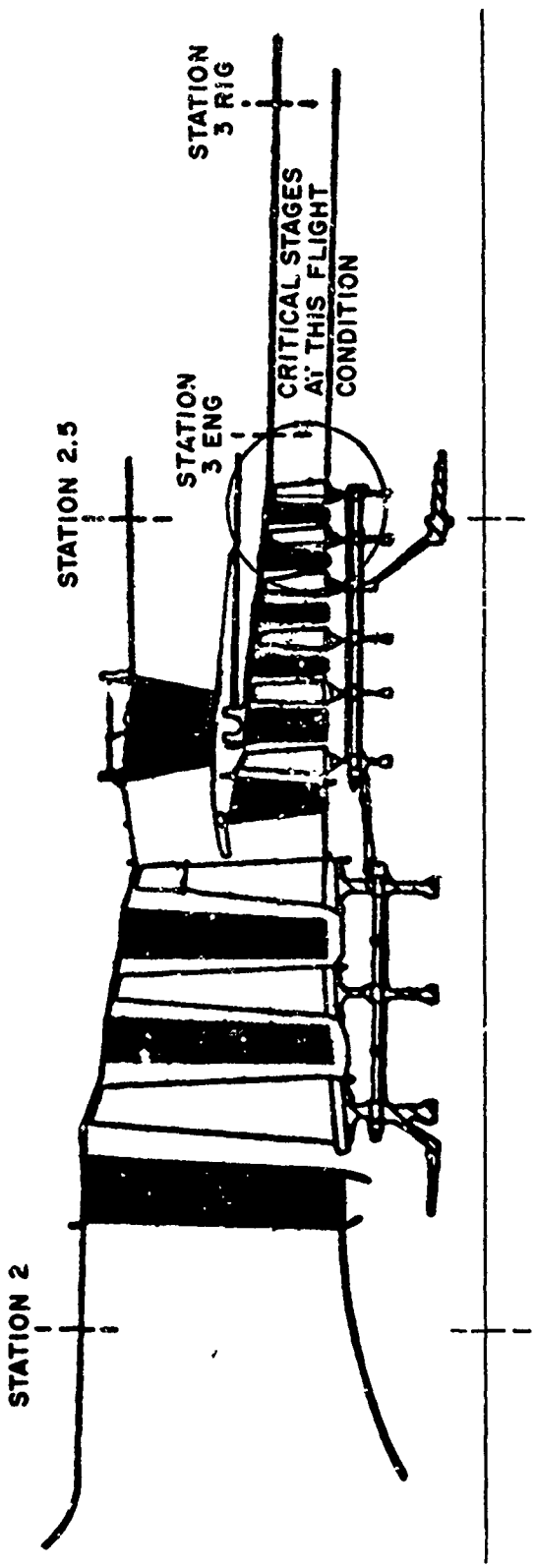

Figure 33. Distortion Transport Time

this test, the last stages of the high pressure compressor tend towards rotating stall. Hence from our time line, we see that about 6 msec of the total 12 msec delay were used up by the transport of the distortion pattern from station 2 where it was detected, to the vicinity of station 3, where it could trigger the surge. The question which remains is the explanation of the other 6 or 7 msec of the delay.

To understand what happened during the interval, let us take another look at the phenomenon of rotating stall, shown in Figure 34. We note once more the rapid, relatively small drops in total pressure. In the test being considered, the instrumentation at station 3 consisted of three pressure transducers, one each on rakes located at 45, 81, and 225° from the top reference line of the system. This is illustrated at the bottom of Figure 34. The pressure traces that were recorded are shown above the instrumentation diagram. We note that the traces seem to have three distinct regimes. The first is composed of extremely rapid, random, and small variations in pressure. The second region, located between the shaded areas, contain a few dips which occur rapidly but are of larger magnitude than those which preceded them. Following the gradual drop-off at the end of the second region, the traces seem to move into a third phase of very large and slow pressure oscillations. Recalling our earlier comments about rotating stall, it would appear that that is the explanation of the middle region of the traces. The first section appears to be normal inlet "noise."

The first significant dip in total pressure within the second region occurs at the 45° probe, and is succeeded by a similar but slightly larger dip of the 81° probe. Another dip (even larger in magnitude)

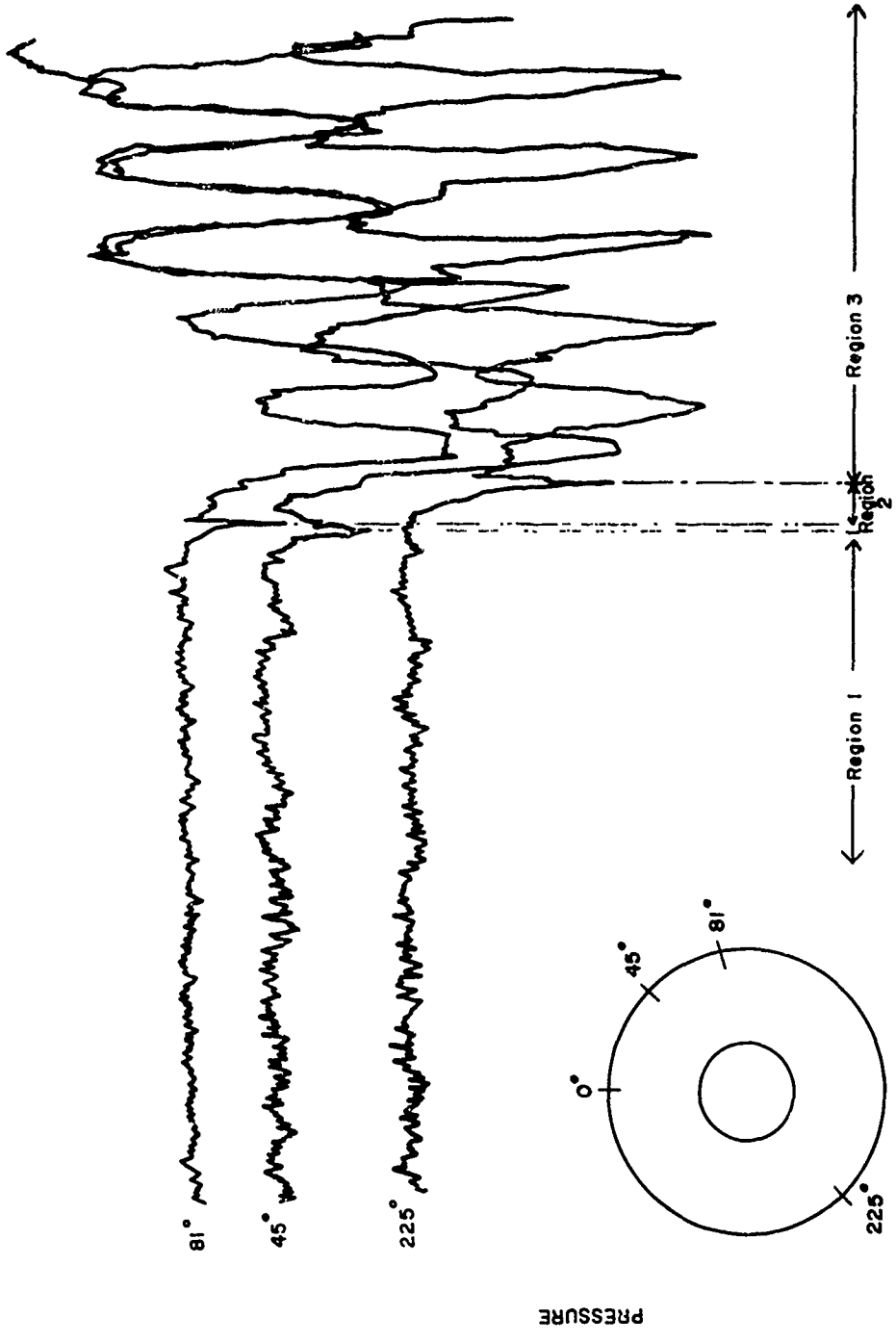

Figure 34. Probe Data Station 3

is felt sometime later in the second region at the 225° probe. Very shortly thereafter, the total pressures at all three probes decay, signalling the onset of the third regime.

The pressure dips in the second area are not cyclical enough to make it that obvious, but the last compressor stage appears to be in rotating stall. This can be seen in Figure 35, where we have taken the time interval from the end of the transport time to the dip at a particular probe at station 3, and plotted it against the circumferential location of the probe. We note that it would appear that we are seeing a low pressure zone that is rotating at a constant speed (about 14 msec per revolution) past the three pressure probes, and growing all the time. This is a pretty fair definition of rotating stall. As the stall cell rotates, it grows, and sometime close to its last sighting at the 225° position, all three probes tail off. This common drop signifies complete flow breakdown; our definition of surge. The third regime is just the reflection of expansion and compression waves discussed previously.

It appears, then, that it took about 6 msec for the rotating stall cell to grow sufficiently large to trigger surge. Within experimental accuracy we seem to have explained the lag time, ignoring as inconsequential the transport time of the stall wave from the stalled stage to the instrument plane. As shown in Figure 36, there is a lag between the time the surge-causing distortion is sensed at the fan inlet plane and the onset of surge, and this lag is composed of transport time, as well as stall cell growth and rotation time.

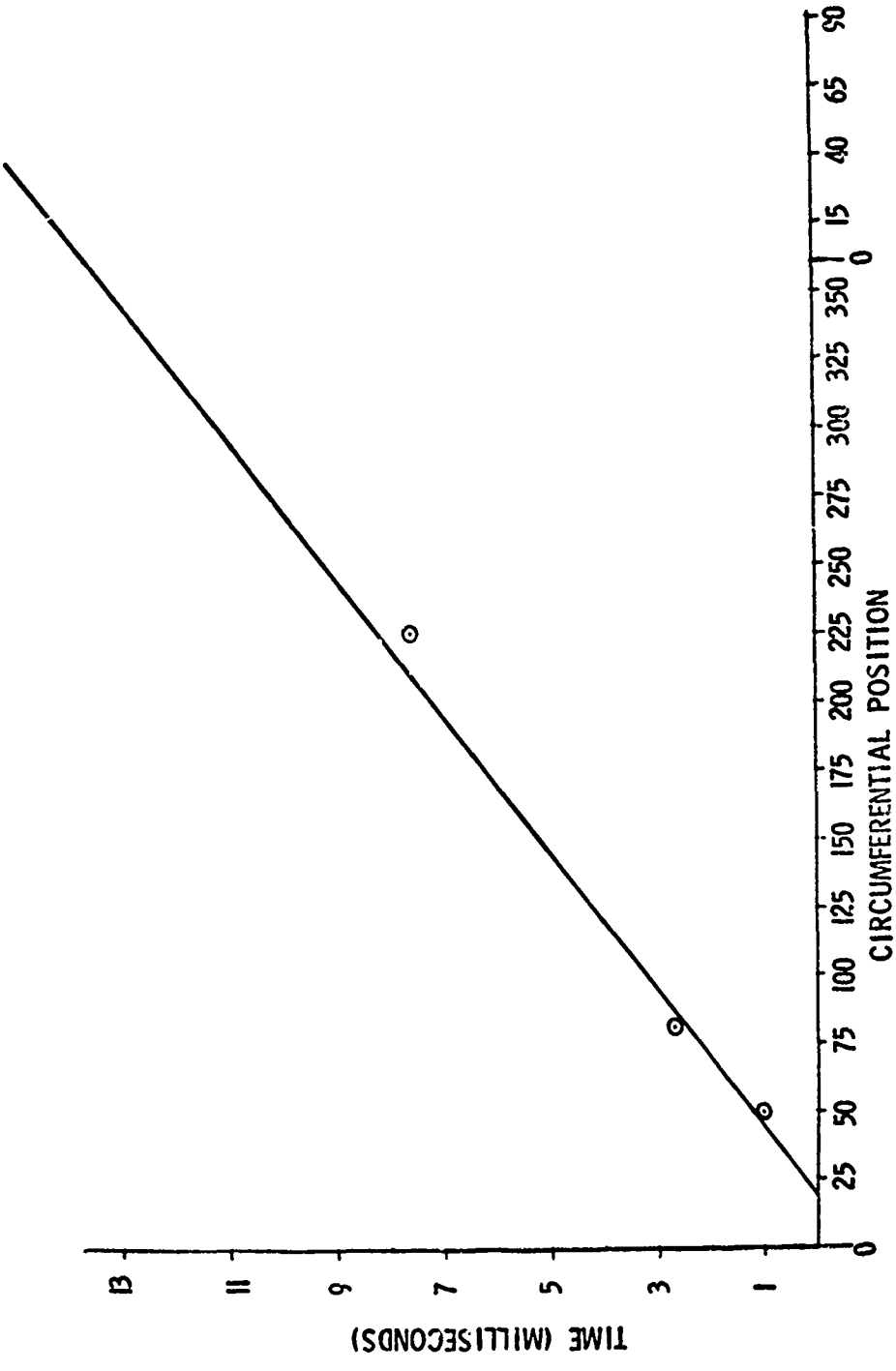

Figure 35. Growth Cell Rotation Rate

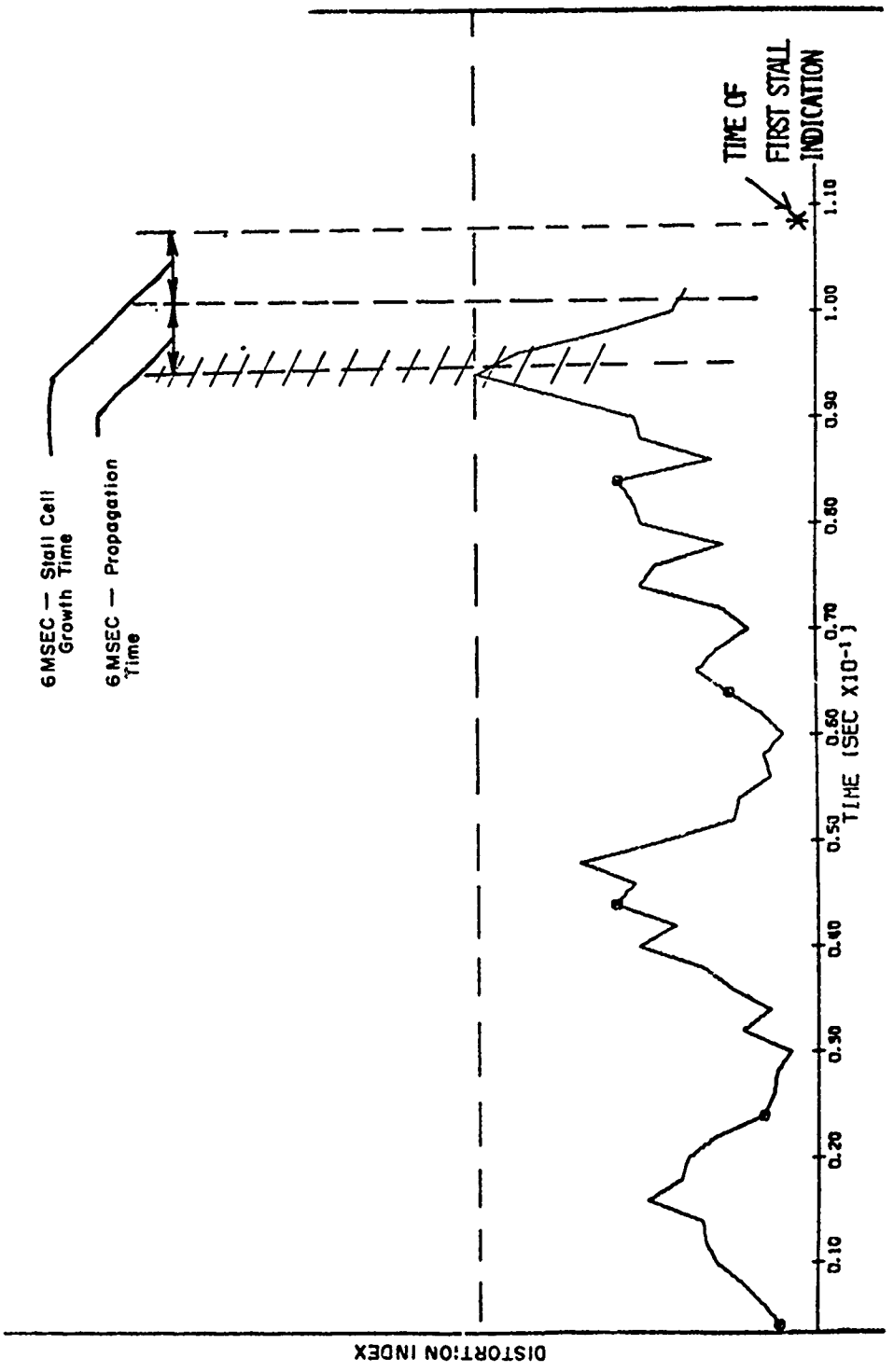

Figure 36. Correlation of Stall with Distortion Pattern

COMPONENT INTERACTIONS

Thus far we have considered only the effect of the distortion pattern on the compressor system as a whole. Actually the effect of distortion on a fan or a compressor (and vice versa) is important and has been investigated. Indeed, the dynamic interactions within a stage (and even across a blade row) is in the early stages of investigation and may prove important to the understanding of the compatibility design problem.

Aside from surging a component, a distorted flow pattern can have other effects. In Figure 37 there is a typical fan map, with the circle as the normal operating point. If distortion is imposed on this fan, the surge line drops down to the dashed line since some of the component's stability margin has been used. Likewise, the distortion has caused flow blockage due to the retarded flow, and a drop in pressure ratio due to efficiency shift, causing the operating point to shift to the square. All these effects must be considered during design.

Additionally, the component affects the distortion pattern as it passes through. In Figure 38 we see a graphical representation of the distortion pattern entering a fan. The numbered isobars refer to a relationship between the pressures on the isobar and the fan average total pressure; e.g., the 1.04 isobar connects points with pressures 4 percent above fan average. The pattern is basically circumferential since this is the general direction of the pressure gradients. The lowest pressure is in a small region at a position of about 9 o'clock, about 8% below the face average. In Figure 39, we see the pattern at

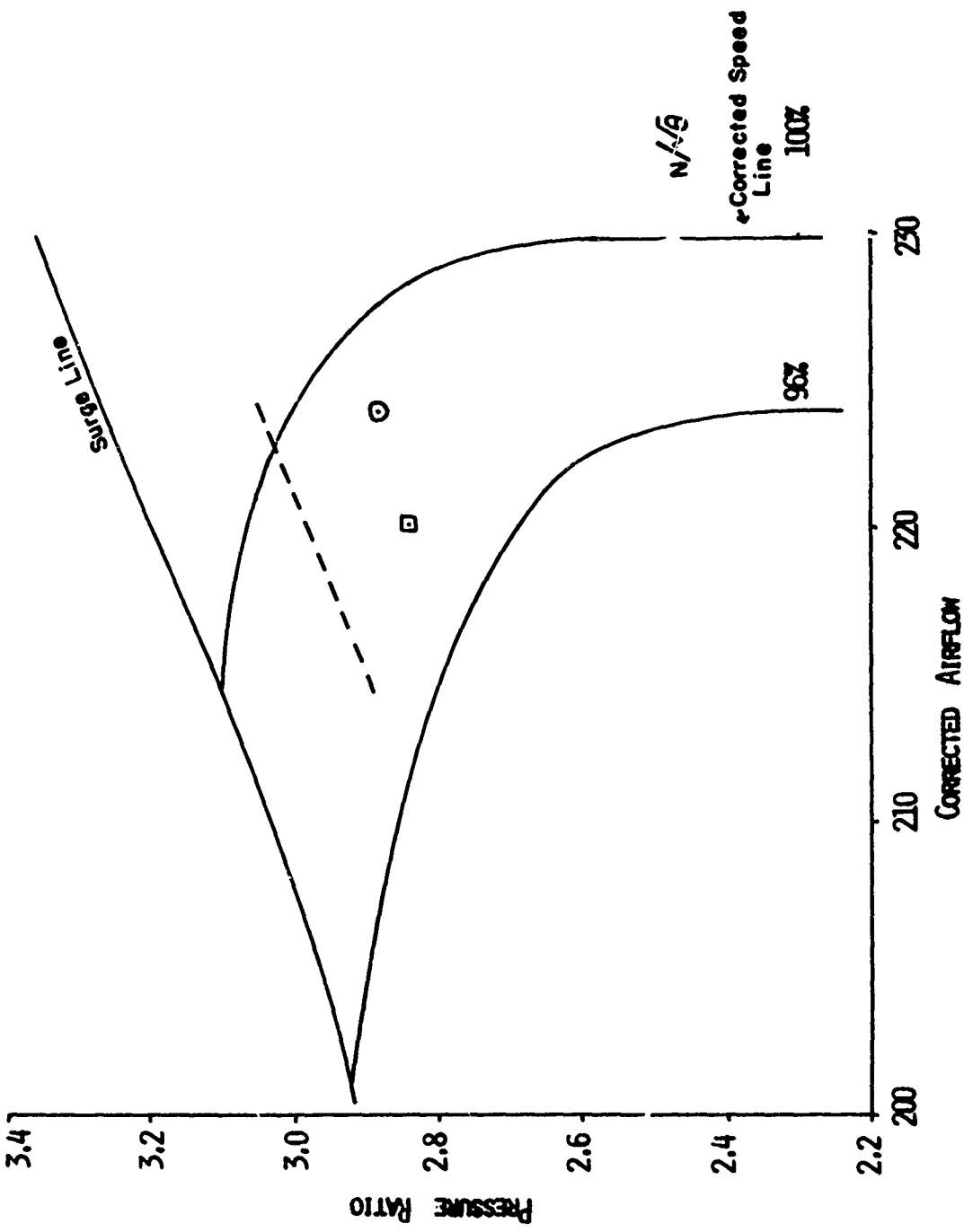

Figure 37. Fan Map

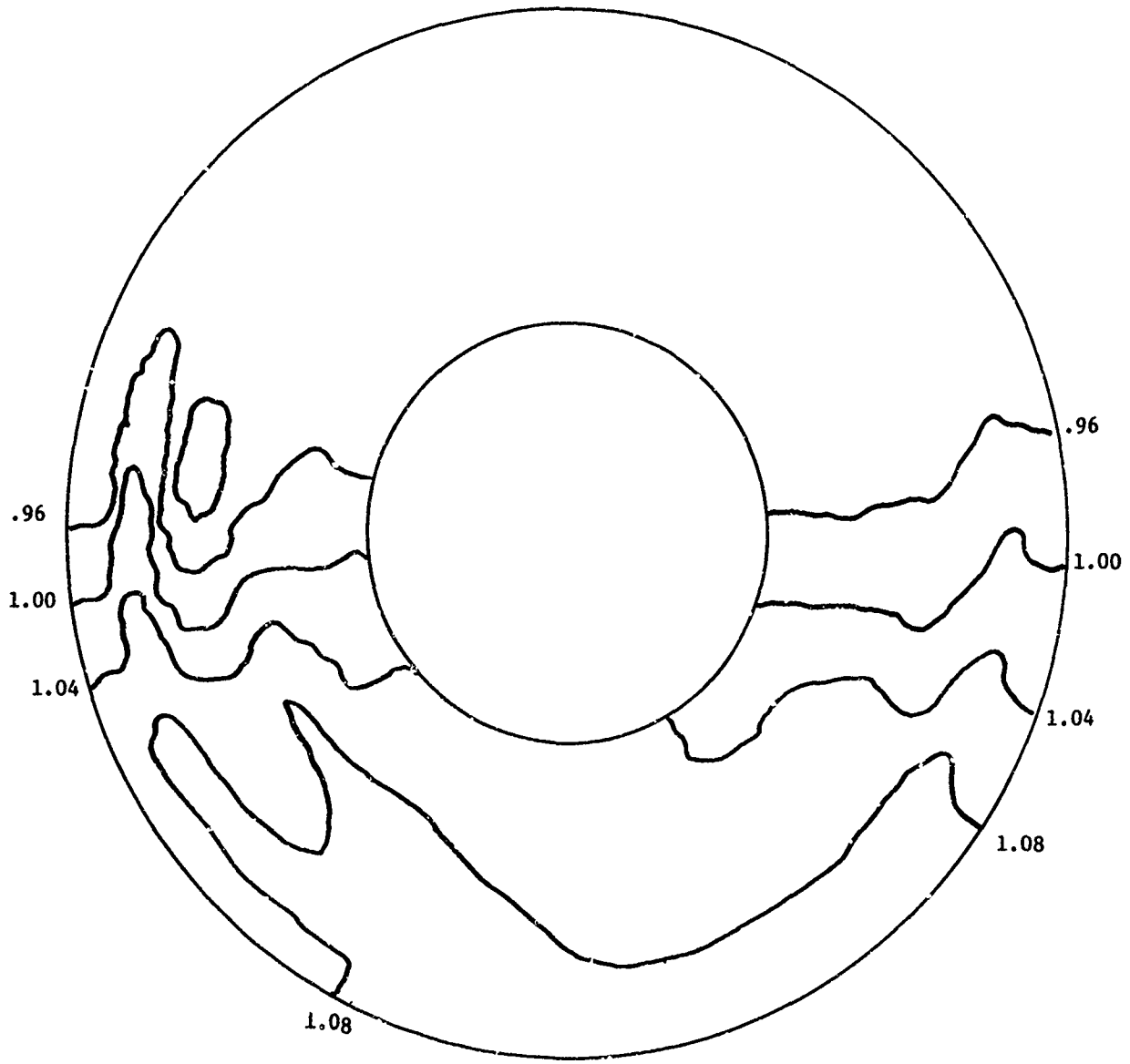

Figure 38. Distortion Pattern Fan Inlet

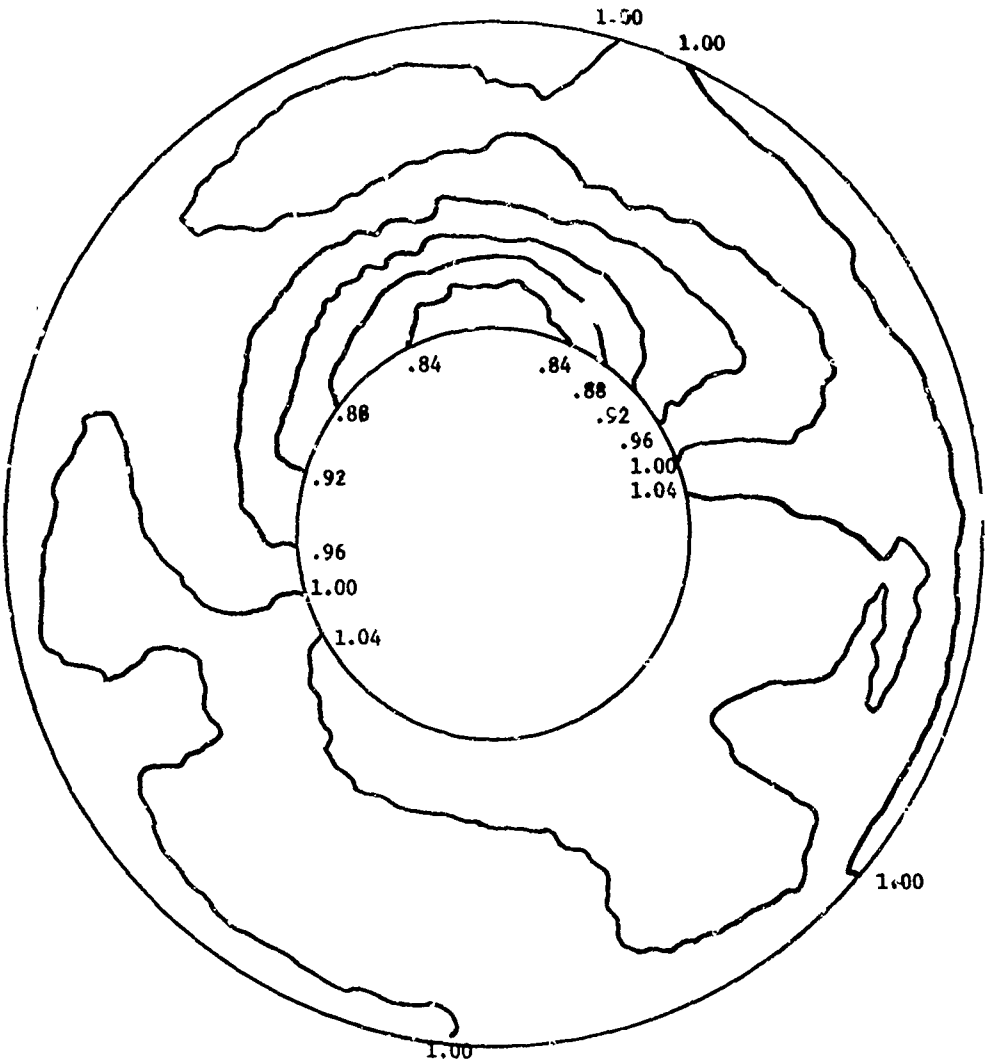

Figure 39. Distortion Pattern Fan Exit

the fan exit. Note the pattern is fairly radial in nature, with the lowest zone at about the 12 o'clock position and some 16% below fan average. This is a more severe pattern than that entering the component.

It has been shown that a component can amplify a distortion pattern. Likewise, through judicious designs, the distortion pattern can be attenuated. In this manner, the critical stages of the compression system can be isolated somewhat, improving the overall resistance to surge.

SUMMARY

Several important phases of the compatibility problem have been discussed here. The most basic is that although inlet flow distortion is a time-variant phenomenon, it appears that only patterns lasting at least for from one-half to one and one-half engine revolutions are felt by this engine. Additionally, the engine transport time for a stall-producing disturbance, as well as the time for the stall cell to grow until it triggers surge, must be accounted for in analyzing inlet-engine distortion tests. If this is not done, the critical phase of analysis --- the finding of the distortion pattern which caused the surge --- can be totally obscured. From the engine side of the problem, we have discussed how individual components of the compression system affects overall engine tolerance to distortion by its transfer characteristics, as well as its own tolerance. The part played by intra-stage effects will have to wait for row by row models to be fully explored.

SECTION III

CONTROL SYSTEMS AND TRANSIENT SIMULATIONS

The discussion in this section pertains to the basic turbine engine control problem and our approach to its solution, and transient simulation, which is an interdisciplinary effort. It ties together the design, development, and test efforts for the engine, its control, and inlet-engine compatibility problems such as distortion.

CONTROL SYSTEMS

Figure 40 depicts the typical modern engine which constitutes our major control program. It is an augmented turbofan engine consisting of a fan, compressor, main burner, two turbines, a mixed flow augmentor, and an exhaust nozzle.

The major objective is to control thrust according to the aircraft requirements and to control the airflow to provide this desired thrust. While meeting these generally external control requirements, various engine internal constraints must be satisfied. The fan and compressor must not be allowed to surge or overspeed, the compressor case to burst, the burners to extinguish, or the turbines to disintegrate. The following engine parameters are available to effect control: variable stator vanes, main fuel flow, augmentor fuel flow, and a variable exhaust nozzle area.

Various parameters are monitored. The airframe provides power lever angle, and aircraft Mach number. At the fan inlet, temperature is sensed, and sometimes pressure; at the compressor inlet, temperature is

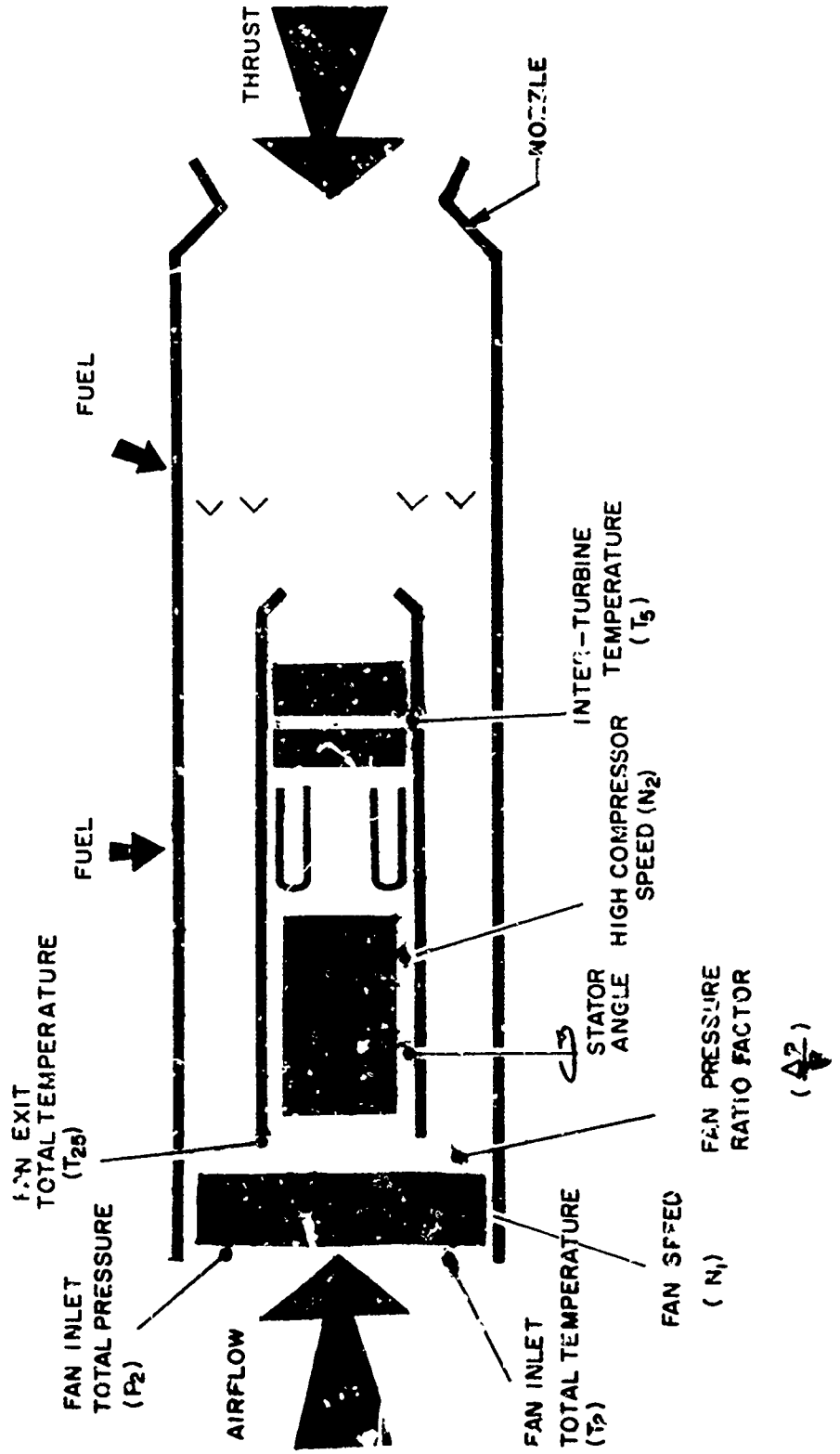

Figure 40. Engine Control Problem

also sensed. Rotor speeds of both spools are monitored. Sometimes fan discharge Mach number is sensed. Finally, since turbine inlet temperature is difficult to measure, inter-turbine temperature is measured.

To simplify this rather complex problem, the core is isolated from the rest of the engine, as shown in Figure 41. This reduces part of the problem to the control of a single spool turbojet. A speed governor is used to control fuel flow-by, nulling out a speed request signal with the sensed speed. During accelerations and decelerations the fuel flow is scheduled to avoid compressor surge, burner blowout and turbine over-temperature. Variable stators are scheduled to the corrected rotor speed.

Shown in Figure 42 is the fan-augmentor control. At low power settings from just below maximum rotor speed through maximum augmentation, nozzle control transfers from a scheduled control to a closed-loop control of engine airflow. That is, a parameter indicative of airflow, such as fan speed, is demanded and compared with the sensed value of speed to generate an error. The nozzle than moves to null out the error. The purpose of this control is to provide constant airflow operation regardless of the level of augmentation. Augmentor fuel flow is simply scheduled by the power lever and the fan inlet total temperature (T_2).

The above control functions are integrated by employing a supervisory control concept, whereby the ruggedness and reliability of hydromechanical hardware is combined with the sophistication of

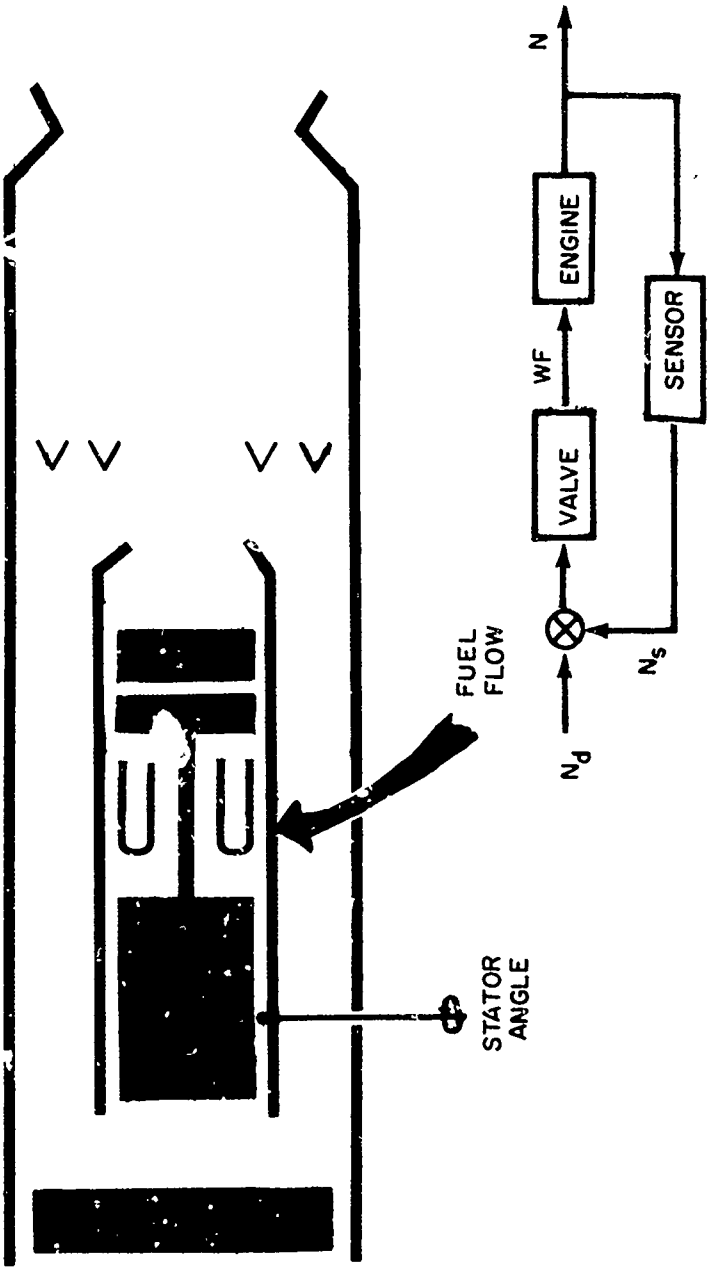

Figure 41. Core Control

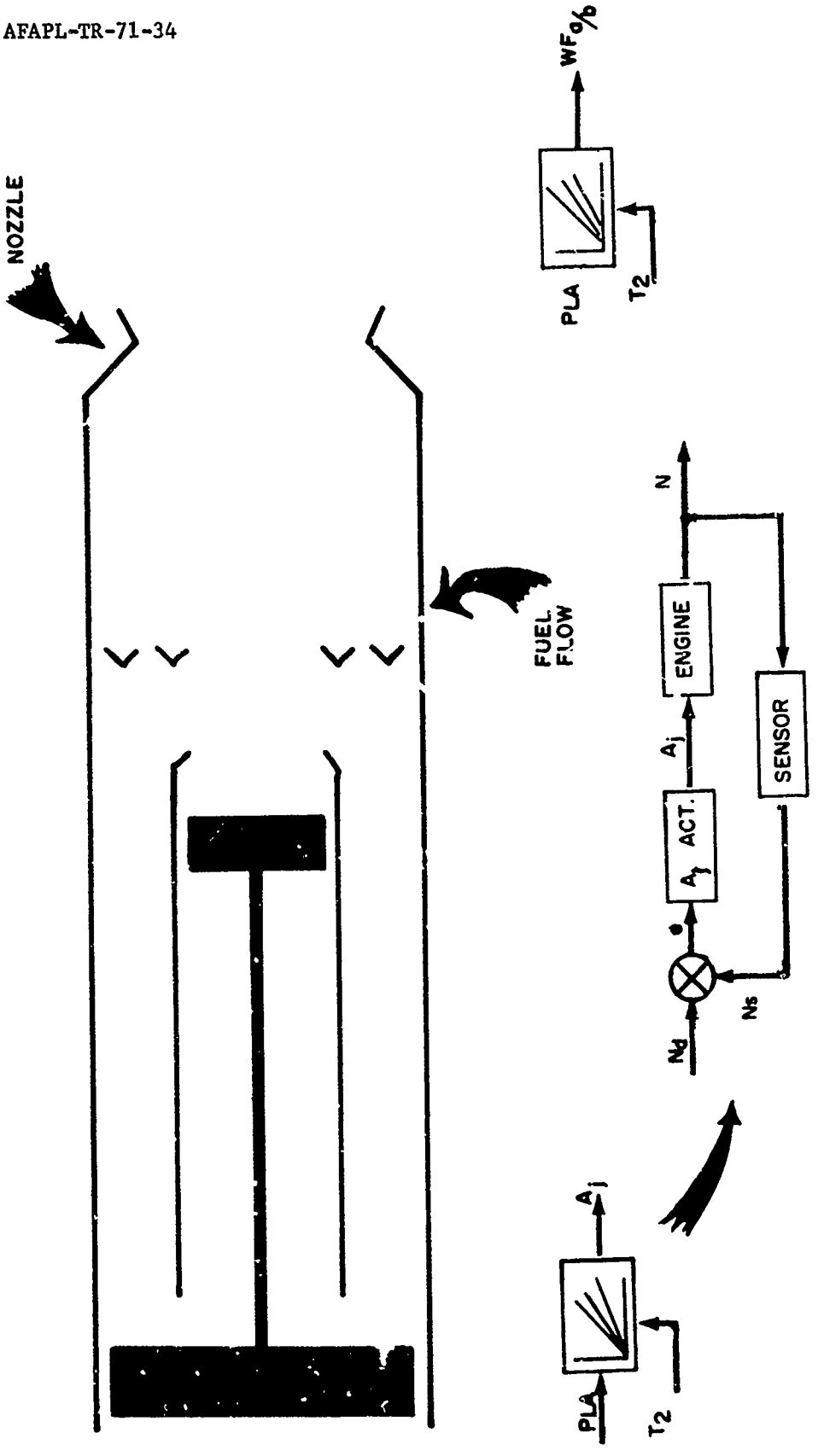

Figure 42. Fan-Augmentor Control

electronics. This is illustrated in Figure 43. The core, augmentor, and the scheduled operation of the nozzle are controlled by a hydromechanical control. This provides a minimum capability which enables at least a safe return home in the event of electronic failure. The electronic supervisory control can trim all the outputs of the hydromechanical control to provide various limits and the important closed-loop control of fan airflow.

TRANSIENT SIMULATION

Transient simulations are digital computer programs which allow the transient behavior of an engine to be simulated. This capability has been developed by industry under the sponsorship of the Air Force. The Air Force now requires an engine manufacturer to deliver a computer deck simulation (as described in Section I) of his engine at various points during a weapons system development progra The purpose of this is to provide a comprehensive flow of data from engine manufacturer to airframe manufacturer.

Figure 44 illustrates a transient simulation. For the sake of illustration, a single spool engine is shown. The components are represented in the simulation with steady-state aerodynamic maps just as in a steady-state simulation. However, dynamic equations are included to integrate the unbalanced torque to generate the instantaneous rotor speed. Other dynamic terms are inserted to account for lags due to the mass storage in the volume of the compressor, heat storage in the turbine, and the lags in the control.

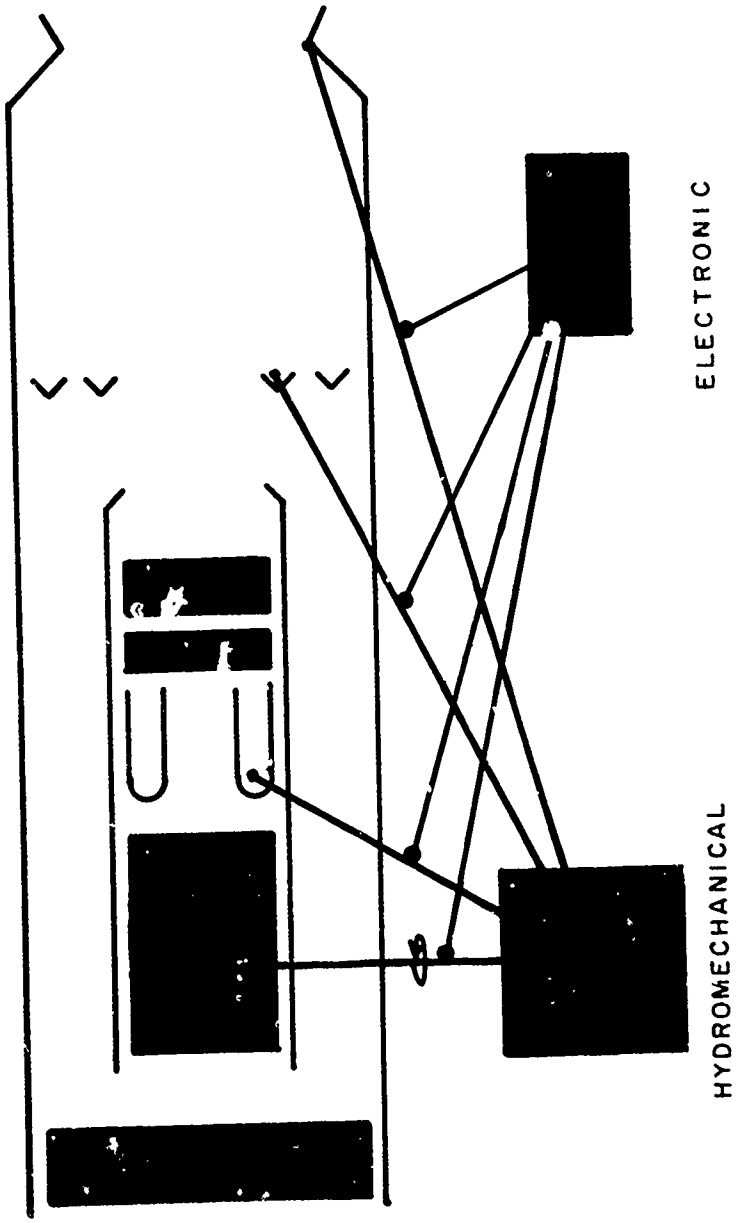

Figure 43. Supervisory Control

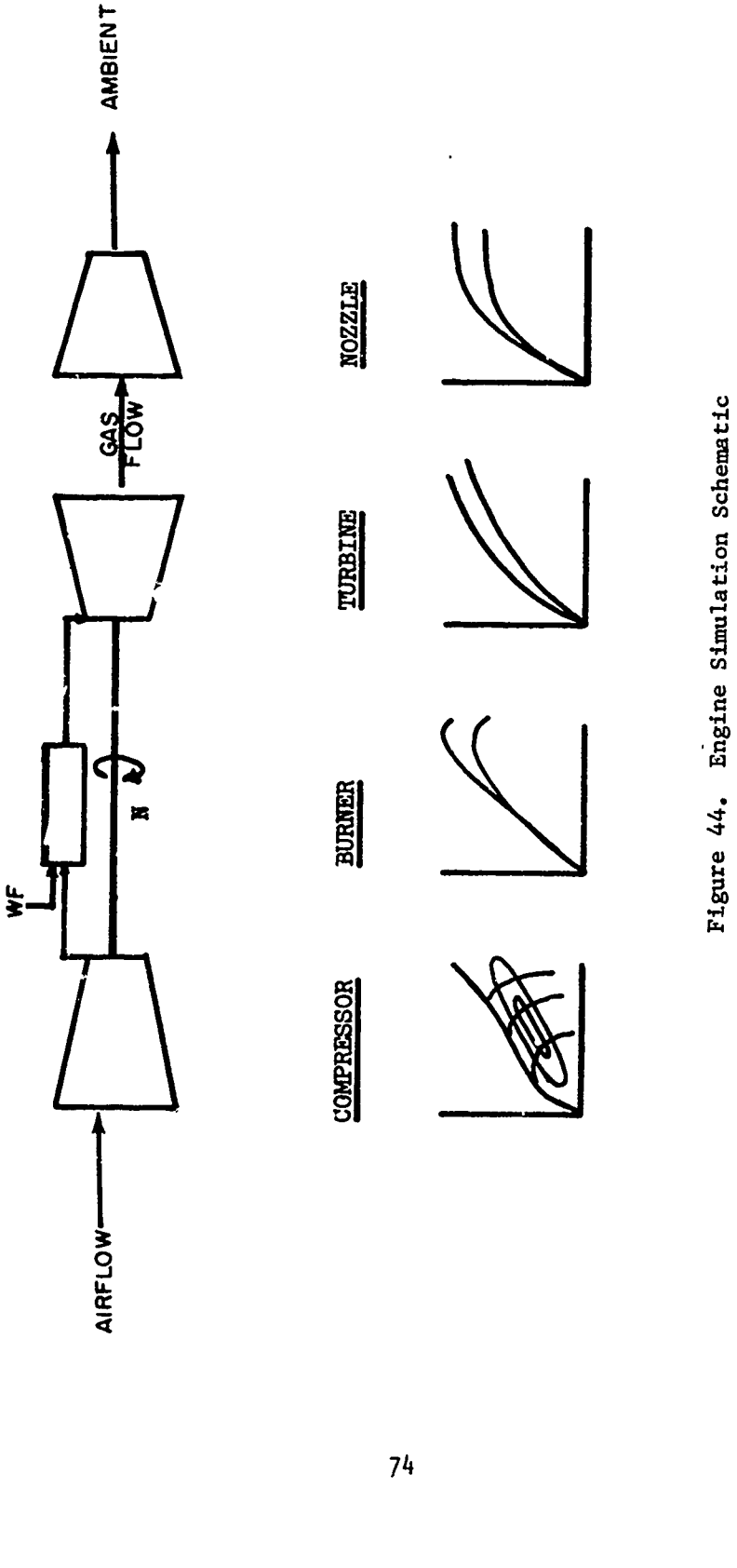

Figure 44. Engine Simulation Schematic

A simulation of this sort allows us to examine any engine parameter versus time as shown in the example of Figure 45. It represents a one-second power lever advance from idle to maximum augmentation for a fan engine. This capability can be used to examine a transient problem involving inlet engine compatibility.

Represented in Figure 46 are the operating characteristics of both the inlet and the engine. The inlet operating lines are indicated at various angles-of-attack and the trajectory of the operating point for a throttle reduction from maximum to idle during level flight and a simultaneous aircraft pitch-up. The simulation results in inlet buzz during the aircraft maneuver.

Figure 47 is a schematic portrayal of the entire system representing the aircraft, inlet, and engine. Generally, the entire simulation is not run on the computer at once because of the size and complexity. Instead, only portions are executed at a time as shown in the following example.

Figure 48 represents the results of a simulation which included the engine, distortion, pressure recovery, and map modifiers. These modifiers depict the effects of distortion on the fan and compressor discussed in Section II of this report. The figure illustrates the result of a power lever movement from idle to maximum augmentation plotted on the typical fan map. Shown are the undistorted surge line, the trajectory of the instantaneous operating point, and the instantaneous surge line reduced as a result of the distortion. The value of this

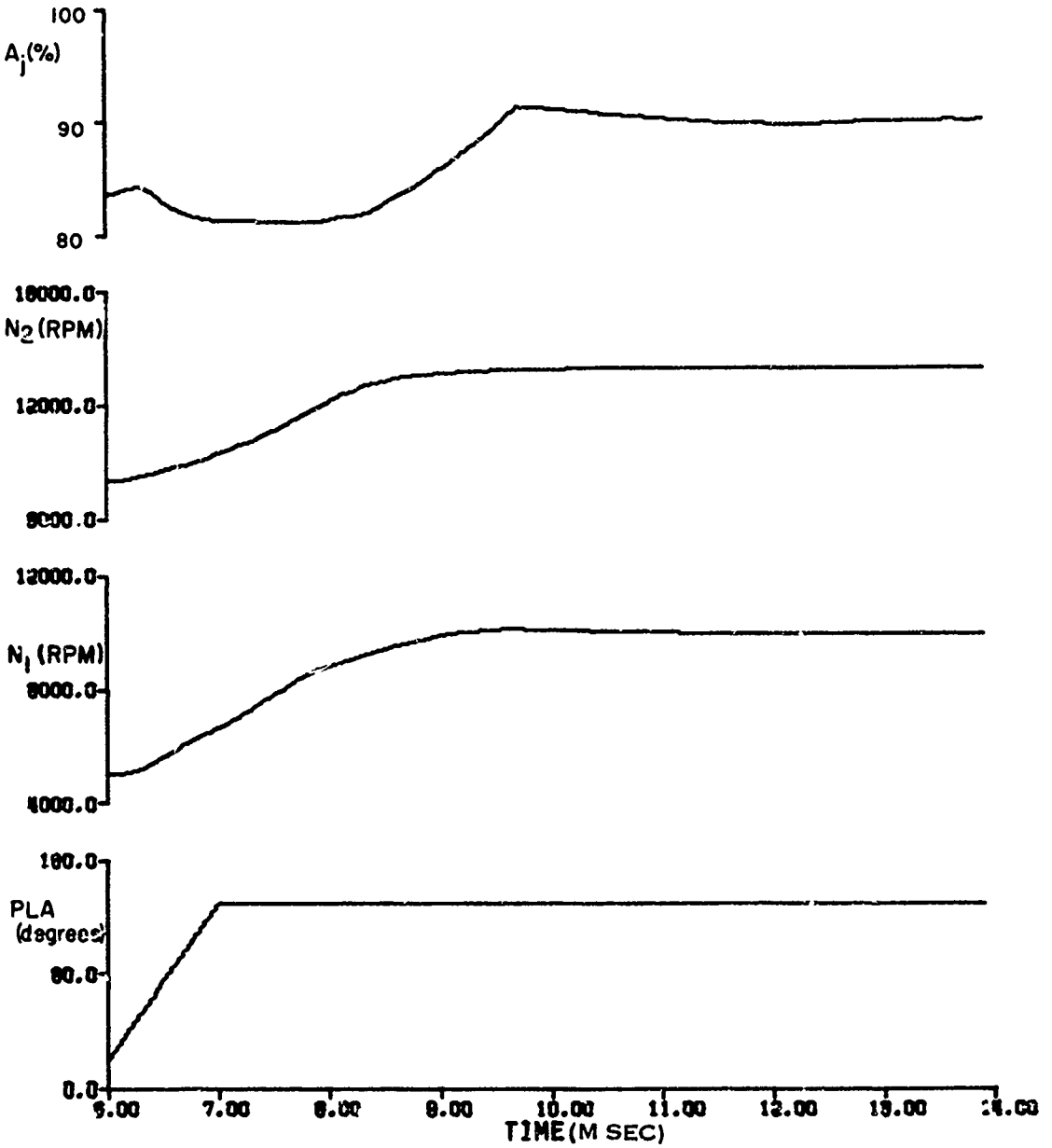

Figure 45. Typical Output of a Simulation

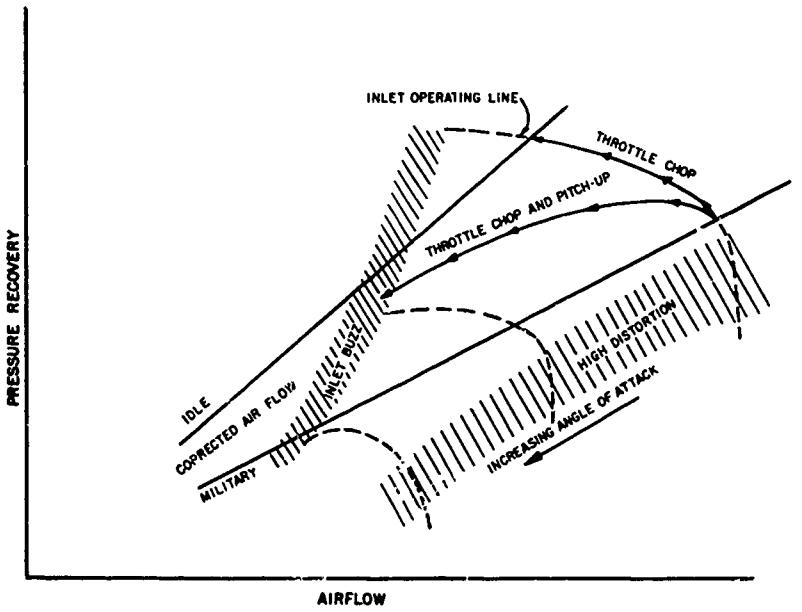

Figure 46. Effect of Aircraft and Engine Transients on Inlet Stability

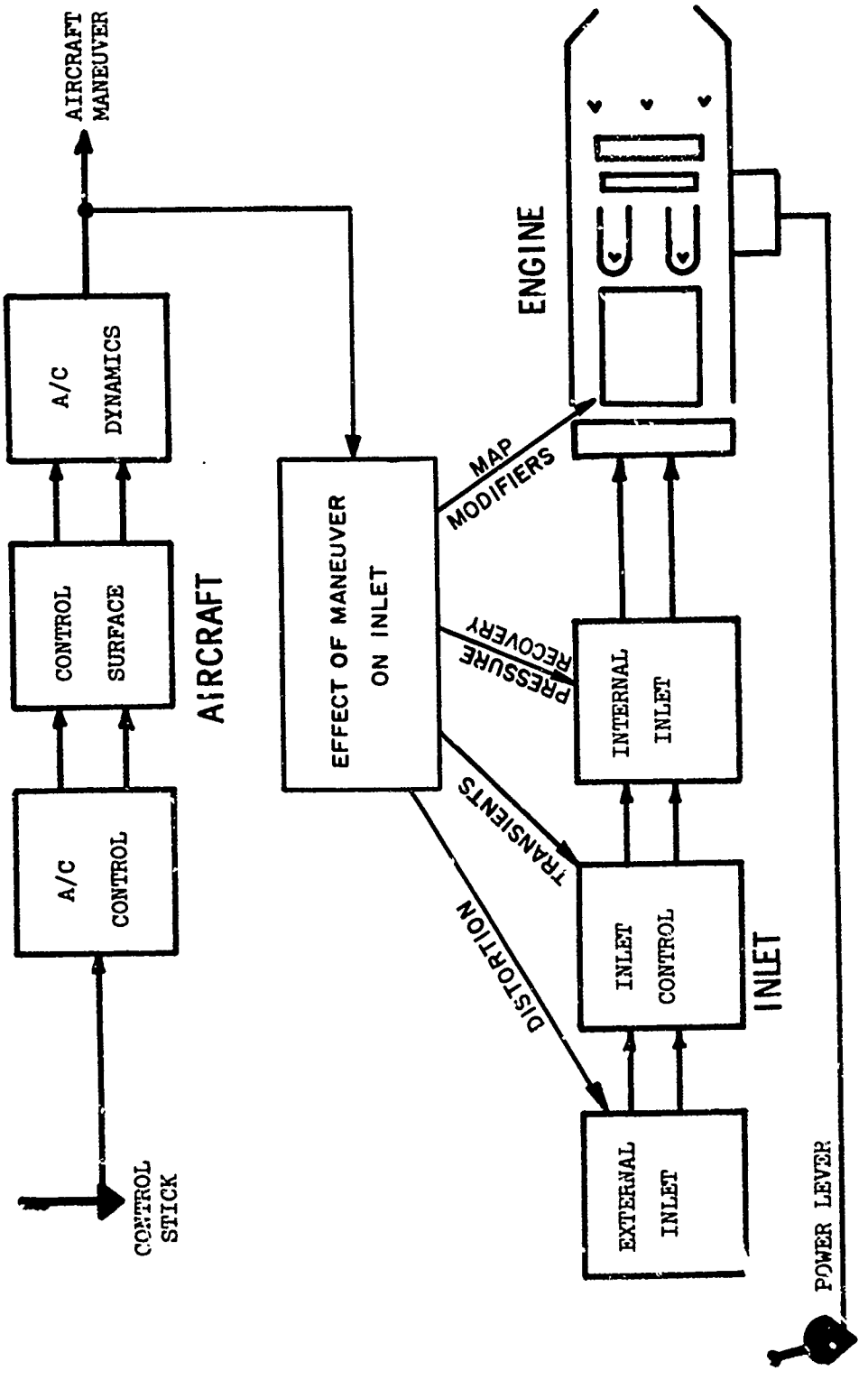

Figure 47. Overall System Simulation

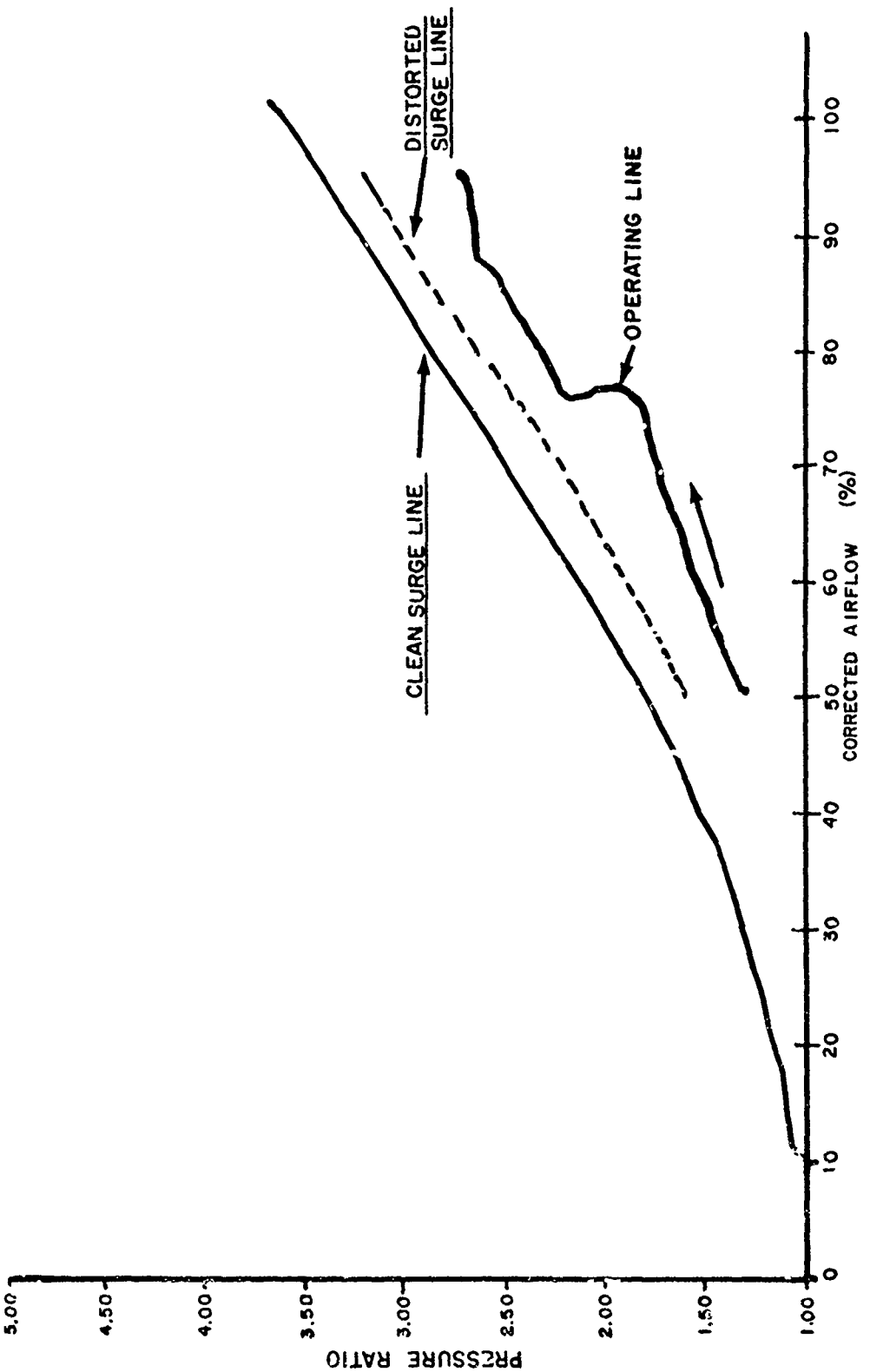

Figure 48. Fan Distortion Phenomenon

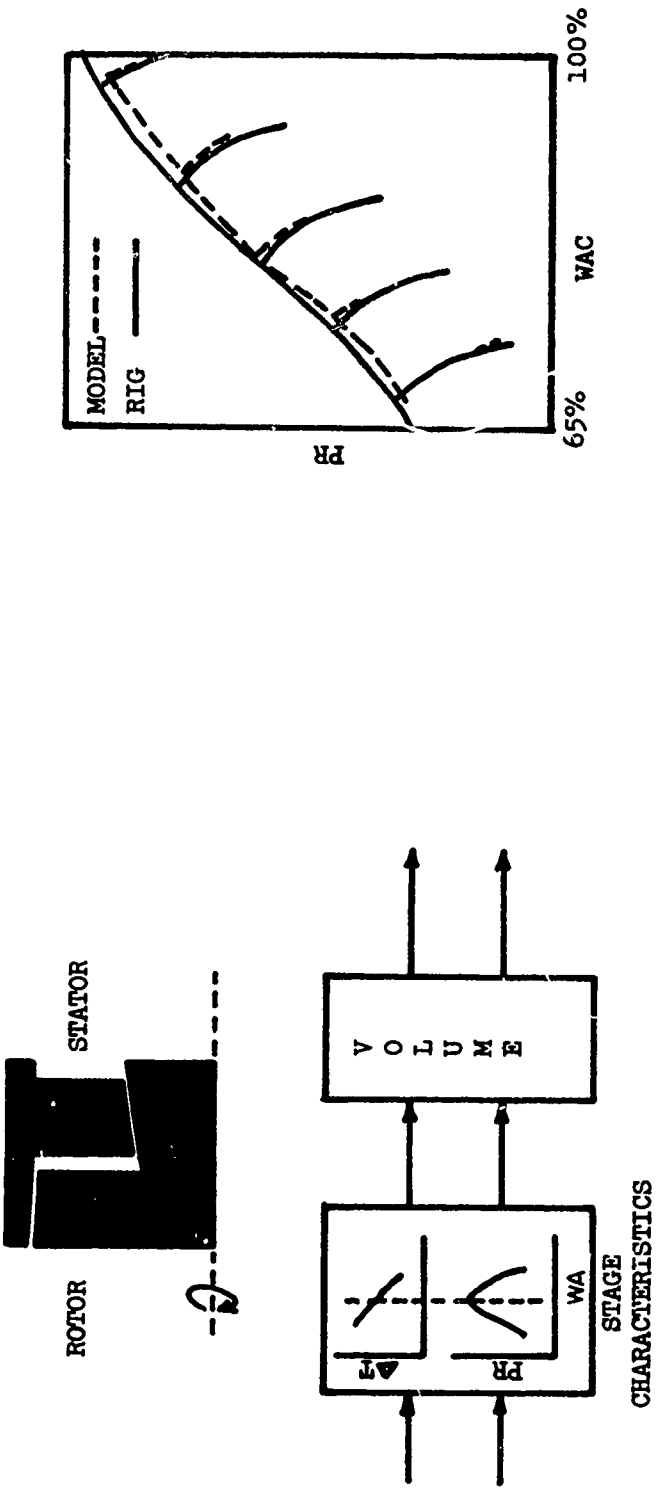

Figure 49. Compressor Stage Model

method of presentation is obvious; you can visually evaluate the surge margin. This is an example of how empirical data concerning distortion and surge are handled.

The turbine engine industry is continuously involved in a more comprehensive search for a better understanding of how distortion causes surge. More sophisticated simulations are being used in this effort, an example of which is the stage-by-stage simulation of a compressor, or fan. In the engine models the compressor is treated as a map and a volume. In the stage-by-stage model, the compressor is divided into stages, depicted by the stage characteristics and a volume, repeating this picture for each stage as shown in Figure 49. An interesting feature of this model is its ability to predict the surge line. Shown is a comparison of a compressor map for rig data and the stage-by-stage model.

The stage-by-stage model has been used to study 180° square wave, circumferential distortion. This was done using a parallel compressor model with two compressors, each experiencing a slightly different inlet pressure, but sharing a common static discharge pressure. Figure 50 shows the results as a distortion level parameter versus the circumferential location around the compressor. The model, of course, predicts square waves at the discharge of the stages. The various data points are typical component test data. The correlation is far from perfect, but trends are correct.

More sophisticated models break up the stages into a row-by-row model. These models use the airfoil characteristics of the rotors and

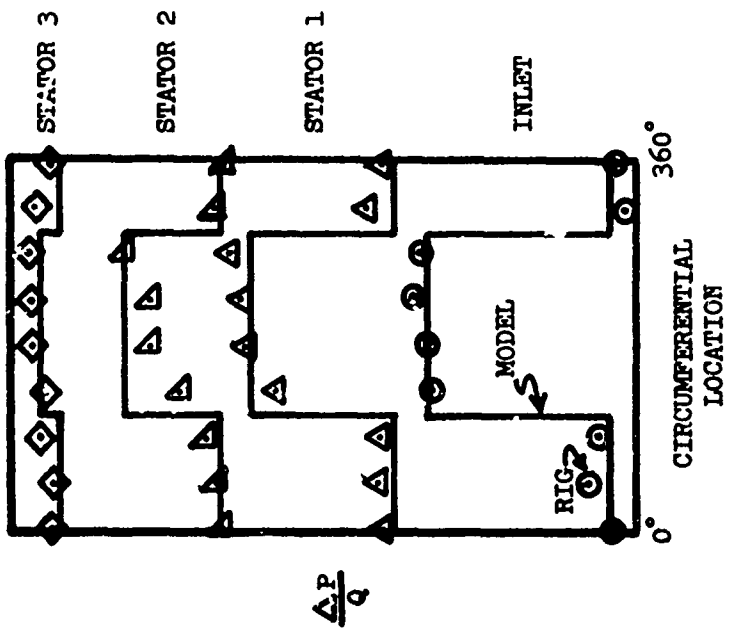

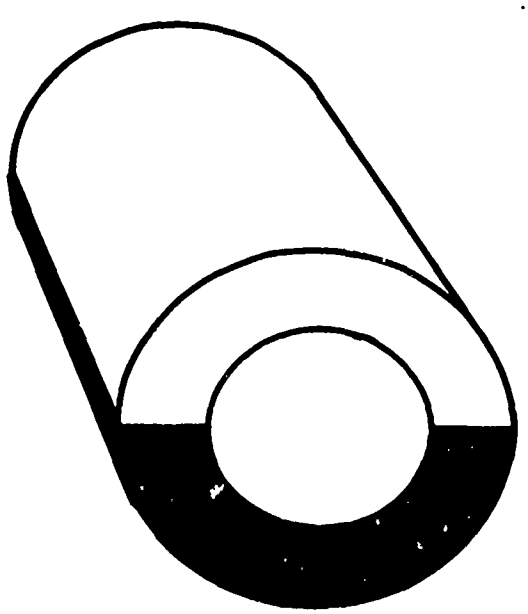

Figure 50. Parallel Compressor

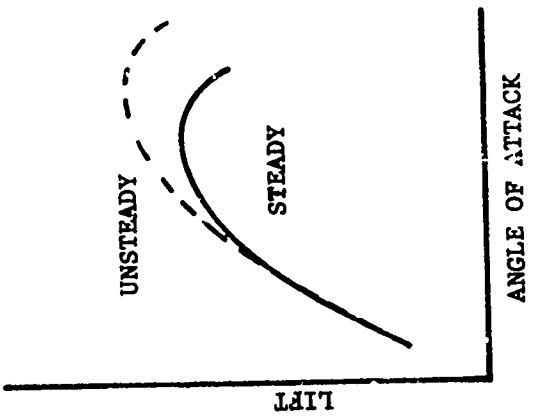

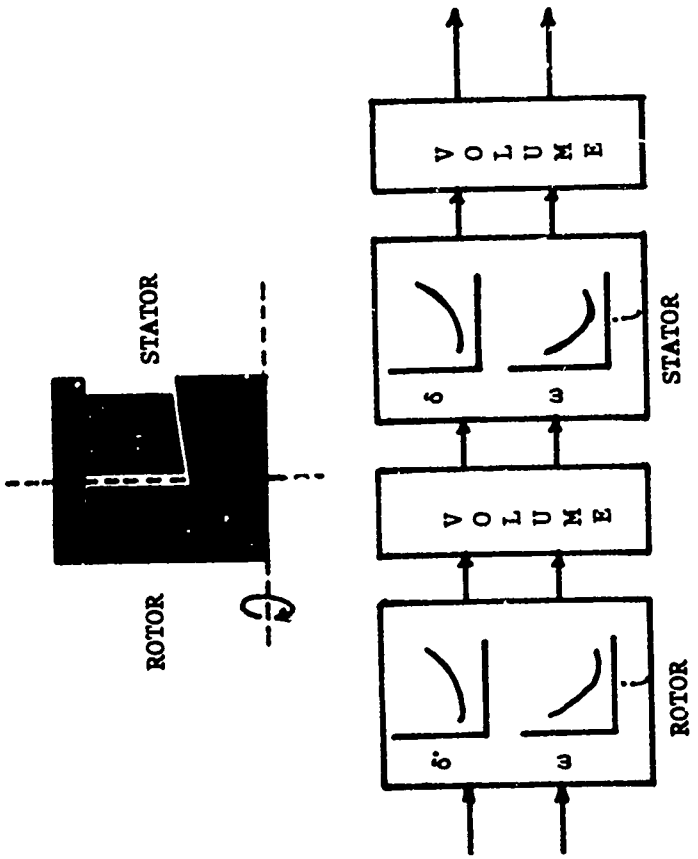

Figure 51. Compressor Row Model

the stators as shown in Figure 51. Results of this effort are preliminary at present. These models also have an interesting feature. Whereas the stage-by-stage model could predict the surge point, the row-by-row model can actually surge in a manner very similar to an actual machine. It is hoped that valuable insight will be gained concerning the mechanism of distortion with this model by incorporating unsteady lift effects.

Any simulation has an upper limit regarding its ability to adequately simulate high frequency phenomena. These limitations are as follows: (1) Engine models are satisfactory to 10 hertz, which makes them adequate for handling power lever and aircraft transients, (2) the stage-by-stage models are good to about 200 hertz, which is approximately one per rev, (3) the row-by-row model is good to 1000 hertz, which should be compatible with the instrumentation used in distortion testing.

SUMMARY

The simulation efforts described in this section are being developed and employed in a coordinated effort aimed at inlet-engine compatibility and to provide a comprehensive design tool for engine control system development.

SECTION IV

A TECHNIQUE FOR PREDICTING INSTALLED INLET AND EXHAUST SYSTEM PERFORMANCE

New types of aircraft entering the Air Force inventory have had the undesirable characteristic of failing to meet mission performance objectives at the outset of the development programs. This failure resulted in part from a lack of the ability to account for the impact of today's increasingly complex mission requirements upon the propulsion systems.

Several of the mission requirements being currently discussed are dictating a trend toward larger propulsion systems with respect to the total aircraft. Some of the reasons for this trend are the higher energy maneuverability requirements for current and projected air superiority missions, supersonic dash requirements for strategic missions, and high takeoff thrust requirements for STOL/VTOL missions. These requirements in themselves do not create the problem. Thus far it has been possible to produce the higher thrust engine cycles required. However, the majority of these current and projected missions also have a requirement for efficient propulsion system operation at the relatively low throttle ratios associated with subsonic cruise operations.

Throttle ratio is defined as the net thrust produced at a given engine power setting relative to the maximum possible net thrust that can be generated at a given Mach number and altitude. As larger thrust propulsion systems are being placed on today's weapon systems, the throttle ratios associated with cruise operations are decreasing. Current high performance, multi-design point aircraft have cruise thrust

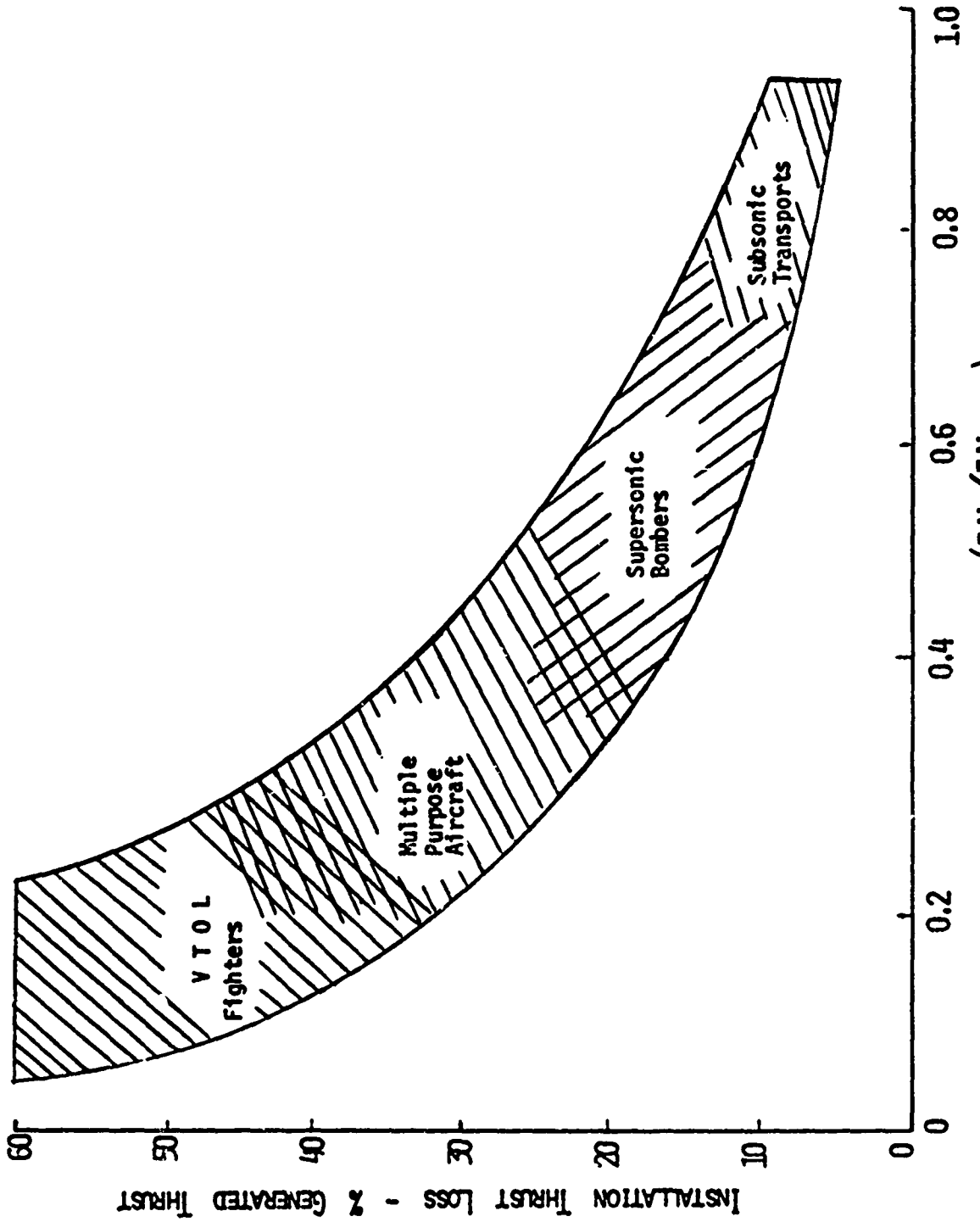

Figure 52. Installation Performance Losses During the Cruise Loiter Operation

requirements on the order of 30% of the maximum available. Future systems requiring STOL takeoff capability will operate at cruise thrust levels approaching 20% of the maximum available generated net thrust. At these low throttle ratios a significant portion of the generated net thrust is being lost. Shown in Figure 52 are typical exhaust system thrust losses at throttle ratios associated with cruise for several classes of current and projected weapon systems. These losses are the result of the flow mismatch, between the inlet, engine, and exhaust systems, which causes the inlet and exhaust systems to operate at off-design conditions during cruise operation. For the inlet, the losses are reflected in the form of increased spillage drag, while for the exhaust system, the losses appear in the form of increased boattail and interference drag. These result from relatively small nozzle exit areas and plumes associated with the small gas flows, nozzle pressure ratios, and temperatures for cruise operations.

To understand this flow mismatch, consider the simplified engine and exhaust system installation shown in Figure 53. The A_{91} shown represents the plume area associated with an isentropic expansion of the exhaust gases to ambient conditions at a given engine power setting. As the throttle ratio is decreased the plume area also decreases and thus fills a smaller area. The ratio of A_{10}, which represents some aircraft cross-sectional area, to this ideal plume area A_{91}, is a measure of how well the exhaust gas stream fills the aft-facing projected area. Consider that any unfilled portion of A_{10} is a source of drag regardless of whether or not the drag is base, boattail, or interference. Shown is the typical variation in A_{10}/A_{91} for current systems. At the low throttle

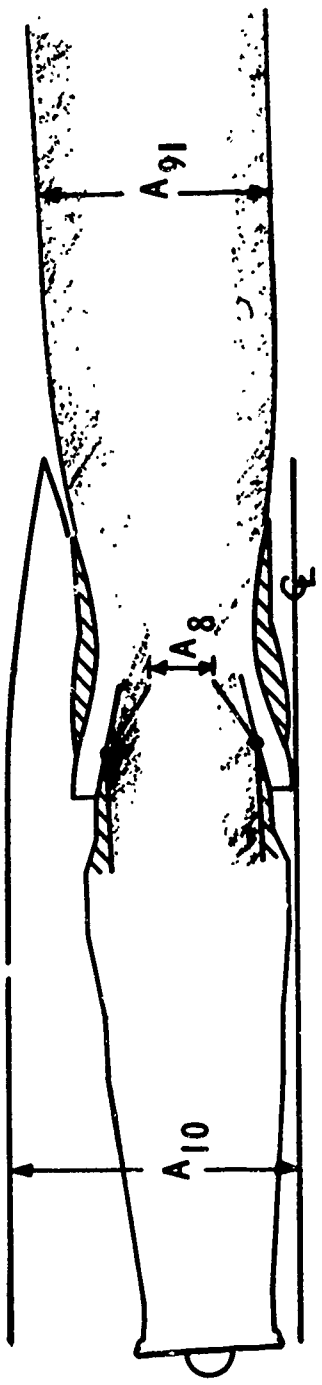

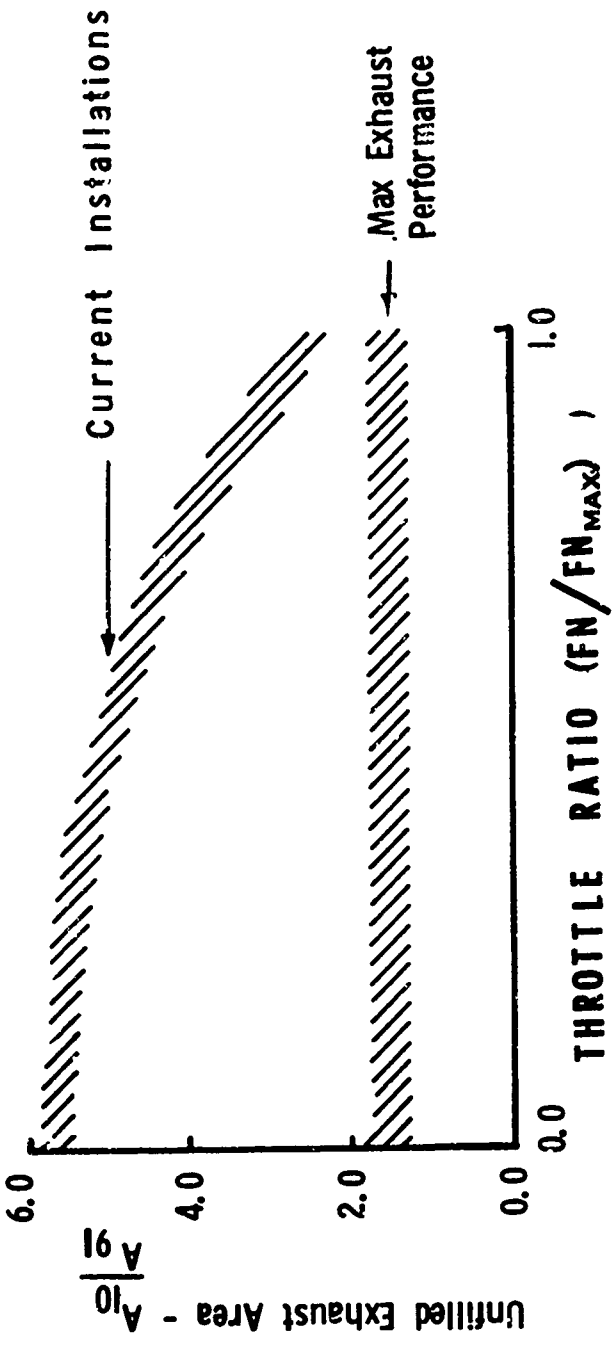

Figure 53. External Exhaust System Thrust Losses (A Function of "Unfilled" Exhaust Area)

ratios associated with cruise operation, the relative large A_{10}/A_{91} ratio is indicative of large performance losses. If the ratio of A_{10}/A_{91} could be minimized as throttle ratio decreases, the external exhaust system losses could be minimized. This desired variation in A_{10}/A_{91} is shown in Figure 53. The question arises as to what are the required variations in the properties of the gas stream delivered to the nozzle throat to maintain a constant A_{10}/A_{91} as the throttle ratio is decreased.

Once again from Figure 53 a mathematical relationship for A_{10}/A_{91} can be expressed in the following manner:

$$\frac{A_{10}}{A_{91}} = \left(\frac{A_{8M}}{A_8}\right)\left(\frac{A_8}{A_{91}}\right)\left(\frac{A_{10}}{A_{8M}}\right)$$

where: A_{8M} = maximum nozzle throat area

A_8 = nozzle throat area at given power setting

Assuming choked flow and using continuity and state relationships, the above expression can be converted to:

$$\frac{A_{10}}{A_{91}} = \left(\frac{1}{\sqrt{T_8/T_{8M}}}\right)\left(\frac{1}{WA/WA_M}\right)\left(\frac{NPR}{NPR_M}\right)\left(\frac{1}{A_{91}/A_8}\right)\left(\frac{A_{10}}{A_{8M}}\right)$$

The required relationships between variations in nozzle temperature ratio, gas flow ratio, and pressure ratio necessary to maintain A_{10}/A_{91} constant at a value of 0.5 are shown in Figure 54 for operation at sea level and Mach 0.85.

In Figure 55 these variations in temperature and nozzle pressure ratio are shown at the same operating point for conventional turbofan and turbojet cycles. Failure to adequately define and account for the

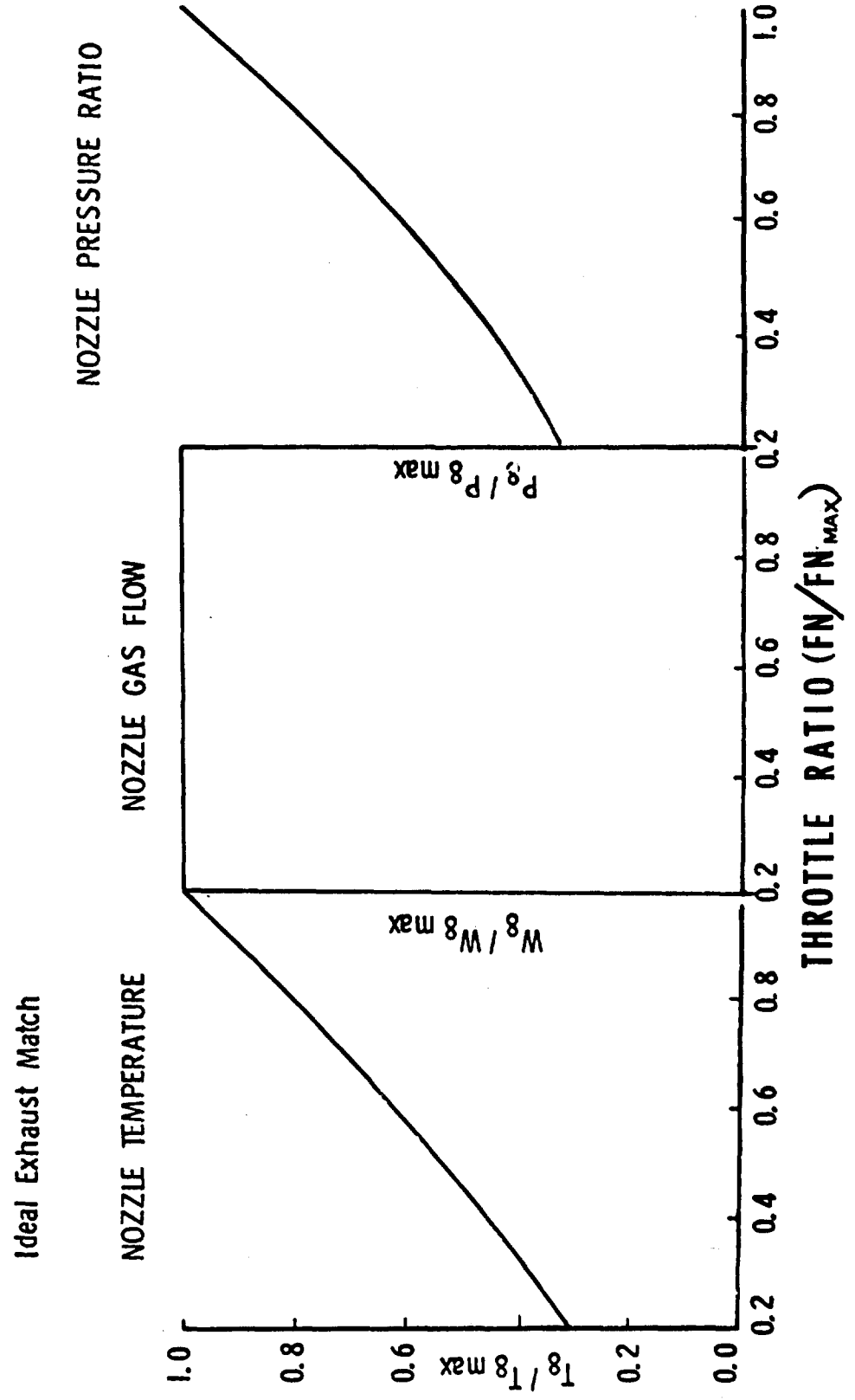

Figure 54. Part-Power Engine Exhaust Performance Match at Sea Level Static and Mach 0.85

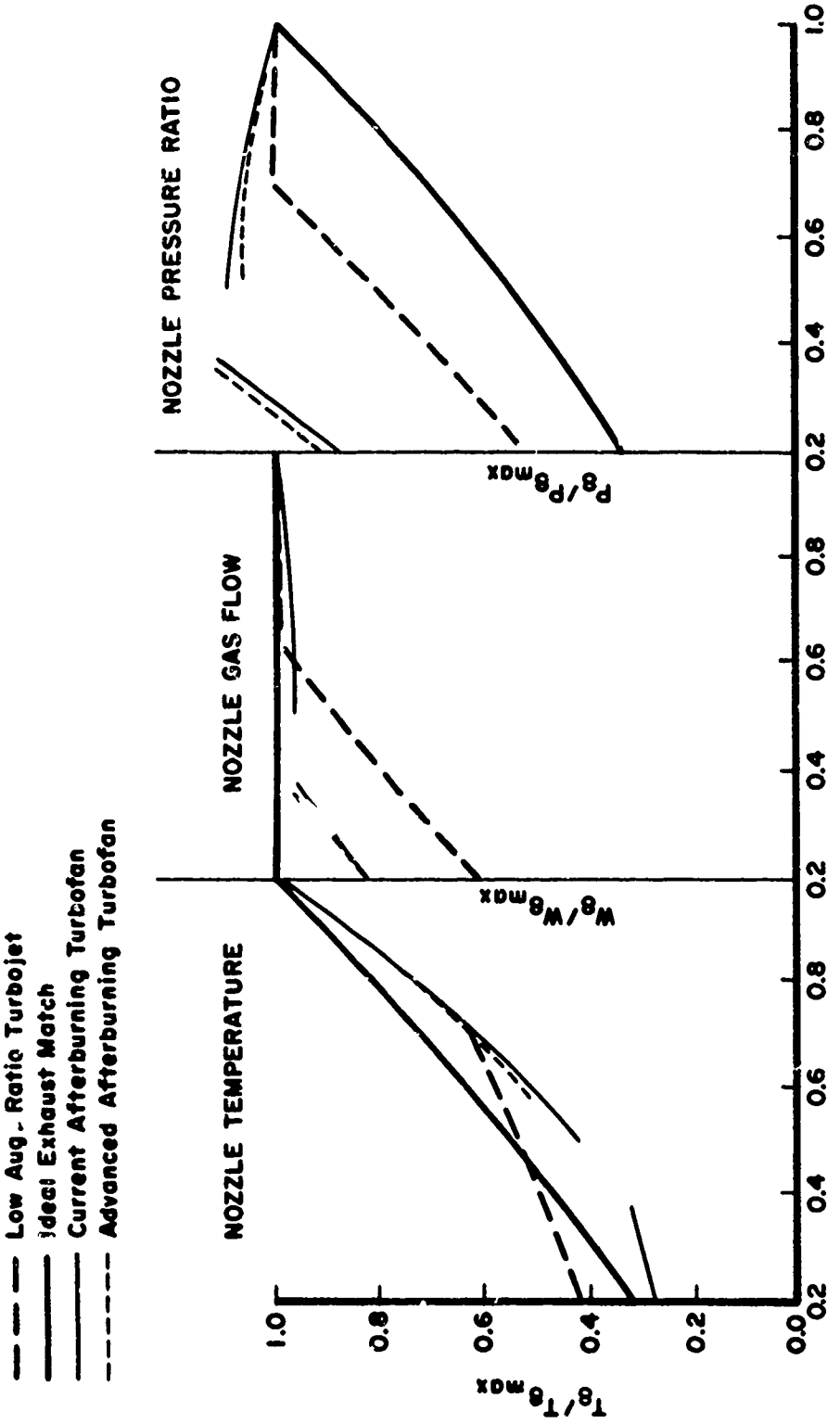

Figure 55. Part-Power Engine-Exhaust Performance Match at Sea Level Static and Mach 0.85

inlet and exhaust system performance losses, implied by these variations, has resulted in large degradations from predicted performance. These degradations usually have not been uncovered until flight test.

During the early phases of a development program, information that would allow accurate assessment of inlet and exhaust system losses is not available. The result is that normally, unrealistically low losses are assumed. For the exhaust nozzle the internal performance is often dictated by a constant C_{TIN} of 0.985 while the external exhaust system losses may not even be accounted for. It is not until the latter phases of a development program, when wind-tunnel test data is available, that realistic assessment of the inlet and exhaust system performance has occurred. Often, however, inconsistencies between the various tests necessary to define system performance have not permitted an accurate assessment. This, in addition to the problems of fully simulating flight conditions, have resulted in flight test performance severely below expectations.

Shown in Figure 56 is an example of the correlation between the initial exhaust system performance estimates and those derived from wind-tunnel testing. Failure to include realistic inlet and exhaust system performance characteristics from program outset leads to optimistic system performance estimates, and may force the engine-aircraft configuration selection process to a seriously sub-optimized system configuration.

Figure 57 shows two levels of exhaust system performance for a given installation. The graph on the right represents the unrealistically

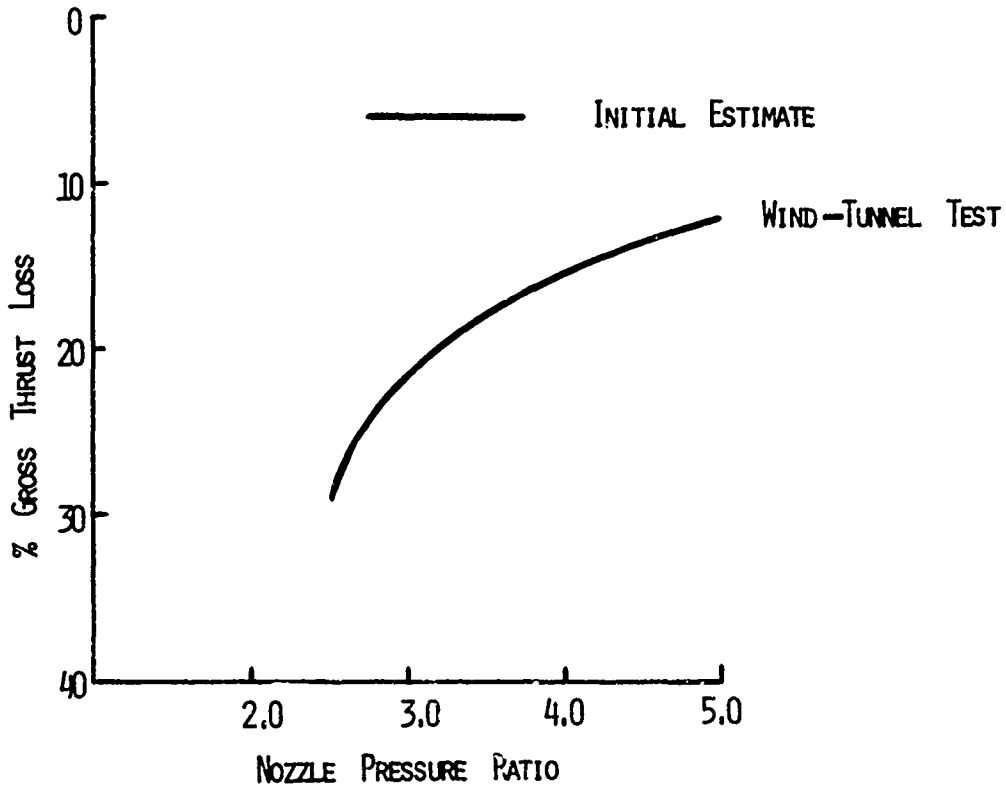

Figure 56. Exhaust System Performance (Typical)

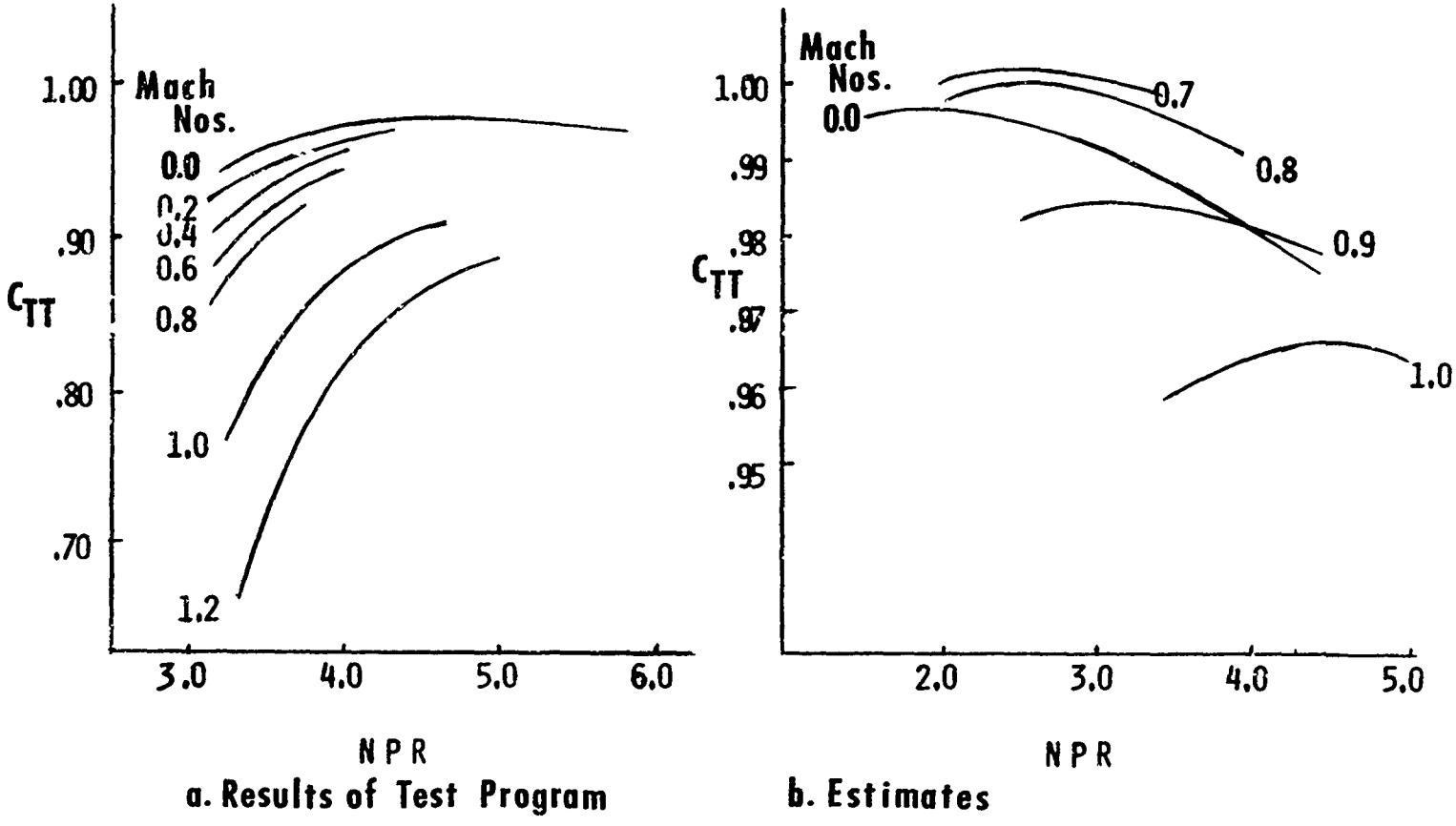

Figure 57. Reference Drag Effect cn C_{TT}

high performance estimates used during the early phases of a development program while those shown on the left are the results of a wind-tunnel test program. At a typical cruise operating point of Mach 0.8, nozzle pressure ratio of three, it can be seen that there are almost ten counts difference in the gross thrust coefficient levels. If, as would normally be the case, the choice of cycle was made based on the initial estimates shown on the right, a turbofan cycle may have been selected over a turbojet in order to take advantage of the improved SFC's inherent with turbofans. However, the higher gross-to-net thrust ratios of the turbofan when combined with the more realistic exhaust system losses shown on the left, can result in significantly greater losses in generated net thrust for the turbofan than those associated with a conventional turbojet for this installation.

INLET AND EXHAUST SYSTEM PERFORMANCE MAP DEFINITION

The difficulties of predicting installed propulsion system performance are compounded by the lack of a universal method of describing inlet and exhaust system performance losses. Inadequate mechanisms now exist for treating these losses in terms understandable and workable intra-company, inter-company, and between companies and government agencies. Without an adequate method of describing propulsion system losses it is difficult and often misleading to optimize engine, aircraft, and mission. Top priority must therefore be given to developing a series of workable "interface parameters" that are understood and used by the people involved in the various disciplines required to define the performance of complex weapons systems.

One possible solution to some of the previously mentioned difficulties of defining and predicting installed propulsion system performance is the use of inlet and exhaust system performance maps. Basically, an inlet or exhaust system map defines the level of throttle dependent losses charged to the propulsion system for a given engine operating point. Although many formats may be used to define these losses, to be acceptable, the parameters used must be meaningful to both engine and aircraft company personnel. Throttle dependent losses are normally expressed in terms of changes in drag, i.e., spillage or boattail, relative to some arbitrarily defined reference conditions.

The losses should be defined such that they can be related to both vehicle performance and engine performance, depending upon whether vehicle or propulsion performance people are working with the losses. The current procedure is to define these maps from a series of wind-tunnel tests. Normally, three test series are conducted to define inlet and exhaust system performance. These are: an aeroforce test to define the inlet and nozzle reference drag levels across a range of engine flow conditions, and inlet system test, and an exhaust system test to determine changes in inlet and afterbody drag levels across a range of engine flow conditions and inlet and nozzle geometry. A parameter used to define exhaust system losses which is useful to the propulsion engineer is the exhaust system gross thrust coefficient, defined as follows:

$$C_{TT} = C_{TIN} + C_{TEX} - 1$$

where:

C_{TT} = Exhaust system gross thrust coeficient

C_{TIN} = Exhaust System internal gross thrust coefficient

C_{TEX} = Exhaust System external gross thrust coefficient

C_{TIN} contains internal friction, over and under expansion, leakage, and divergence augularity losses, while C_{TEX} contains the exhaust system external losses:

$$C_{TEX} = (F_{GID} - \Delta D)/F_{GID}$$

where:

F_{GID} = Ideal gross thrust derived by isentropically expanding the gas at nozzle entrance conditions to ambient pressure.

ΔD = The drag of the external surfaces of the exhaust system referenced to a known base condition.

The conditions chosen for the aero reference test have a definite impact upon the resulting levels of drag assigned to the inlet and exhaust systems. Therefore, it is essential that all individuals involved completely understand the test procedures, reference conditions, and performance integration system being used for making system performance projections. Typical inlet and exhaust system performance maps are shown in Figure 58 and 59.

Since resources are often not available during the early phases of a development program to conduct wind-tunnel model tests, carefully generalized empirical data and analytical procedures can be used to generate inlet and exhaust system maps. The resulting estimates, although not exact,would ensure that representative installation losses are included when making weapons system performance predictions. From these preliminary estimates, those installations having greatest performance potential may be selected for continued development. For each

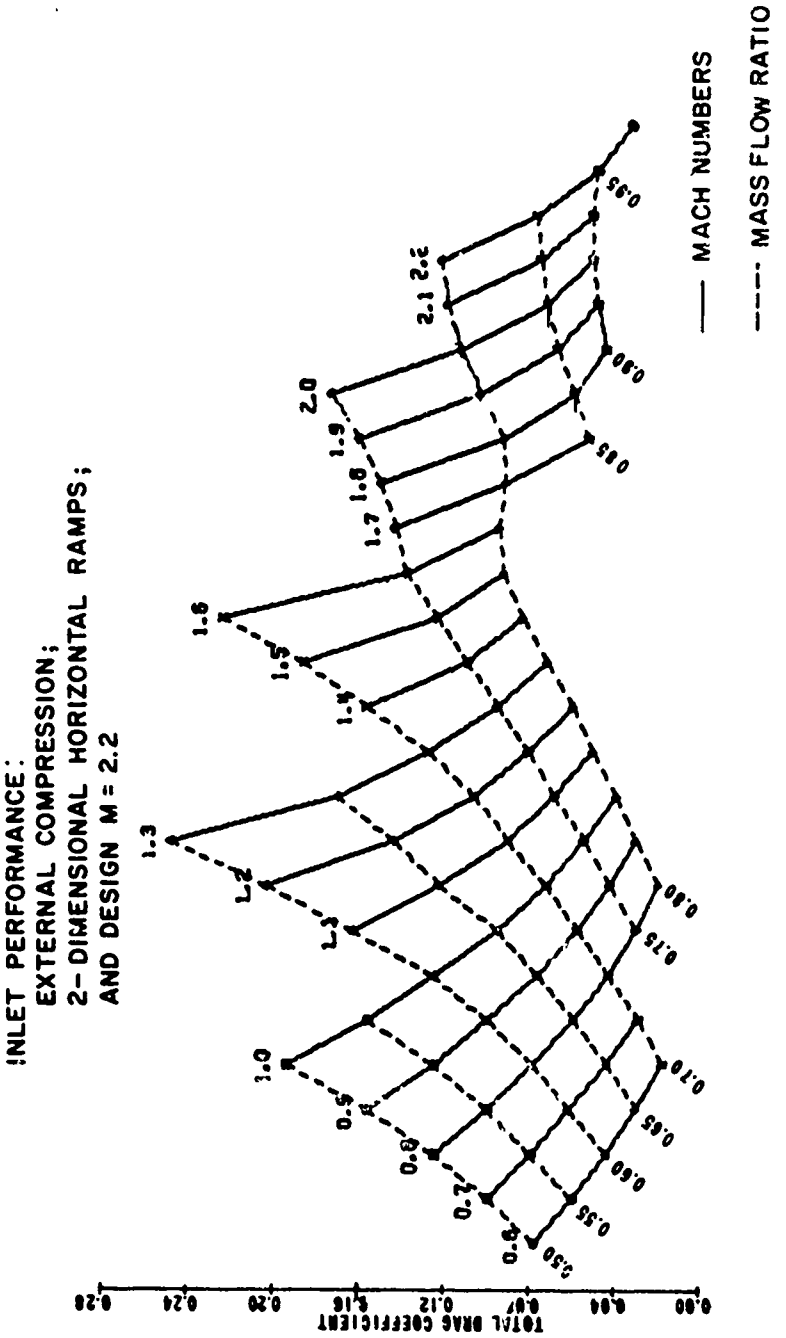

Figure 58. Thrust Losses Due to Excessive Inlet Airflow

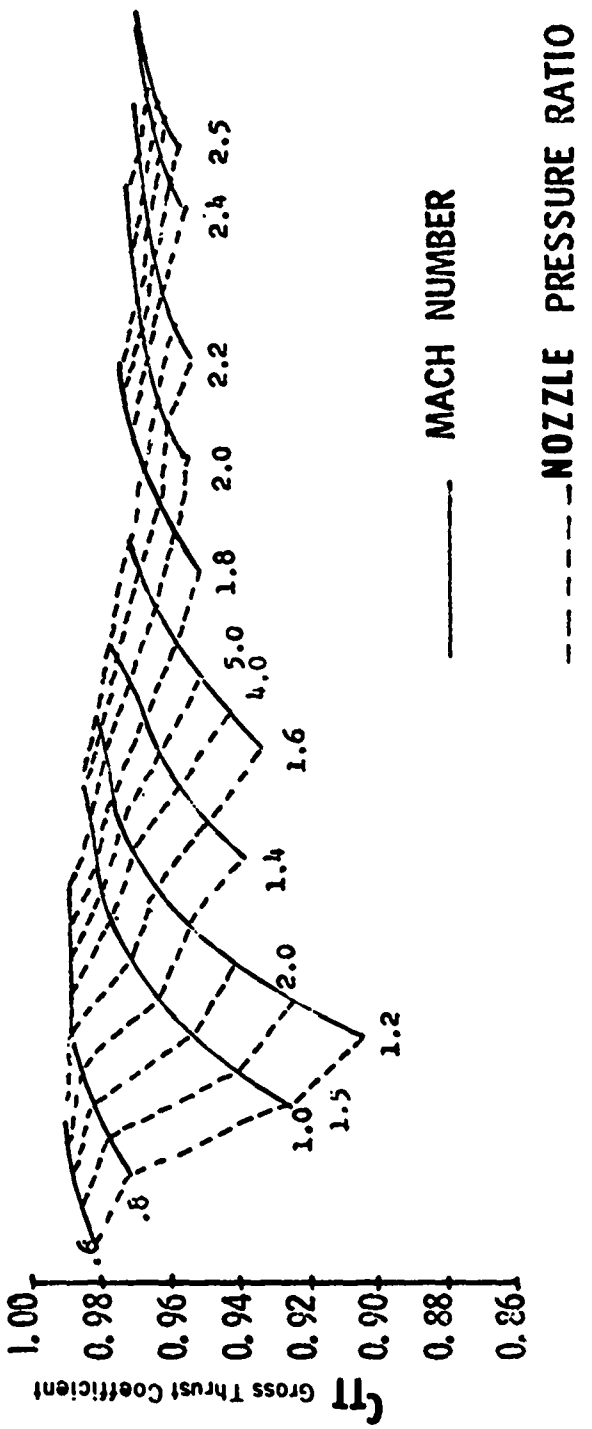

Figure 59. Exhaust System Installed Performance

of these, the engine configuration which best matches the given installation can then be defined.

When the resources for wind-tunnel testing become available, pretest inlet and exhaust system performance maps can be estimated and used to identify areas of uncertainty where additional data is needed. From these, the tests and instrumentation necessary to define performance across the required operating range may be defined. Pretest estimates can then be used during the wind-tunnel tests to check the results and make any necessary corrections to the test techniques, data reduction, and instrumentation being used.

SUMMARY

By using inlet and exhaust maps derived from valid wind-tunnel test data in conjunction with engine performance simulations, discussed Section I of this report, the installed propulsion system performance can be assessed at the necessary engine operating points. Figure 60 is a typical exhaust system performance map for a Mach number of 0.9 at sea level. Shown on this map is the engine operating line (A-B-C-D-E) from maximum afterburning to an idle power condition, expressed in terms of A_8/A_{8M} and nozzle pressure ratio. Using this as a base, changes in cycle parameters which affect the operating line can now be investigated in an attempt to minimize these exhaust system losses. However, any proposed change must be examined relative to the inlet to determine if the resulting changes in inlet performance negate those gains made in the exhaust system.

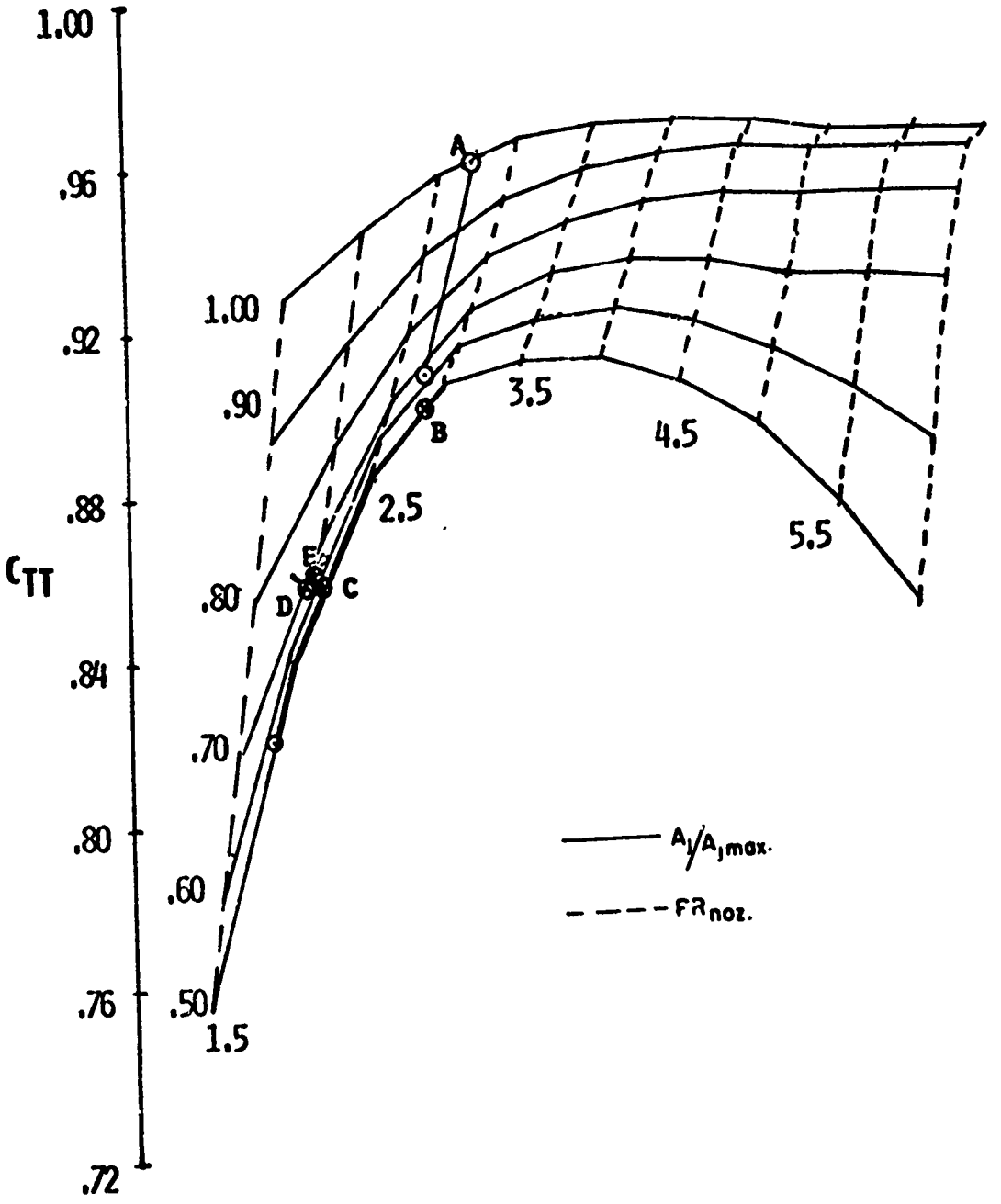

Figure 60. Nozzle Operating Line at Sea Level Static and Mach 0.9

Timely synthesis and use of inlet and exhaust system performance maps can reduce the number and severity of unexpected performance problems which are encountered during the progress of systems development programs.